Targeted CNS Delivery via Nanoparticulate Drug Delivery Systems

Dissertation zur Erlangung des Doktorgrades
der Naturwissenschaften (Dr. rer. nat.)
der Fakultät für Chemie und Pharmazie
der Universität Regensburg

vorgelegt von

Mira Oswald
aus Dieburg

im Jahr 2017

Promotionsgesuch eingereicht am: 21.04.2017

Die Arbeit wurde angeleitet von: Prof. Dr. Achim Göpferich

Diese Doktorarbeit entstand in der Zeit vom Dezember 2012 bis März 2016

bei der Merck KGaA, Pharmaceutical Technologies, Darmstadt, in Zusammenarbeit mit dem Institut für Pharmazeutische Technologie der Universität Regensburg.

Für meine Lieben

Daß etwas schwer ist, muß ein Grund mehr sein, es zu tun.

Rainer Maria Rilke (1875-1926)

Table of contents

Chapter 1

Targeting the blood-brain barrier: a review of rabies virus targeting strategies

Submitted to Molecular Pharmaceutics

Abstract

The transport of drugs across the blood brain barrier is challenging. The use of peptide sequences derived from viruses with a CNS-tropism is one elegant option. A prominent example is the rabies virus glycopeptide (RVG), which is said to enable a targeted brain delivery. Although the entry mechanism of rabies virus into the CNS is very well characterized, it is unknown whether RVG-functionalized drug delivery systems (DDS) follow this pathway. RVG-functionalized DDS present themselves with modifications of the RVG peptide sequence and different physicochemical properties compared to rabies virus. To our surprise, the impact of these changes on the functionality is completely neglected. This review explores virus-related CNS targeting strategies by comparing RVG-functionalized DDS with regard to their peptide modification, physiochemical properties and their behavior in cell culture studies with a special focus on the original pathway of rabies virus entry into the CNS.

Introduction

In brain targeted delivery, short virus peptide sequences with a central nervous system (CNS)-tropism have gained great popularity as a potential targeting motif [1, 2]. Although classical CNS delivery approaches target receptors, which are directly located on the endothelial cells of the blood-brain barrier (BBB) [3, 4], it is unknown, if drug delivery systems (DDS), which are functionalized with virus peptide sequences, follow this pathway [2]. An interesting fact is that for many viruses, entry into the CNS starts at the peripheral nervous system (PNS) [5]. By entering through the PNS, viruses benefit from the tremendously long nerve tracts which enable their transport from the periphery to the CNS via the spinal cord, circumventing the highly regulated BBB [2, 6]. Hitherto, the question of whether the uptake mechanism into the CNS of particles carrying only motifs of virus proteins is identical to that of the whole virus is still unanswered.

Especially short peptide sequences derived from virus proteins, which are responsible for the transport of the virus into the brain, are selected for the functionalization of DDS [7-9]. This functionalization causes significant deviations from the physicochemical properties of the original viral particle. The peptide sequences of the virus have to be modified to enable covalent linkage to the DDS. In addition, the DDS itself has certain characteristic physicochemical properties which could drastically change the uptake mechanism of the original sequence. To our surprise, the impact of physicochemical properties of virus-functionalized DDS on the targeting effect have been completely neglected so far.

One prominent strategy for virus-related CNS targeting is the use of rabies virus. Due to its known CNS-tropism [10], rabies virus peptide sequences have a widespread application for the modification of DDS (see table 1, 2). Although the targeted delivery to the CNS was proved by in vitro and in vivo analyses (see table 3), the uptake mechanisms and impact of physicochemical properties on the cellular uptake mechanism are not discussed. This is surprising since the pathway of the rabies virus is very well known and therefore well suited for the precise analysis of uptake patterns and transport mechanisms of virus-modified DDS.

The goal of this review is to elucidate the impact of physicochemical properties on the cellular uptake by comparing the properties of the virus with that of rabies virus glycoprotein modified DDS in the literature. We will start with a description of the fate of rabies virus on its way into CNS, including a detailed description of relevant receptors with regard to the cellular uptake mechanism. We will then review the different types of rabies virus glycoproteins available for DDS modification with a special emphasis on the design and the physicochemical properties of DDS. Finally, we will review in vitro and in vivo work with respect to cell uptake and brain

tropism. By doing so we intend to contribute to a better understanding of virus-related CNS targeting strategies.

1. Rabies virus – a role model for CNS-targeting?

1.1. Rabies virus

The reason for using rabies virus peptide sequences for CNS targeting strategies can be explained by the pathology of rabies virus infections, which is accompanied by neuroinvasion and neurotropism of viral particles [11]. The virus is bullet-shaped with a length of 180 nm and a diameter of 65 nm [12]. The virion is surrounded by a lipid layer, which carries the rabies virus external glycoprotein (RVG) [11]. RVG is organized as a trimer and covers the complete surface of the virus. RVG consists of 500 amino acids (aa) and has two major antigenic sites [11] and is responsible for cellular entry and virus fusion [10, 11, 13].Therefore, RVG is a prime candidate for use as a CNS-targeting motif.

1.2. Infection pathway of rabies virus into the CNS

In accordance with the uptake mechanism of most CNS-tropic viruses, the rabies virus uses axonal transport to reach the CNS [14] (Figure 1). The pathway of the rabies virus starts in the periphery with the infection of a dermal or muscular wound [2, 10]. The journey to the CNS starts directly at the neuromuscular junctions (NMJ) [9, 10, 15]. These are specialized synapses between muscles and motor neurons, responsible for the innervation of muscles. Published data suggests that the rabies virus follows an interesting pathway, entering the postsynaptic muscle membrane first and not the presynaptic neurons. In accordance with uptake mechanisms of other viruses, the first interaction with cell membranes could be mediated by electrostatic interactions with gangliosides, lipids and carbohydrates [10, 16-22]. The nicotinic acetylcholine receptor (nAchR) is responsible for the first entry into the muscle cells ❶. It is hypothesized that the initial entry into muscle cells is used for the multiplication of the rabies virus and, therefore, results in a more efficient infection of the neurons ❷ [10, 23]. After the infection of muscle cells with the rabies virus, the virus spreads from the muscle into the synapse ❸. The resulting approach enables the virus to have close contact with the cell membrane. The entry into motor neurons could again be mediated by electrostatic interactions (adsorptive-mediated) [10, 16-22] as well as the binding at specific receptors (receptor-mediated), which are located in the NMJ at the motor neurons ❸ [6]. Receptors, like neuronal cell adhesion molecule (NCAM) and low-affinity nerve growth factor (p75NTR), have been described as potential portals for rabies virus entry into the neuron.

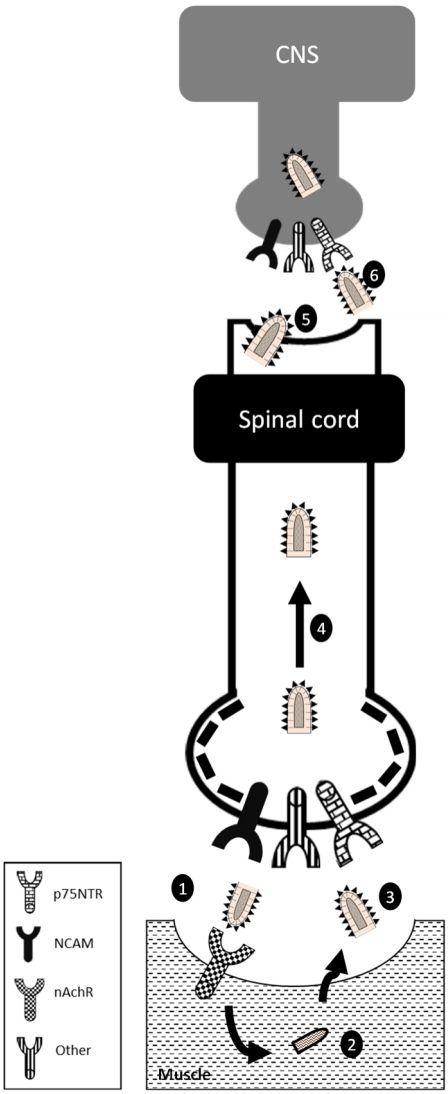

Figure 1 Scheme of the long axonal transport of rabies virus from the periphery to the CNS. The classical pathway suggests a prior infection of peripheral muscle cells ❶. After the binding of rabies virus to the acetylcholine receptor (nAchR), rabies virus enters the muscle cell and replicates ❷. From here, the rabies virus spreads into the neuromuscular junction (NMJ). The entry into neurons is achieved by electrostatic interactions (adsorptive-mediated) and receptor-mediated interactions ❸. The neuronal cell adhesion molecule (NCAM) and the neurotrophin (p75NTR) receptor are believed to open the portals for rabies virus into the nervous system ❸. Rabies virus travels in a retrograde manner to the cell body of the motorneurons ❹, which is located in the spinal cord. Hereby, it is hypothesized that either the whole virus or the capsid alone travels to the cell body. From here, the neurons are connected to the central nervous system (CNS). Rabies takes advantage of this network and moves from neuron to neuron ❺-❻ until it hits the CNS.

However, the fact that NCAM- and p75NTR-deficient mice could still be infected with rabies [21, 24] shows that the complexity of the entry mechanism of the virus is still not completely understood [25]. So far, the published data clearly reveals the involvement of nACH-, NCAM- and p75NT receptors in the pathogenesis of the rabies virus. However, the complete pathway is still unraveled, including the identification of all relevant receptors needed for the uptake. For example, it is of high interest to determine if the interaction with the presynaptic neurons is dependent on the preceding interaction with the nAchR, which is located at the postsynaptic muscle cell membrane and would have hence require a specific order of receptor interaction [25], or if rabies virus can directly enter the presynaptic neurons [23].

1.3. Rabies virus receptors

For a solid understanding of rabies virus receptor interactions, the following section provides a deep insight into the designated receptors, starting with their structure and their occurrence and then going into the potential receptor binding sites of the rabies virus.

The **nicotinic acetylcholine receptor** (**nAchR**) was the first receptor discovered to be responsible for the entry of rabies virus into CNS. Its involvement in the pathogenesis of rabies was first revealed after the intramuscular injection of mice with rabies virus. Virus antigen could be detected 1 hour after injection by immunofluorescence at the NMJ [22]. This observation directly reflected the pathogenesis of rabies and confirmed that the initial infection is transmitted by the bite of an animal [22]. Lentz et al. analyzed the binding of the rabies virus glycoprotein to the acetylcholine receptors by using the α-1-subunit [19]. The α-1-subunit receptor belongs to the class of muscle subunits (α1, ß1, δ, ε and ϒ), which is one of three major classes of nAchR subunits. Entry via the muscle subunit describes the classical pathway of rabies virus with an initial muscle infection in the periphery [23]. An interesting question is if other nAchRs could further play a role in the transport of rabies virus to the CNS by enabling the synaptic passage between neurons [5, 17]. nAchRs are widely distributed in the nervous system and could, therefore, serve as potential door-opener for a fast infection of the CNS. Furthermore, the interaction of rabies virus with the α-subunit could indicate that rabies is also able to interact with other nAchR subtypes. An important note is that the muscular subunit α1 as well as the neuronal subunit α7 can both be inhibited by the nAchR antagonist α-bungarotoxin [17]. Therefore, some authors assume that α7 is also able to interact with rabies virus and, therefore, might also play a role in the uptake of rabies virus into the CNS [17, 21]. Furthermore, the mammalian brain mostly contains the α4ß2 or α7 receptor subtypes. Thus, a deeper investigation of the α4ß2 or α7 is of high interest [17, 26].

After the observation that several lymphocyte cell lines could be infected with rabies virus strains, challenge virus standard (CVS) and Evelyn Rotnycki Abelseth (ERA) [27], M. Thoulouze et al. analyzed RV-susceptible and non-susceptible cell lines with regard of surface molecules, which could enable the uptake of rabies virus. They figured out that all RV-susceptible cell lines express two isoforms of the **neural cell adhesion molecule 140 and 180** (**NCAM-140 and 180**) on their surface. NCAM, also known as CD56, D2CAM, Leu19 or NKH-1, belongs to the immunoglobulin superfamily and is a cell adhesion molecule. Members of this family can be found on neurons, astrocytes, myoblasts, myotubes, activated T cells and NK cells [24]. Due to their expression on neurons and lymphocytes, other viruses such as

adeno-, coxsackie and herpes simplex virus use NCAM for entering the CNS as well [28]. Thoulouze et al. found that the recombinant expression of NCAM in NCAM negative cells enhanced their susceptibility to rabies virus, whereas blocking the NCAM receptor in NCAM positive cells using antibodies led to a decrease. In addition, the mortality of NCAM-deficient mice was compared to wild-type animals upon infection with the CVS strain of RV. A delayed mortality was noted for NCAM-deficient mice (mean length of survival 10 d for wild-type and 13.6 d for NCAM-deficient mice). The neutralization of RV infection by soluble NCAM, which was composed of the five immunoglobulin (Ig)-like domains and the two fibronectin domains, proved that the ectodomain is a potential binding site for rabies virus.

p75 neutrophin receptor (NTR) was identified as another relevant receptor for rabies virus binding. It was discovered by screening a neuroblastoma cell library for soluble RVG [29]. The neutrophin receptor, also known as low-affinity receptor for nerve growth factor, is a type I transmembrane protein of the tumor necrosis factor receptor family [17]. It is important during early neuronal development and in different pathological conditions, such as neurodegeneration and epilepsy [30]. In adults, its prevalence is limited to the peripheral and central nervous system. The ectodomain of the receptor consists of four cysteine-rich domains (CRD). In contrast to other members of the tumor necrosis factor family, its ligands are organized as dimers [29]. Different CRD mutants were used to analyze the interaction between RVG and p75NTR. These experiments revealed CRD1 is a RVG binding site, as the antigen bound to all mutants, except those who had a deleted CRD1. Gluska et al. analyzed the interaction of p75NTR and rabies virus with respect to the uptake into axons and tracked the transport machinery by live cell imaging [31]. EGFP-tagged rabies virus was applied to dorsal root ganglion (DRG) explants, which were cultured in a microfluidic system in presence of fluorescent antibody against p75NTR. They found that both, the rabies virus and p75NTR, were internalized together. In addition, rabies virus infection of p75NTR knockdown DRG cultures revealed lower infection rates, which emphasizes the role of p75NTR as rabies receptor. Furthemore, p75NTR dependent uptake causes a faster transport of rabies virus [31].

1.4. CNS entry

After the successful receptor binding on the motorneurons, the whole virus is endocytosed via clathrin-mediated uptake [32-34]. Next, the virus is transported to the cell bodies. This transport was described for the whole virion as well as for the capsid alone ❹ [10]. It has been reported that the rabies virus phosphoprotein, which is part of the rabies capsid, interacts with the dynein light chain LC8 [16, 35], this interaction requires the uncoating of the rabies virus after cell

entry. The acidic environment of the endosomal compartment leads to conformational changes of the rabies virus glycoprotein and causes the fusion of the virus with the endosomal membrane [16]. On the other hand, there is also evidence for the transport of the whole virion. It is based on the assumption that the external rabies virus glycoprotein is not only responsible for the entry into the cells, but is also a decisive factor for the long-distance transport across the axons (intra-neuronal transport) [36]. Rabies virus travels in a retrograde manner from the periphery to the cell body of the motorneuron ❺, which is located in the spinal cord. These cell bodies are in synaptic contact with motor centers in the brain [8, 15]. Thereafter, the chain-like connection of neurons via synaptic junctions allows the entry of rabies virus into the CNS ❺-❻. Therefore, the infection of rabies virus heavily relies on the ability of rabies virus to interact with receptors and cell membrane structures, enabling the synaptic passage and entry into the subsequent neuron [5]. The exact mechanism however, remains unclear [11].

2. RVG-Primary sequence and modification: from pathogenesis to use as CNS-targeting motif

The targeted journey of rabies virus from the periphery to the brain points directly to a key element of the virus which is responsible for its CNS- tropism, the external surface glycoprotein RVG. This glycoprotein contains short peptide sequences, which hold the relevant information for the receptor-interaction with the above-mentioned receptors. Nowadays, a key strategy in designing CNS-targeted DDS is functionalizing the DDS with such uptake-relevant short peptide sequences. Using this strategy will give us a better understanding of the pathogenesis of rabies and allow concomitantly the transport of such systems into the CNS. With the investigation of the receptor binding of RVG to the nAchR, Lentz et al. provided us with better understanding of significant structural elements within the primary sequence of RVG which are necessary for successful receptor binding. A second aspect of major interest has been the assessment of the physicochemical properties of the peptide sequences. As rabies virus takes advantage of the electrostatic interactions for binding to the host cell membranes, a description of physicochemical properties is important. An interesting fact, which is often neglected is that the functionalization of DDS requires the modification of virus peptide sequences to enable the linkage to the DDS. These modifications could impact the sensitivity of RVG to its receptors and its physicochemical properties. We will, therefore, shed some light on relevant peptide sequences, their physicochemical properties and the impact of RVG modifications on their functionality.

2.1. Receptor-binding studies of RVG

The interaction of RVG with the nAchR was somewhat anticipated due to the structure similarities of RVG to curare-mimetic snake venom toxins, which also bind with high affinity to the nAchR [37]. The sequence alignment of the primary sequences of the snake venom toxin Naja melanoleuca (the residues 1-71) and RVG (residues 151-237) revealed 26 matches [37]. Further Lentz et al. showed that different cholinergic antagonists, neurotoxin peptides and RVG peptides were able to inhibit the binding of nAchR-antagonist α-Bungarotoxin to the synthetic peptides of the α-subunit of the ray torpedo californica and human acetylcholine receptor (residues 173-204) [37]. The IC50-values for RVG and neurotoxin peptides were comparable to those of cholinergic agonists and antagonists. The rabies virus CVS strain residues 175-203 (CVS 29mer), a homologous segment of the RVG, was the most effective of the rabies glycoprotein peptides in inhibiting α-bungarotoxin ($1.2x10^{-6}$M and $2.5x10^{-6}$M) [37], showing its receptor binding capabilities to nAchR.

2.2. Physicochemical properties of RVG peptide

The physicochemical properties of RVG play an important role in the cell uptake behavior of the rabies virus. The peptide has a good water solubility with an isoelectric point at pH 9.7, causing a positive net charge under physiological conditions. The positive charge of RVG at pH 7.4 explains the adsorptive interaction of rabies virus in addition to the receptor-mediated uptake [17, 21, 22, 24]. Since heparan sulphate proteoglycans lead to a negative charge of the plasma membrane surface, the uptake of positively charged substances is believed to be driven by the electrostatic interactions[1, 38].

2.3. RVG-peptide modifications

For CNS targeted delivery, DDS have frequently been functionalized with RVG peptide. The anchoring of RVG on a DDS is one of the most critical steps during formulation. The functionalization requires modifications of RVG to enable covalent coupling or adsorption of the peptide to the DDS. The different modifications of the RVG peptide and resulting changes of physicochemical properties are explained in detail hereinafter. Table 1 lists the RVG derivatives that have been used to date.

Table 1: Peptide properties of RVG-29 peptide and its modifications estimated by peptide calculator of Innovagen.
Mod.=modification, N= number of residues, M_W= molecular weight, pI= isoelectric point, dR= D-arginine; RVG-29= rabies virus glycopetide 29mer; C= cysteine; G= glycine; R= Arginine; H= Histidine; GST= glutathione.

RVG peptide sequence+ Linker	Mod.	N	M_W [g/mol]	pI [pH]	Net charge at pH7	Ref.
RVG		29	3267	9.7	2	[39-42]
RVG+C	C-Terminal	30	3370	8.75	1.9	[3, 43-45]
RVG+GGGGC		34	3542	8.75	1.9	[46, 47]
RVG+GGGG9dR		41	4844	12.25	11	[48-53]
RVG+HHHH rRrRrRrRr		42	5221	12.25	11.3	[54]
Recombinant fusion protein GST-RVG29-9R-His		47	5666	12.25	11.5	[55]
RVG-Protamine		54	6458	12.17	14	[56]
RVG+9D/LR		41	4844	12.25	11	[57]
RVG+ Biotin		29	3267	9.7	2	[58, 59]

2.3.1 Addition of positively charged peptides

RVG peptides have frequently been conjugated to nucleic acids. In this strategy, the RVG peptide acts as a navigator, leading the complex to the CNS. Because nucleic acids carry a negative charge, they can be utilized to form electrostatic complexes with positively charged peptides.

Therefore, by adding positively charged residues to the RVG sequence, the resulting peptide forms complexes with nucleic acids. An example is the complex formed by attaching the cell-penetrating peptide (CPP) nona arginine to the C-terminal of the RVG peptide sequence [48, 49]. The addition of nona-arginine leads to an increase of the isoelectric point and a positive net charge. The construct is positively charged even at neutral pH values. Nucleic acids can be condensed and complexed by such molecules. A short sequence of glycine or histidine serves as a linker between RVG and nona-arginine, minimizing undesired interactions. The RVG part of the whole molecule is still available for the receptor-interaction [47-49, 51, 54, 55, 60]. The addition of the positively charged nonapeptide favors not only the adsorption of nucleic acids, but also facilitates the cell uptake of the DDS [57].

The increased uptake of nona-D-arginine RVG compared to nona-L-arginine RVG was shown by Zeller et al [57]. The use of racemic arginine led to a higher resistance against proteases and showed reduced toxicity [57, 61]. Therefore, racemic arginine is promising for the use as CPP for brain delivery.

Beside short oligonucleotides, Ye et al. aimed to formulate DNA-complexes with RVG. They used the protamine RVG instead of the nona-arginine peptide, as nona-arginine RVG was not able to bind their DNA [56].

2.3.2 Maleimide-thiol-coupling

Besides the modifications of RVG with positively charged peptides, further modifications by coupling RVG peptide directly to DDS were undertaken. One of the most well-known coupling reactions is the maleimide-thiol-coupling. Maleimides react with thiols to form stable thio-ether bonds [62]. One reason for the popularity of this coupling reaction is that peptides can easily be functionalized with cysteines to introduce a thiol group [63]. An interesting fact is that the original RVG sequence already contains a cysteine residue, which is located in the middle of the sequence and amenable for maleimide-thiol coupling [39, 40]. A coupling reaction with this native cysteine could, however, impact the binding affinity of the RVG peptide to the described receptors.

Evidence of the importance of this cysteine for the receptor binding was given by Lentz et al. The native cysteine belongs to the matches, which have been identified via the sequence alignment of the RVG sequence and the snake neurotoxin peptide sequence [37]. Therefore, this cysteine could be involved in the receptor binding. Further the results of Lentz et al. imply a reduced receptor interaction for RVG peptide sequences without cysteines in their primary sequence. A good example is the RVG peptide CVS-10 mer, which consists of the residues 190-199 of the CVS strain and contains no cysteine. Compared to the CVS-29, which contains a cysteine in the middle of the sequence, CVS-10 mer showed a decreased binding to synthetic peptides of the Torpedo and Human acetylcholine receptor α-subunit with IC_{50} values of $7.2x10^{-5}$M, compared to $1.2x10^{-6}$M for the CVS-29 mer [37]. To avoid such a loss of receptor affinity, one elegant approach is to modify the peptide with an additional cysteine on the C-terminal site [43-46, 64-66]. A disadvantage of this strategy is the risk of obtaining undesirable side products. Furthermore, if the central cysteine is not protected, the maleimide group is able to react with both cysteines. In addition, the presence of the two cysteines may facilitate disulfide-bond formation that decrease the number of free thiol-groups.

2.3.3 Biotin/streptavidin coupling

Chen et al. used biotin/streptavidin coupling for the attachment of RVG to albumin nanoparticles [59]. Streptavidin mediated the linkage between RVG by carrying an additional biotin on C-terminal, and the nanoparticles. Since the interaction between streptavidin and biotin is one of the strongest non-covalent interactions with a dissociation constant of $1.3x10^{-15}$M, it is very well suited as conjugation technique [67].

2.3.4 Control peptides

To verify the receptor-mediated uptake of RVG-functionalized DDS, a comparison of these delivery systems to negative controls is mandatory. In the literature two different examples, the RV-Matrix peptide and scrambled RVG, have been used. Their length and physicochemical properties are similar to that of the RVG peptide. However, they are supposed to have no CNS-targeting effect. While the RV-Matrix peptide was obtained from rabies matrix virus protein [48, 50-53, 56], the scrambled RVG peptide was synthesized by changing the amino acid sequence [49].

Table 2 gives detailed information of the published rabies virus glycopeptide (RVG-29) targeted drug-delivery-systems (DDS). By screening all DDS with regard to formulation type, RVG-29-modification and modification type, use of negative control and cargo, the table gives an overall view and comparison of the common DDS. Furthermore, the table provides information about the physicochemical characterization including conjugation yield, size, surface charge and stability analysis.
+ GGGG9dR= RVG-29 + glycine linker + nine arginine residues; +C= RVG-29 with additional cysteine on C-terminal; +GGGGC = RVG-29 + glycine linker with additional cysteine on C-terminal; +HHHHrRrRrRrRr= RVG-29 + histidine linker + nine arginine residues; AFM= Atomic force microscopy; Asp= Aspartate; BCA= bicinchoninic acid; BPEI= bioreducible polyethylenimine; CD= cyclodextrins; CPT= Camptothecin; DIR= 1,2′-Dioctadecyl-3,3,3′,3′-Tetrematheylindotricarbocyanine Iodide; DLS= Dynamic light scattering; DNA= desoxyribonucleic acid; DSPE= 1,2-Distearoyl-sn-glycero-3-phosphoethanolamine; DTT= Dithiothreitol; EDC= 1-Ethyl-3-(3-dimethylaminopropyl)carbodiimide; FBS= fetal bovine serum; FRET= Förster resonance energy transfer; Glu= Glutamate; GSH= gluthation; GTA= methoxy PEG and trimethylammonium groups; ITZ= Itraconazole; miRNA;= microRNA; mPEG-Mal= Monofunctional PEG Maleimide; n.t= not tested; N/P-ratio= nitrogen/phosphate ration; NC= nanocarrier;; NR= nanorod; NHS-PEG-Mal/ Mal-PEG-SCM= N-hydroxy-succinimid-polyethylene glycol-maleimide; NMR=Nuclear magnetic resonance NR= Niele red; PAH= polyasparthydrazide; PAM-ABP= poly(cystaminebisacrylamidediaminohexane) grafted with 9–11 residues of the amino acid arginine with a molecular weight of ~4.45 × 10 3 Da/mole; PAMAM= polyamidoamine; PBS= Phosphate buffered saline; PCR= polymerase chain reaction; pDNA= plasmid DNA;PEG= Polyethylenglycole; PLGA= poly (lactic-co-glycolic acid; RPMI=Roswell Park Memorial Institute RVG-Mat= RVG-Mat (MNLLRKIVKNRRDEDTQKSSPASAPLDDG); RV-Mat= rabies virus matrix protein; SCM-PEG-Mal- Maleimide PEG succinimidyl carboxymethyl; Scrambled RVG-(WESYRTRAIPKCSPGTDPMINPFTRGNGN); SDS-PAGE= sodium dodecyl sulfate polyacrylamide gel electrophoresis; siRNA= small interfering RNA; SMPT= 4-succinimidyloxycarbonyl-α-methyl-α-[2-pyridyldithio]toluene; SNALPs= stable nucleic acid lipid particles; SSPEI= disulfide crosslinked bioreducible polyethylenimine; TMC= trimethylated chitosan; w/o= without; w= with; wt= weight; wt= wild type.

No.		RVG peptide sequence	Neg. control	DDS	Cargo	Conjugation yield	Linker	Size	Surface charge	Agarose gel electrophoresis	Serum stability	Ref.
1	Electrostatic interaction	RVG	-	RVG-conjugated BPEI	pDNA	Fluorescence activity of tryptophan: RVG:BPEI-SH (molar ratio 1:11,8) GPC analysis	NHS-PEG5k-Mal	≥4 wt ratio size decreased to 200 nm	Neutral surface charge at ≥4	BPEI-SS-PEG-RVG was able to form polyelectrolyte complexes with pDNA at wt ratio of 0.75	Stable in 10% serum in RPMI at 37°C over 48h; Stable up to 50% serum RPMI in size and surface charge	[40]
2		RVG	-	RVG-conjugated SSPEI	miRNA	n.a	NHS-PEG5k-Mal	Polymer/miR-124a wt of 6.6 : 290.5 nm	6.6 wt ratio (polymer/miRNA) change to positively charged values	0.8-6.6 wt ratio (polymer/miRNA) form stable complexes	6.6 wt ratio polymer/miRNA complexes were incubated with 10 % FBS remained stable over 4 h	[39]
3		+C	-	RVG-peptide linked siRNA/TMC-PEG	siRNA	^{1}H-NMR→ 26% (by weight)of RVG-peptide linked to TMC-PEG	Mal-PEG-SCM	N/P-ratio from 96/1 to 12/1: 308±16 nm to 134±19 nm siRNA loading prior to RVG-linkage: 135±7 nm siRNA loading after RVG-linkage: 207± 2 nm	N/P-ratio from 96/1 to 12/1: 9.0±2.5 mV to 4.6±1.3 mV	Stable complexes formed at N/P ratio of ≥48/1 and ≥24/1	Incubation with 50% serum for 72 h	[43]
4		+GGGGC	-	PAM-ABP: poly (amido amine) PAMAM dendrimer grafted with 9-11 arginine residues	pDNA	Possible coupling products RVG linked C-terminal or with Glu and Asp residues 1,2 and 3 molecules of RVG conjugate with each PAM-ABP molecule at peptide:polyplex conjugation ratios of 2,4 and 8 → detection of thiol group by Ellman´s assay	EDC-NHS via Carboxy-group at Arginin-residues of PAM-ABP	Size decrease in dependence of carrier:DNA ratio (5→20) from 188±9 nm to 152±9 nm for the Bare-nanocarriers, other NC similar results in size decrease	Increase of surface charge in dependence of carrier:DNA ratio (5→20) from 11.4±1.8 mV to 21.1±3.8 mV	RVG-PAM-ABP (ratio 2:1) complete condensed at a 3-fold ratio of carrier:DNA, peptide:polymer ratios of 4:1 and 8:1	Environment-Sensitive DNA release: 5mM DTT (reducing agent) → 70% of DNA was released in 2 hours	[46]

No.		RVG peptide sequence	Neg. control	DDS	Cargo	Conjugation yield	Linker	Size	Surface charge	Agarose gel electrophoresis	Serum stability	Ref.
5	Electrostatic interaction	+C	-	Polyion complex RVG peptide tagged PEGylated polyaspart-hydrazide derivatives	siRNA	Fluorescence intensity of tryptophan: molar ratio of conjugate RVG to PEG 0.32:1	SCM-PEG-Mal	COOH-PEG-g-PAHy-GTA/siRNA (100:1): 221±9.35 nm RVG-PEG-g-PAHy-GTA/siRNA (100:1): 248±10.32 nm	COOH-PEG-g-PAHy-GTA/si RNA (100:1): 2.78±1.82 nm RVG-PEG-g-PAHy-GTA/siRNA (100:1): 9.81±3.74 nm	>50:1 COOH-PEG-g-PAHy-GTA/siRNA with PEG 1/3/5% were able to complex siRNA → 3% PEG micelles were chosen for further studies	50% FBS at 37°C siRNA was protected more than 24h	[44]
6		+C	-	PAMAM-PEG-RVG29/ DNA Nano-particles	Plasmid pEGFP-N2	NMR	NHS-PEG-Mal	150±16.7 nm	-	Complete encapsulation at ratio of 10:1 of PAMAM to DNA	-	[45]
7		+C	-	Dendigraft-Poly-Lysine-RVG29-FRET Nano-device		UV-absorbance	Sulfo-LC-SMPT	DLS: ~5 nm AFM:30 nm	-	-	Incubation in serum, GSH at 37°C, Activated caspase 3 at 37°C for 2 h	[3]
8		+C	-	Modified β-cyclodextrins: cationic amphiphilic CD and neutral PEGylated derivative		^{1}HNMR: estimated by number of maleimides in the intermediated species → 4 RVG peptides conjugate per cylcodextrin molecule	SMPT	Coformulation of CD1 with CD2 and RVG→ CD1:CD2:CD4 Increase in size >200 nm, PDI <0.4	Charge decrease from 35 – 20 mV	CD1:CD2:CD4 (molar ratio 1:1.5:0.5) complexed with siRNA mass ratio (1:10)	Aggregation in 50% OptiMEM of CD:siRNA (mass ratio 10) nanocomplexes → no size increase for complexes with higher molar content of CD2 Incubated with 50% FBS protection up to 24 h	[65]

No.		RVG peptide sequence	Neg. control	DDS	Cargo	Conjugation yield	Linker	Size	Surface charge	Agarose gel electrophoresis	Serum stability	Ref.
9	Electrostatic interaction	+GGGG9dR	RV-Mat	siRNA-RVG-9dR	siRNA	n.a	none	n.a	n.a	RVG-9dR was able to bind siRNA in dose dependent manner	stable over 8h in 50% FBS	[48]
10		+GGGG9dR	Scrambled RVG	siRNA-RVG-9dR	siRNA	n.a	none	n.a	n.a	n.a	n.a	[49]
11		+GGGG9dR	RV-Mat	Liposome-siRNA-peptide complexes	siRNA	n.a	none	siRNA:liposomes: RVG-9r (100:10/100/1000:1000 pmol → 178±20 nm	siRNA:liposomes: RVG-9r 100:10/100/1000:1000 pmol →6.25±0.75/9.78±0.98/ 19.89±4.46 mV (with increasing concentration of liposome)	n.a	Incubation with 90% mouse serum at 37°C → addition of 100 pmol prevent degradation for at least 4 hours	[52]
12		+GGGG9dR	RV-Mat	RVG9R-siRNA	siRNA	n.a	none	n.a	n.a	n.a	n.a	[51]

No.		RVG peptide sequence	Neg. control	DDS	Cargo	Conjugation yield	Linker	Size	Surface charge	Agarose gel electrophoresis	Serum stability	Ref.
13	Electrostatic interaction	GGGG+9dR	RV-Mat	n.a	n.a	n.a	none	n.a	n.a	n.a	n.a	[50]
14		+HHHH rRrRrRrRr	-	RVG-9rR/pDNA	pDNA	n.a	none	N/P ratio: ≥3 → 80 nm (Size of naked pDNA was 308±24 nm)	N/P ratio: ≥ 2 → 27 mV	Complete encapsulation of pDNA at N/P ratio: ≥3	Stability proved after Incubation with 10% serum for 20 min by gelelectrophoresis	[54]
15		Recombinant fusion protein GST-RVG29-9R-His	-	RVG29-9R-6His/pDNA	pDNA	SDS-PAGE	none	N/P ratio: ≥ 2 → 118-172 nm (Size of naked pDNA was 323 nm)	N/P ratio: ≥ 2 → 14.2 mV	Complete encapsulation at N/P ratio: ≥ 2, (shielding of surface charge with mPEG-Mal)	Stability proved after incubation with 10/30/50 and 90% mouse serum in 0.01M PBS for 4 and 8 h at 37°C	[55]
16		RVG-Protamine	RV-Mat	RVG-protamine-DNA complexes	pDNA	n.a	none	n.a	n.a	Complete binding at a w/w ratio DNA/RVG-Protamine of 1:10	n.a	[56]

No.		RVG peptide sequence	Neg. control	DDS	Cargo	Conjugation yield	Linker	Size	Surface charge	Agarose gel electrophoresis	Serum stability	Ref.
17		RVG+9D/LR	-	RVG-9DR-siRNA And RVG-9LR-siRNA	siRNA	n.a	none	RVG-9DR-siRNA: 208.6±20.4 nm RVG-9LR-siRNA=203.5±3.5 nm	RVG-9DR-siRNA: 24.2±0.3 mV RVG-9LR-siRNA=28.8±0.7 mV	Complete binding at Peptide-siRNA complexes (100 pmol; 10:1 peptide:siRNA)	Both complexes stable for at least 3 hours exposed to RNase A; after incubation with 50% human AB serum only RVG-9DR-siRNA complex remained stable over 24h in contrast to RVG-9LR-siRNA (3h)	[57]
18	Cysteine modifications	+GGGGC	-	RVG peptide conjugated pluronic-based nano-carrier w and w/o chitosan	β-Galact osidase	^{1}HNMR and Fluorescence intensity of tryptophan : 81% (1.8 wt% of the nanocarrier)	NHS-PEG-Mal (MW 2.1K)	Size was measured at 4/25/37°C: At 37°C <70 nm	At 25°C: Bare-NC: 2.1±1.3 mV Chito-NC: 12.8±2.4 mV RVG-Bare-NC:1.9±2.4 mV RVG-Chito-NC:11.3±0.6 mV	-	β-Galactosidase release: loaded nanocarrier in dialysis membrane (300 kDa) in PBS with 10%FBS 100 rpm at 37°C	[64]
19		+Biotin	-	PLGA nanoparticles	Campt o-thecin	-	Avidin-Biotin-Linkage	RVG-PLGA-DiR : 188 ± 44 nm RVG-PLGA-NR: 162 ± 64 nm RVG-PLGA-CPT: 204 ± 45 nm RVG-PLGA: 253 ± 69 nm	RVG-PLGA-DiR : 0.36± 1.76 mV RVG-PLGA-NR: -0.88± 2.98 mV RVG-PLGA-CPT: -2.50± 1.19 mV RVG-PLGA: -2.71± 1.33 mV	-	Incubation in PBS+ 2% Tween-80 at 37 °C	[58]
20		+GGGG9dr	RV-MAT-9r	SNALPs	siRNA	BCA Protein Assay: 12.2± 1.9 nmol RV-Mat-9r/µmol 15.8±0.2 nmol RVG-9r	DSPE-PEG-Mal	RV-Mat-9r liposomes : 190.0± 22.9 nm (PDI: <0.3) RVG-9r liposomes: 195.8± 4.5 nm (PDI: <0.2)	-	-	Incubation at 37°C in presence of RNase (0.01 or 0.1 mg/ml) or serum (10%FBS)	[53]

No.		RVG peptide sequence	Neg. control	DDS	Cargo	Conjugation yield	Linker	Size	Surface charge	Agarose gel electrophoresis	Serum stability	Ref.
21		+C	-	RVG peptide modulated liposomes	Protamine-condensed siRNA	-	DSPE-PEG-Mal	91±6 nm	-21.8±1.7 mV	n.a	n.a	[66]
22	Exosomes	RVG	-	RVG targeted exosomes	siRNA	-		n.a	n.a	n.a	n.a	[42]
23		RVG	-	RVG targeted exosomes	siRNA	Quantitative PCR	Lamp2b fused to RVG peptide	~80 nm	n.a	n.a	n.a	[41]
24	Biotinylated RVG	+Biotin	-	RVG29-anchored nanoparticle	Itra-conazole	n.a	Strept-avidin-biotin	RVG29-ITZ-NPs: 89.3 ± 1.9 nm	-33.1±0.9 mV	n.a	Drug release in 10% FBS	[59]

3. RVG-functionalized DDS

RVG was used as a CNS targeting motif in a wide variety of DDS. These DDS differ from each other in their different RVG peptide modifications, the type of DDS functionalization as well as the physicochemical properties of the resulting DDS. Table 2 gives a summary of the published RVG-functionalized DDS, providing detailed information on their formulation, design and characterization. The main characteristics of the materials with respect to composition and therapeutic potential will be discussed below.

3.1. Nucleic acid-RVG-polymer-complexes

RVG peptide was used for the non-viral delivery of genes to the CNS using cationic polymers for nucleic acid complexation. Complexes with nucleic acids are formed by electrostatic interactions of positively charged polymers and negatively charged nucleic acids, leading to the formation of so-called polyplexes. Disulfide branched polyethylenimine (PEI) [39, 40], trimethylated chitosan [43], poly(cystaminebisacrylamidediaminohexane) grafted with 9-11 residues of arginine (PAM-ABP) [46], polyasparthydrazide [44], polyamidoamine [45], poly-L-lysines [3] and β-modified cyclodextrins [65] have all been used as polycationic material for complexation with nucleic acids. The attachment of the peptide to the polymer was carried out via the use of heterobifunctional linkers such as N-hydroxy-succinimid-polyethylene glycol-maleimide (NHS-PEG-Mal) [39, 40, 44, 45, 43], (4-succinimidyloxycarbonyl-α-methyl-α-[2-pyridyldithio]toluene) (Sulfo-LC-SMPT) [3] or 3-(Maleimido)propionic acid N-succinimidyl ester [65]. Amine-reactive NHS ester enabled the coupling to the polymer, whereas a maleimide or pyridine-2-thione functionality was used for the covalent coupling of the RVG sequence. Besides the original RVG sequence [39, 40], RVG sequences with an additional cysteine [3, 43, 44, 65] have been used for the formation of nucleic acids-RVG-polymer-complexes. The impact of the use of the native cysteine for the coupling reaction has already been discussed above (see 2.3.1).

Another strategy was employed by Beloor et al., who used 1-Ethyl-3-(3-dimethylaminopropyl)carbodiimide (EDC)/NHS as coupling agent to activate the carboxy group of the C-terminal of RVG peptide and bind it to the arginine residues on a polymer [46]. However, it cannot be excluded that the free carboxy groups of glutamate and aspartate in the RVG sequence can react with the polymer as well. This could result in a variety of orientations of the RVG peptide that could directly impact the receptor binding affinity, as each type of reaction product results in a different presentation of RVG peptide to the receptor. Introducing PEG-chains as a spacer between DDS and RVG reactive groups is a frequently used option.

Furthermore, the PEGylation of DDS can increase their biocompatibility and extend their circulation time in the bloodstream [68]. The presentation of RVG peptide on the distal end of a PEG-chain might facilitate binding, in contrast to functionalized DDS without spacer. This was shown for antiHER2 antibody fragments (Fab´) targeted liposomes [69, 70].The quantitative analysis of the final amount of RVG peptide was estimated by different analytical approaches. Son et al. used the fluorescence of tryptophan in the RVG sequence and measured the increase in molecular weight of RVG-functionalized polymers by GPC analysis [40]. The successful coupling could also be shown by ^{1}H-NMR analysis by the disappearance of the maleimide peak. The amount of RVG was calculated by integrating the ^{1}H-NMR spectra [65, 43]. Another approach was the quantification of RVG by using Ellman´s assay to detect free thiol groups of the cysteine in the RVG sequence [40].

Polyplexes of nucleic acids and RVG-polymer were characterized by measuring size, surface charge and gel retardation which depends on the RVG-polymer to nucleic acid ratio. By increasing the electrostatic interactions between nucleic acid and polymer, the size of complexes decreased. Agarose gel electrophoresis was used to identify the required ratio of siRNA or DNA (P) to RVG-polymer conjugates (N) or to analyze serum stability of complexes.

3.2. Nucleic acids-RVG-9R/protamine-complexes

Similar to RVG-polymer-complexes, RVG-nona-arginine or protamine conjugates are formed by electrostatic interactions between positively charged poly-arginine or protamine sequences and negative charged nucleic acids. The described nona-arginine sequences consisted either of D-arginine [48, 51, 52, 57, 50], L-arginine [57] or alternating D-and L-arginine residues [54]. Ye et al. used protamine as complexing component [56]. The poly-arginine and - protamine conjugates can be directly synthesized without the use of additional linker chemistry and are added on the C-terminal of the RVG peptide. Similar to the polymer complexes, the formation was characterized by the analysis of size, surface charge and gel retardation. Again, the positive charge is a common property for all complexes.

3.3. RVG-functionalized nanoparticles

Nanoparticles have some advantages in comparison to polyplexes with respect to their stability. The encapsulation protects nucleic acids against degradation and PEGylated nanoparticles show prolonged blood circulation time [60, 64, 71].

In contrast to polyplexes, functionalization with RVG takes place after the formulation of nanoparticles. The use of chitosan-conjugated pluronic-based micelles as transport system with the additional RVG-peptide modification, enabling receptor-mediated uptake is one example

of RVG-functionalized nanoparticles [64, 72]. To form these micelles, RVG peptide was conjugated at the C-terminal to a NHS-PEG-Mal linker on the polymeric micelle. The conjugation yield was estimated by ^{1}H-NMR analysis and the fluorescence of tryptophan in the RVG peptide sequence. The sizes of the different polymeric micelles were determined at different temperatures to show the thermosensitive effect of the pluronic. Surface charge was analyzed at 25°C and showed the impact of chitosan-modification of the polymeric micelles. Bare polymeric micelles had neutral charge and showed no change in surface charge after RVG modification and encapsulation with β-Galactosidase. However, the additional modification with chitosan caused a shift to positive values of the polymeric micelles (~12 mV). β-Galactosidase release was estimated in 10% FBS at 37°C. RVG peptides were presented on the distal end of PEG-chains with free N-terminals. The additional modification of chitosan allowed the binding via receptor and electrostatic interactions.

Cook et al. encapsulated camptothecin in RVG-functionalized PLGA particles. Functionalization was achieved by an avidin-biotin-linkage, presenting RVG-peptide with a free N-terminal [58]. Besides nanoparticles, RVG-functionalized liposomal formulations are described as well. Tao et al. presented RVG-functionalized liposomes as a DDS for the delivery of siRNA. The liposomes were composed of 1,2-dioctadecanoyl-sn-glycero-3-phosphoethanolamine (DSPE), cholesterol (CHO) and 1,2-distearoyl-sn-glycero-3-phosphoethanolamine-N-[maleimide(polyethylene glycol)-2000] (DSPE-PEG-2000-Mal) [66]. Due to the thiol-reactivity of the maleimide group, coupling reactions could take place either with the cysteine located in the middle or on the C-terminal of the RVG peptide.

Furthermore, liposomes containing positively charged phospholipids were used for the delivery of nucleic acids. They are also referred to as stable nucleic acid lipid particles [53]. Conceicão et al. used 1,2-dioleoyl-3-dimethylammonium-propane (DODAP) as the positively charged lipid in their formulation. The liposomes were further functionalized with RVG-nona-arginine, conjugated by the reaction of DSPE-PEG-2000-Mal with the cysteine located in the middle of the RVG sequence. Another interesting approach was shown by Pulford et al. This group encapsulated siRNA-RVG-nona-arginine complexes into positively charged liposomes to enhance the stability of the siRNA complex [52]. In contrast to the other DDS, in this study, the RVG-peptide was not present on the outer surface of DDS, but rather hidden by a positively charged lipid bilayer of liposome.

3.4. RVG-functionalized exosomes

Exosomes are natural nano-vesicles which are secreted by numerous cell types [42, 41, 73]. Because of this, they are an excellent DDS, mimicking natural cell vesicles [74]. Due to their cell-like membrane structure, exosomes are less likely to elicit a foreign body response, thus causing less adverse effects [74]. In the literature, two exosome formulations were presented as promising BBB-targeted DDS for gene delivery [41, 42]. In these studies, researchers used self-derived dendritic cells for exosome production. An advantage of exosomes is that they contain a number of membrane proteins, which are exclusively expressed on the exosomal surface [75]. Lamp2b is one such exosomal membrane protein, which can be used to functionalize exosomes, by fusing the RVG peptide to the extra-exosomal N terminus [41, 42]. The RVG-Lamb2b functionalized exosomes were analyzed with regard to their size using nanoparticle tracking analysis and electron microscopy. The successful expression of RVG Lamp2b was assessed with quantitative PCR. Loading of exosomes was achieved with electroporation [41, 42].

Table 3: Summary of the performed in vitro experiments of RVG-functionalized DDS. The table gives an overview of the cellular uptake studies of the RVG-modified DDS. Each DDS is listed along with its physicochemical properties, the used cargos and cells as well as the studies performed on the cellular uptake.

No.	DDS	Cargo	Cell line	Physicochemical characterization	Cellular uptake	Ref.
1	RVG-conjugated BPEI	Firefly luciferase coding sequence region in pcDNA3.1 (+) vector	Neuro2a (nAchR-positive) HeLa (nAchR -negative)	RVG: unmodified sequence Size: ~200nm Charge: 0	**Confocal microscopy**: Higher extent of uptake of polyplexes and gene expression in Neuro2a cells than in HeLa **Competitive inhibition assay:** Free RVG peptide was able to compete the uptake of BPEI-SS-PEG-RVG/pDNA (6.4 fold decrease of gene expression) Negative control: BPEI-SS-PEG/pDNA polyplex	[40]
2	RVG-conjugated BPEI	Cy5.5-labeled miR-124a oligomer CMV promoter driven Gaussia luciferase vector	Neuro2a (nAchR-positive) HeLa (nAchR –negative)	RVG: unmodified sequence Size: 290.5nm (Polymer/miR.124a wt of 6.6) Charge:+	**Fluorescence intensity:** 3-fold higher fluorescence activity in Neuro2a compared to HeLa **Detection of miR-124a release from RVG-SSPEI/miR-124a-complex:** Decrease of gaussialuciferase activity compared to Negative control: RVG-SSPEI +scrambled miRNA	[39]
3	RVG-peptide linked siRNA/TMC-PEG	PPIL2 siRNA Carboxyfluorescein-labeled siRNA	Neuro2a (nAchR-positive) HeLa (nAchR-negative)	RVG: +C Size: siRNA/TMC-PEG-RVG :~ 200nm Charge: +	**FACS:** Increase of MFI 1.6-1.8 fold compared to unmodified complexes in Neuro2a, but not in HeLa Negative control: siRNA/TMC-mPEG complexes **CLSM:** Uptake of modified complexes **In vitro gene silencing:** Expression of BACE1 was 57% for unmodified complexes and 50% for RVG-modified complexes	[43]
5	Polyion complex RVG peptide tagged PEGylated polyaspart-hydrazide derivatives	PPIL2 siRNA Negative control siRNA FAM-labeled siRNA Cy5-labeled siRNA	Neuro2a (nAchR-positive) HeLa (nAchR-negative)	RVG: +C Size: RVG-modified micelles: ~ 250nm Charge: +	**FACS/CLSM:** Cellular uptake of RVG-modified micelles significantly higher in Neuro2a compared to HeLa Negative control: COOH-PEG-g-PAHy-GTA/FAM-siRNA micelles **In vitro gene silencing:** Reduced expression of BACE1 detected by Western Plot analysis	[44]

No.	DDS	Cargo	Cell line	Physicochemical characterization	Cellular uptake	Ref.
6	PAMAM-PEG-RVG29/DNA	pEGFP-N2 and pGL2-control vector	BCECs	RVG: +C Size: ~150nm Charge: n.a	**Cellular uptake by fluorescent microscopy:** Cellular uptake of PAMAM-PEG-RVG29 Negative control: PAMAM-PEG/DNA **Cell uptake mechanism:** ➔ Receptor-mediated uptake was reduced at 4°C ➔ Receptor-mediated uptake could be competitive inhibited by free RVG peptide ➔ Incubation with acetylcholine, mecanylamine and nicotine had little influence on the uptake ➔ The cellular uptake was reduced after the incubation with free GABA ➔ Receptor-mediated uptake was reduced by the endocytotic pathway inhibitor filipin, **Transport studies** Papp of PAMAM-PEG-RVG29/DNA NPs was higher compared to PAMAM/DNA NPs	[45]
7	Dendigraft-polylysine-RVG29-FRET	Cy5 labeled nine amino acid pepitde	SH-SY5Y	RVG: +C Size: ~5nm Charge: n.a	**In vitro caspase-3 activation model**: RVG-modified nanodevice was able to detect caspase-3-activity	[39]

No.	DDS	Cargo	Cell line	Physicochemical characterization	Cellular uptake	Ref.
8	RVG-Modified β-Cyclodextrins	Fluorescein-tagged siRNA GAPDH siRNA	U87 HeLa	RVG: +C Size: RVG-modified cyclodextrin formulation (R3): ~250 nm Charge: +	**Cellular uptake in U87:** Negative control: free siRNA, cationic CD siRNA complex, PEGylated CD Control: Lipofectamine + siRNA RVG-tagged PEGylated cyclodextrin co-formulation R3 showed the highest uptake in comparison to untargeted co-formulations **Competitive inhibition assay:** Preincubation with RVG results in significant decrease in uptake of targeted co-formulations in U87 cells, no effect in HeLa cells **GAPDH knockdown analysis:** Negative control: naked siRNA, cationic cyclodextrin w/o siRNA Positive control: Lipofectamine+siRNA Cationic cyclodextrin siRNA nanocomplex: 80% reduction Cationic cyclodextrin w/o siRNA : No effect PEGylated cyclodextrin : No significant knockdown RVG-tagged PEGylated cyclodextrrin siRNA nanocomplex: 27% reduction	[65]
9	siRNA-RVG-9dR	Biotinylated RVG or RVG-Mat Anti GFP siRNA	Neuro2a (nAchR-positive) BHK21 292T HeLa CHO (nAchR-negative)	RVG: GGGG+9dR Size: n.a Charge: n.a	**Cellular uptake of RVG-peptide:** Uptake of RVG instead of RVG-Mat in Neuro2a Uptake of RVG in Neuro2a (nAchR positive) No uptake in non-neuronal cell lines Competitive inhibition of RVG by α-bungarotoxin in dose-dependent manner **Cellular uptake of RVG-9R/siRNA complexes:** Uptake of FITC-siRNA/RVG-9R complexes in a dose-dependent manner in contrast to RV-Mat-9R/siRNA complexes Positive control: Lipofectamine **GFP-silencing:** Lipofectamine and RVG-9R/siRNA complexes were able to decrease GFP-expression	[48]

No.	DDS	Cargo	Cell line	Physicochemical characterization	Cellular uptake	Ref.
10	siRNA-RVG-9dR	FITC-siRNA	Raw 264.7 N9 Primary splenic macrophages of wild type and AchR knockout mice	RVG: GGGG+9dR Size: n.a Charge: n.a	**nAchR-expression:** Expression of nAchR on Raw 264.7, N9 and primary macrophages of wild type but not of knockout mice **Cellular uptake of RVG-FITC on primary macrophages:** Negative control: scrambled RVG-FITC RVG-FITC but not negative control showed uptake in primary macrophages of wild type mice No uptake of FITC-RVG in primary macrophages of nAchR knockout mice **Cellular uptake of RVG-9dR/FITC-siRNA complexes:** RVG-9dR complexes transduced 90% of FITC-siRNA inN9 cells and 65% in Raw 264.7 cells RVG-9dR complexes were able to transduce siRNA into primary macrophages of wild type mice, but not into nAchR-knockout mice **Gene silencing in Raw 264.7 cells:** 70% reduction of GFP expression	[49]
11	Liposome-siRNA-peptide complexes	PRP (cellular prion protein) siRNA	Neuro2a (nAchR-positive) HEK293 HeLa 4T1 (nAchR-negative)	RVG: GGGG+9dR Size: ~180 nm Charge: +	**Uptake to Neuro2a (MFI):** PRP-siRNA/RVM-9r w/o liposome: no uptake PRP-siRNA/RVM-9r w liposome: 15% PRP siRNA-RVG-9r w/o liposome: 8% PRP siRNA-RVG-9r with liposome: 85% **Competitive inhibition of RVG-9r with liposome in Neuro2a:** Excess of unlabeled RVG-9r or RVM-9r **Cell specificity (MFI):** PRP-siRNA/RVG-9r with liposome: Neuro2a: 90+5% HEK292: 67+7% 4T1 and HeLa:<5% **PrP siRNA-RVG-9r LSPC suppress expression:** PrP-siRNA/RVG-9r w liposome: 30+8% PrP-siRNA/RVM-9r w liposome:99+3% RVG-9r-control w liposome:98+2% Liposome alone: 99+2%	[52]

No.	DDS	Cargo	Cell line	Physicochemical characterization	Cellular uptake	Ref.
12	RVG9R-p137	p137-RVG9r	SH-SY5Y HEK293 U373	RVG: GGGG+9dR Size: n.a Charge: n.a	**α3/α5nAchR-expression in SH-SY5Y, HEK293, U373:** Expression of α3/α5nAchR subunits in SH-SY5Y and U373 cells **Cellular uptake in α3/α5nAchR –positive U373 cell line** Negative control: naked siRNA, RVMat9R-p137 and RVG9R-pXef Cellular uptake of RVG9R-p137 complexes in contrast to negative control **Protection of SH-SY5Y from rotenone-induced cell death:** Negative control: RVG9R- scrambled p137, RVMat9R-p137 Reduced cell death after incubation with RVG9R-p137-complexes	[51]
14	RVG-9rR/pDNA	pEGFP	Neuro2a (nAchR-positive) HeLa (nAchR-negative)	RVG: HHHHrRrRrRrRr Size: ~80 nm Charge: +	**Cellular uptake of RVG29-9rR/pDNA in Neuro2a:** RVG29-9rR/pEGFP-N1 Negative control: 9rR/pEGFP-N1, naked plasmid Uptake of RVG29-9rR/pEGFP-N1 in Neuro2a in contrast to negative control No uptake in HeLa cells Inhibition of endocytosis at 4°C Internalization indicated by LysoTracker **Luciferase expression assay:** Positive control: Lipofectamine RVG29-9rR delivered pEGFP in Neuro2a but not HeLa Highest DNA efficiency at N/P ratio >3 in Neuro2A cells (55.9%) Higher transfection efficiency compared to positive control	[54]
15	RVG29-9R-6His/PDNA	pRNAT-U6.3/Hygro encoding green fluorescent protein	Neuro2a (nAchR-postive) HeLa BV-2 BHK-21 (nAch-negative)	RVG: +9R-6His Size: <200 nm Charge: +	**Neuro2a cells-based ELISA:** Detection by anti-His antibodies → Uptake of RVG29-9R-His/pDNA was only detectable by Neuro2a cells but not HeLA cells **Specificity of cell recognition:** Positive control: Lipofectamine (33% in Neuro2a) Complex was only taken up by Neuro2a cells Transfection efficiency [%]: 28% Neuro2a, 0.9% in BV-2, 3.3% in HeLa and 3.3% in BHK-21	[55]

No.	DDS	Cargo	Cell line	Physicochemical characterization	Cellular uptake	Ref.
17	RVG+9D/LR-siRNA	GFP	Neuro2a (nAchR-postive)	RVG: +9R Size: ~200 nm Charge: +	**Cellular uptake :** Uptake of 9DR/LR (higher uptake of 9DR after 24h) 9DR-GFP higher uptake compared to 9LR-GFP RVG-9DR/LR-siRNA complexes showed enhanced uptake in Neuro2a cells **Gene silencing (Increase of GFP-negative cells %):** Positive control: Lipofectamine Negative control: 9DR/LR-siRNA RVG-9LR-siRNA: 69.8 ± 2.7% RVG-9DR-siRNA: 42.1 ± 23.4% Lipofectamine : 46.6 ± 19%, **Cellular trafficking:** Detailed information please refer to reference	[57]
20	Brain targeted SNALPS	Si-EGFP FAM labeled siRNA siMutAtax3	Neuro2a (nAchR-positive) HT-22 HeLa (nAchR-negative)	RVG: GGGG+9R Size: < 200 nm Charge: n.a	**Cellular uptake:** Negative control: Non-targeted SNALPs, RV-MAT-9R targeted liposomes Increase in uptake of RVG-9R targeted liposomes in Neuro2a and HT-22 cell line, but not in HeLa **siRNA delivery in Neuro2a cells:** Uptake indicated of RVG-9R targeted liposomes encapsulated FAM-labeled siRNA **Uptake inhibition:** Uptake was reduced at 4°C and inhibited by free RVG peptide **Gene silencing:** RVG-9R targeted liposomes encapsulated siMutAtax3 decreased mutant ataxin-3 levels	[53]
21	RVG-peptide modulated liposomes	FAM-labeled siRNA EGFP-siRNA+Protamine	BMM U87	RVG: +C Size: ~90 nm Charge: -	**Cellular uptake in BMM cells:** Increase of uptake of RVG-liposomes and RVG-liposomes containing siRNA **GFP expression silencing:** Negative control: naked GFP-siRNA, RVG-liposome Common liposome, CRGD and RVG modified liposomes encapsulated with GFP-siRNA showed similar reduction in GFP expression (~ 20%)	[66]

No.	DDS	Cargo	Cell line	Physicochemical characterization	Cellular uptake	Ref.
22	RVG targeted exosomes	siRNA alpha-synuclein	SH-SY5Y	RVG: unmodified sequence Size:n.a Charge:n.a	**Gene silencing:** Positive control: Hiperfect transfection reagent RVG exosomes showed higher efficiency than positive control	[42]
23		GAPDH siRNA BACE1 siRNA	C2C12 (muscle) Neuro2a	RVG: unmodified sequence Size: ~80 nm Charge: n.a	**Gene silencing:** Positive control: Lipofectamine Negative control: naked siRNA, unmodified exosomes GAPDH silencing could be achieved by RVG modified exosomes in Neuro2a cells but not in C2C12 BACE1 silencing was dose dependent for RVG modified exosomes and could be inhibited by α- bungarotoxin	[41]
24	RVG29 anchored nanoparticle	Itraconazole	bEND3		**Cellular uptake on bEND3:** FITC-RVG29-ITZ-NP: 52.15 ± 3.41 FITC-ITZ-NP: 22.62 ± 2.51	[59]

4. In vitro testing of RVG-functionalized DDS

In vitro testing of RVG-functionalized DDS should give us an answer of whether or not the functionalization with RVG enables a targeted delivery into the brain. By using RVG as a CNS targeting peptide, the functionalized DDS should follow the pathway of rabies virus. Therefore, the cells lines and in vitro experimental designs used should reflect the pathway of the rabies virus. The uptake mechanism of rabies virus was described as a combination of receptor- and adsorptive-mediated uptake. According to the classical pathway of the rabies virus, especially muscle cells and neurons are of utmost relevance, and could be therefore, used for the in vitro testing of RVG-functionalized DDS.

4.1. Interaction of RVG-functionalized particles with primary cells and cell lines

The in-vitro effect of RVG-functionalized DDS on cells was investigated in several studies (Table 3). Figure 2 gives an overview of the used cell lines, including their origin and receptor expression. The uptake of RVG-functionalized DDS by neuronal cell lines, such as Neuro2a expressing nAchR (nAchR-positive), versus to non-neuronal cell lines, like HeLa, BHK-21, 292T, CHO, HEK293, 4T1, BV-2 and C2C12 which do not express nACH-receptors (nAchR-negative) [24, 39-41, 43, 44, 48, 52-55, 57], was investigated by a number of groups. Neuro2a cells are derived from mouse neuroblastoma. An important question is the involvement of the neuronal nAchR subunits. According to the classical pathway of rabies, only the interaction of RVG with the nAchR subunit α 1, which is typically expressed in muscles cells, has been described. The uptake of RVG-functionalized DDS in Neuro2a cells allowed researchers to draw conclusions about the receptors relevant for the uptake of the rabies virus and RVG-functionalized DDS, as Neuro2a cells express several neuronal nAchR subunits as well as NCAM and p75NT receptors. Therefore, this cell line is ideal for the investigation of the cell uptake of RVG-functionalized DDS by receptor-mediated effects [24, 76].

Although the rabies virus does not belong to the group of viruses which enter the CNS via the BBB [5, 10, 11, 77], the uptake of RVG-functionalized nanoparticles was also assessed using brain capillary endothelial cells (BCECs) [45] and the mouse brain endothelial cell line bEnd.3 [59]. The uptake of RVG-functionalized nanoparticles in these cell lines shed new light on the uptake characteristics of RVG-functionalized DDS. These studies revealed RVG-functionalized DDS also target non-neuronal cells at the BBB. The bEnd.3 is an immortalized mouse endothelial cell line, which expresses several typical BBB transporters and receptors, like glucose- and l amino acid transporters and the p-glykoprotein receptors as well as important tight junctions proteins [78]. Due to its BBB functionality, this cell line is widely used for

testing interaction of DDS with the BBB [4, 66, 79]. The observed uptake of RVG-functionalized DDS in these cells could be a result of the involvement of further unknown rabies receptors, but could also be due to electrostatic interactions between the RVG-functionalized DDS and the endothelial cell membrane. Further experiments are required to create a complete picture of the pathway of RVG-functionalized DDS.

The in vitro testing on human glioblastoma cell line U87 aimed at the application of RVG-functionalized DDS for the treatment of cancer [51, 65, 66]. The use of the SH-SY5Y cell line directly addresses the application of RVG-functionalized DDS in parkinson disease [3, 42, 51, 80]. The SH-SY5Y is a neuronal tumour cell line [81]. Interestingly, it expresses several neuronal nAchR subunits, the α3, α5, β2 and β4 as well as the α7-subunit [51, 82, 83]. The α7-subunit is the prime candidate for the receptor-binding of RVG-functionalized DDS among the nAchR subunits. Like the α1-subunit, which was used for the receptor-binding studies of RVG, the α7-subunit is also able to bind the antagonist α-bungarotoxin. This fact demonstrates structural similarities between the two subunits, which might also enable the binding of rabies virus and RVG-functionalized DDS on the neuronal α7-subunit. With regard to pathological conditions of the brain, microglia cells play an important role as immune barrier [1, 4, 49]. Expressing the α7 subunit of nACHR on their surface, Kim et al. investigated the RVG targeting effect on macrophages (Raw 264.7), the glial cell line (N9) as well as primary macrophages, which were obtained from wild type mice [49]. The group used the wild-type primary macrophages to assess the binding of the RVG peptide. The results assume that the FITC-labeled RVG was also able to bind at the primary macrophages via the α7 subunit [49].

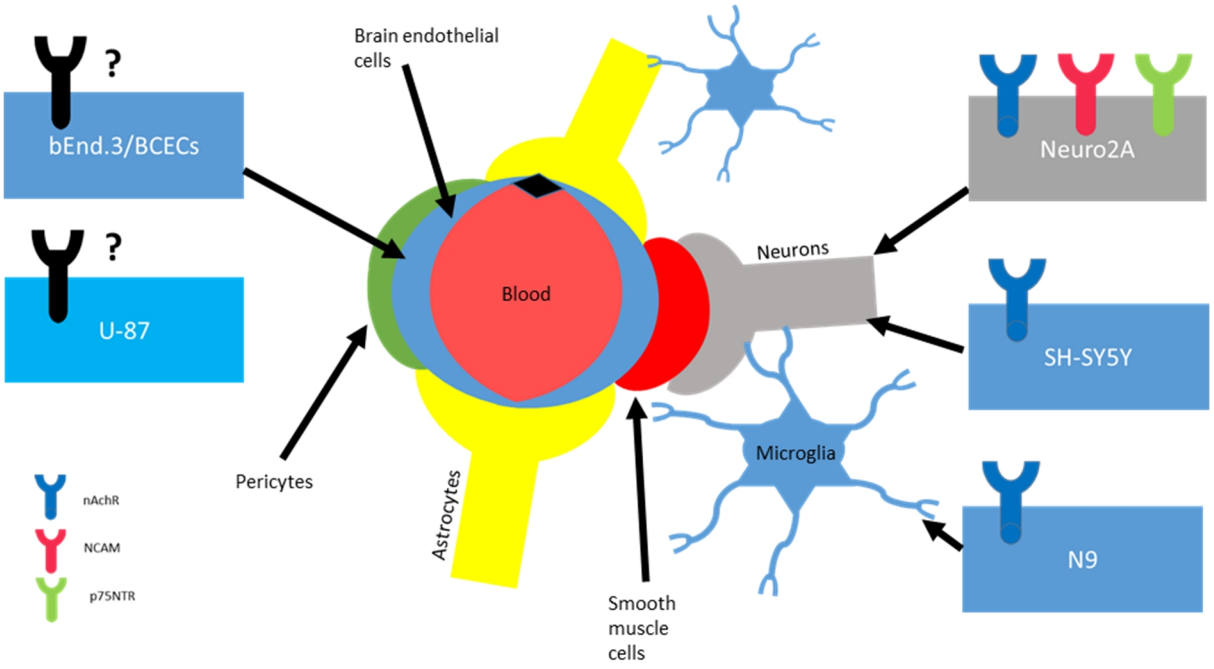

Figure 2: Overview of the cells used for the in vitro testing of RVG functionalized DDS, including their location and their receptor expression. Neuronal cell lines directly mirror the classical pathway of rabies virus along the axonal nervous system. This includes neuronal cells like the Neuro2a and the SH-SY5Y cell lines, which are said to express several identified rabies receptors, like nAcHR, NCAM and p75NTR. Microglia cells, like N9, play a role in the immune response of the brain and are also expressed with nAchRs. The use of brain endothelial cells directly target a potential uptake of RVG functionalized DDS across the blood brain barrier (BBB). The mouse endothelial cell line bEnd.3 and brain capillary endothelial cells (BCECs) have been used. In contrast to the nAchR-expressing cells, no rabies virus receptors have been identified. This is the same for the glioblastoma cell line U-87, which shows the application of RVG-functionalized DDS in the field of cancer therapy.

4.2. Receptor-mediated uptake

The first step of the analysis of RVG-functionalized DDS should be the proofing selective uptake of the targeting peptide RVG itself. This was impressively shown by the work of Kumar et al., who proved the selective uptake of biotinylated RVG peptide compared to the RV-Mat peptide, which was used as negative control, on Neuro2a cells [48]. The preliminary investigation of the uptake of RVG peptide alone was also performed by Kim et al. They showed that FITC-labeled RVG peptide was taken up by primary macrophages of wild type mice. In contrast, primary macrophages of nAchR-knockout mice showed no uptake of RVG-peptide [49].

The mechanism of receptor-mediated uptake of the RVG-functionalized DDS was analyzed by cellular uptake studies conducted at 4°C compared to 37°C [45, 54] or by the competitive inhibition with free RVG peptide [40, 48, 52, 65], agonists or antagonists. This was, for instance, shown by Liu et al, who analyzed the cellular uptake of RVG-functionalized nanoparticles BCECs. The results suggested a receptor-mediated uptake via the GABA receptor, which was indicated by a reduced uptake after the pre-incubation with free GABA. The prior incubation with potential inhibitors of the nACHR (acetylcholine, mecanylamine and

nicotine) caused no reduced uptake of RVG-functionalized nanoparticles [45]. The suggested pathway is of high interest and the involvement of GABA in the pathogenesis of rabies was not described. Further investigations are required.

In addition to the inhibition studies, BCECs were incubated with different endocytosis inhibitors to investigate the endocytosis mechanism. Furthermore, the nACHR-receptor-specificity for Neuro2a was proved by the reduced uptake of RVG-peptide after the incubation with α-bungarotoxin [48, 41].

4.3. Do RVG-functionalized DDS follow the classical rabies virus pathway?

The analysis of RVG-functionalized DDS brought new insights. The higher uptake of RVG-functionalized DDS in neuronal cells compared to non-neuronal cells clearly revealed an uptake mechanism that is similar to that of rabies virus. However, it is questionable whether RVG-functionalized DDS enter the CNS via the long axonal transport system like the rabies virus. The fact that RVG-functionalized DDS also showed cellular uptake in brain endothelial cells, suggests that the uptake mechanism of these DDS differs from that of rabies virus. Two major aspects have to be taken into account. First the presentation of RVG peptide on the surface on DDS and, second the overall surface net charge. The orientation of RVG molecule on the surface is highly dependent on the type of DDS and the selection of the RVG modification. To our surprise, the presented data revealed that the different ways of RVG orientation on DDS surface had no impact on the cellular uptake. Therefore, it is arguable that RVG-functionalized DDS are endocytosed via highly selective receptor interactions. The results of Lentz et al. clearly showed that the receptor binding affinity at the α-1-subunit depends on the primary sequence of the RVG peptide [22]. These facts emphasize an uptake of RVG-functionalized DDS, which is mediated via the electrostatic and hydrophobic interactions between the RVG-peptide coupled onto the surface of the DDS and cell membranes [17]. The complete picture of the uptake of RVG-functionalized DDS can only be given by a precise analysis of receptor interactions.

5. In vivo

The question of whether the RVG-functionalized DDS are actually up taken into the CNS is finally answered by the in vivo analysis of RVG-functionalized DDS and was shown for most of the presented DDS. The targeted uptake into CNS was shown for RVG-functionalized DDS and compared to the uptake of the used cargo of the DDS [54], the unmodified DDS [39, 40, 43, 44, 66] or the used DDS functionalized with scrambled versions of RVG instead of the CNS-leading RVG sequence [48, 52]. Besides the proof of CNS targeting by using fluorescent cargos, active cargoes were used to detect luciferase activity [45, 54] , caspase-3 activation [3], or the expression or silencing of genes [41, 42, 48, 52]. As the performed in vivo experiments mainly focused on the final delivery of the RVG-functionalized DDS into the brain rather than showing the complex fate of RVG-functionalized DDS to its final destination, the in vivo experiments are not discussed in detail.

While Kumar et al. were one of the first to show the potential of RVG as CNS targeting motif, the group of Cook argued the CNS targeting potential of RVG. Kumar et al. showed that mice infected with japanese-encephalitis virus (JEV) could be treated with the antiviral siRNA/RVG-9R complex (80% of survival). In contrast, mice treated with siRNA alone, luciferase siRNA, or siRNA complexed with RV-MAT-9R died within 10 days. The results of Cook et al. challenged the CNS targeting potential of RVG [58]. They quantified the delivery of the fluorescence marker DiR, encapsulated in RVG functionalized or biotin-functionalized nanoparticles, to the specific CNS regions. These results suggested only minimal evidence of a targeted uptake via the spinal cord into the CNS. A higher uptake of RVG-functionalized nanoparticles was only shown in the cortex region. This observation led to the assumption of the participation of $GABA_B$ receptors in the entry mechanism of rabies virus, as these receptors are mainly located in this region. Cook et al. further referred to the results of Liu et al., who showed that the uptake of RVG-functionalized nanoparticles was inhibited by GABA in brain endothelial cells [45]. This is an interesting hint as the GABA receptor is not described as a rabies receptor and should, therefore, be taken into account for a deeper analysis of receptor participation.

6. Summary and conclusion

Rabies virus carries a decisive factor for the entry into the CNS, controlled by the external surface glycoprotein RVG. Although the complete infection pathway of the rabies virus is still not understood, nAchR, NCAM-1, p75NTR as well as the interaction with carbohydrates, gangliosides and lipids hold a stake in its entry into CNS. It is assumed that the virus uses a dual entry strategy of receptor and electrostatic interaction. This was further emphasized by the identification of 29-mer peptide derived from RVG, binding to α-1-subunit of nAchR, and the fact that this peptide has an overall positive charge under physiological conditions, enabling electrostatic interactions with the cell membranes. For the functionalization of DDS, the RVG sequence underwent modifications. The impact of these modifications with regard to the uptake mechanism still needs to be investigated. The functionalization with RVG was applied to several DDS like for the delivery of nucleic acids with polymer or polyarginine complexes, nanoparticles and exosomes. The targeting effect was proved by the increased uptake of targeted DDS in neuronal compared to non-neuronal cells. Although the classical pathway of rabies virus is along the long axonal nervous system, the uptake of RVG-functionalized DDS in brain endothelial cells and macrophages emphasize a versatile uptake strategy for these DDS. The functionalization of DDS with the RVG sequence resulted in changes of the primary sequence of RVG and in different physicochemical properties compared to RVG. Interestingly, the uptake into the used cells was independent from all changes, which could be due to the significance of positive charges of the molecules for the cell uptake.

Nevertheless, for the identification of the uptake mechanism of targeted DDS, impact factors like modification of peptide and physicochemical properties should be taken into account. The results assumed a dual-approach of receptor binding and electrostatic interactions, which cannot be reduced to a unique key-lock principle. Although the potential CNS targeting has been proved by in vivo experiments, they were not able to record the pathway of RVG-functionalized DDS. Especially the contradictory results of Kumar et al. and Cook et al. showed that is it important to record the track of RVG-functionalized DDS and taking the structure modifications of RVG and the DDS own physicochemical properties into account.

Reference list

1. Chen, Y. and L. Liu, *Modern methods for delivery of drugs across the blood-brain barrier*. Advanced Drug Delivery Reviews Delivery of Therapeutics to the Central Nervous System. 2012. p. 640-665.
2. Salinas, S., G. Schiavo, and E.J. Kremer, *A hitchhiker's guide to the nervous system: the complex journey of viruses and toxins.* Nat Rev Micro, 2010. 8(9): p. 645-655.
3. Liu, Y., et al., *Targeted imaging of activated caspase-3 in the central nervous system by a dual functional nano-device.* Journal of Controlled Release, 2012. 163(2): p. 203-210.
4. Cardoso, F.L., D. Brites, and M.A. Brito, *Looking at the blood–brain barrier: Molecular anatomy and possible investigation approaches.* Brain Research Reviews, 2010. 64(2): p. 328-363.
5. Koyuncu, O.O., I.B. Hogue, and L.W. Enquist, *Virus Infections in the Nervous System.* Cell host & microbe, 2013. 13(4): p. 379-393.
6. McGavern, D.B. and S.S. Kang, *Illuminating viral infections in the nervous system.* Nat Rev Immunol, 2011. 11(5): p. 318-329.
7. Lentz, T.B., S.J. Gray, and R.J. Samulski, *Viral vectors for gene delivery to the central nervous system.* Neurobiology of Disease, 2012. 48(2): p. 179-188.
8. Avila-Olias, M., et al., *Inspired by nature: fundamentals in nanotechnology design to overcome biological barriers.* Therapeutic Delivery, 2012. 4(1): p. 27-43.
9. Kim, K.S., *Mechanisms of microbial traversal of the blood-brain barrier.* Nat Rev Micro, 2008. 6(8): p. 625-634.
10. Schnell, M.J., et al., *The cell biology of rabies virus: using stealth to reach the brain.* Nat Rev Micro, 2010. 8(1): p. 51-61.
11. Dietzschold, B., et al., *Concepts in the pathogenesis of rabies.* Future virology, 2008. 3(5): p. 481-490.
12. Modrow, D.F.U.T.H.S.S., *Viren mit einzelsträngigem, kontinuierlichem RNA-Genom in Negativstrangorientierung*. Molekulare Virologie, 2010. p. 263-323.
13. Cantin, E.M. and J.J. Rossi, *Molecular medicine: Entry granted.* Nature, 2007. 448(7149): p. 33-34.
14. Koyuncu, O.O., D.H. Perlman, and L.W. Enquist, *Efficient Retrograde Transport of Pseudorabies Virus within Neurons Requires Local Protein Synthesis In Axons.* Cell host & microbe, 2013. 13(1): p. 54-66.
15. Lentz, T.L., et al., *The acetylcholine receptor as a cellular receptor for rabies virus.* The Yale Journal of Biology and Medicine, 1983. 56(4): p. 315-322.
16. Albertini, A.A.V., et al., *Molecular and Cellular Aspects of Rhabdovirus Entry.* Viruses, 2012. 4(1): p. 117-139.
17. Lafon, M., *Rabies virus receptors.* Journal of NeuroVirology, 2005. 11(1): p. 82-87.
18. Ugolini, G., *Advances in viral transneuronal tracing.* Journal of Neuroscience Methods, 2010. 194(1): p. 2-20.
19. Lentz, T.L., *Rabies virus binding to an acetylcholine receptor α-subunit peptide.* Journal of Molecular Recognition, 1990. 3(2): p. 82-88.
20. Lentz, T.L., *Structure-function relationships of curaremimetic neurotoxin loop 2 and of a structurally similar segment of rabies virus glycoprotein in their interaction with the nicotinic acetylcholine receptor.* Biochemistry, 1991. 30(45): p. 10949-10957.
21. Tuffereau, C., et al., *The rabies virus glycoprotein receptor p75NTR is not essential for rabies virus infection.* Journal of virology, 2007. 81(24): p. 13622-13630.
22. Lentz, T.L., et al., *Is the acetylcholine receptor a rabies virus receptor?* Science, 1982. 215(4529): p. 182-184.

23. Hemachudha, T., et al., *Human rabies: neuropathogenesis, diagnosis, and management.* The Lancet Neurology, 2013. 12(5): p. 498-513.
24. Thoulouze, M.-I., et al., *The Neural Cell Adhesion Molecule Is a Receptor for Rabies Virus.* Journal of Virology, 1998. 72(9): p. 7181-7190.
25. Grove, J. and M. Marsh, *The cell biology of receptor-mediated virus entry.* The Journal of Cell Biology, 2011. 195(7): p. 1071-1082.
26. Gotti, C. and F. Clementi, *Neuronal nicotinic receptors: from structure to pathology.* Progress in neurobiology, 2004. 74(6): p. 363-396.
27. Thoulouze, M.I., et al., *Rabies virus infects mouse and human lymphocytes and induces apoptosis.* Journal of Virology, 1997. 71(10): p. 7372-7380.
28. Soroka, *Structure and Function of the Neural Cell Adhesion Molecule NCAM*. Advances in Experimental Medicine and Biology, ed. V. Berezin. 2010.
29. Langevin, C., et al., *Rabies Virus Glycoprotein (RVG) Is a Trimeric Ligand for the N-terminal Cysteine-rich Domain of the Mammalian p75 Neurotrophin Receptor.* Journal of Biological Chemistry, 2002. 277(40): p. 37655-37662.
30. Dechant, G. and Y.-A. Barde, *The neurotrophin receptor p75NTR: novel functions and implications for diseases of the nervous system.* Nat Neurosci, 2002. 5(11): p. 1131-1136.
31. Gluska, S., et al., *Rabies Virus Hijacks and Accelerates the p75NTR Retrograde Axonal Transport Machinery.* PLoS Pathogens, 2014. 10(8): p. e1004348.
32. Piccinotti, S., T. Kirchhausen, and S.P.J. Whelan, *Uptake of Rabies Virus into Epithelial Cells by Clathrin-Mediated Endocytosis Depends upon Actin.* Journal of Virology, 2013. 87(21): p. 11637-11647.
33. Piccinotti, S. and S.P.J. Whelan, *Rabies Internalizes into Primary Peripheral Neurons via Clathrin Coated Pits and Requires Fusion at the Cell Body.* PLoS Pathogens, 2016. 12(7): p. e1005753.
34. Xu, H., et al., *Real-time Imaging of Rabies Virus Entry into Living Vero cells.* Scientific Reports, 2015. 5: p. 11753.
35. Jacob, Y., et al., *Cytoplasmic Dynein LC8 Interacts with Lyssavirus Phosphoprotein.* Journal of Virology, 2000. 74(21): p. 10217-10222.
36. Klingen, Y., K.-K. Conzelmann, and S. Finke, *Double-Labeled Rabies Virus: Live Tracking of Enveloped Virus Transport.* Journal of Virology, 2008. 82(1): p. 237-245.
37. Lentz, T.L., E. Hawrot, and P.T. Wilson, *Synthetic peptides corresponding to sequences of snake venom neurotoxins and rabies virus glycoprotein bind to the nicotinic acetylcholine receptor.* Proteins: Structure, Function, and Bioinformatics, 1987. 2(4): p. 298-307.
38. Hervé, F., N. Ghinea, and J.-M. Scherrmann, *CNS Delivery Via Adsorptive Transcytosis.* The AAPS Journal, 2008. 10(3): p. 455-472.
39. Hwang, D.W., et al., *A brain-targeted rabies virus glycoprotein-disulfide linked PEI nanocarrier for delivery of neurogenic microRNA.* Biomaterials, 2011. 32(21): p. 4968-4975.
40. Son, S., et al., *RVG peptide tethered bioreducible polyethylenimine for gene delivery to brain.* Journal of Controlled Release, 2011. 155(1): p. 18-25.
41. Alvarez-Erviti, L., et al., *Delivery of siRNA to the mouse brain by systemic injection of targeted exosomes.* Nat Biotech, 2011. 29(4): p. 341-345.
42. Cooper, J.M., et al., *Systemic exosomal siRNA delivery reduced alpha-synuclein aggregates in brains of transgenic mice.* Movement Disorders, 2014. 29(12): p. 1476-1485.
43. Gao, Y., et al., *RVG-Peptide-Linked Trimethylated Chitosan for Delivery of siRNA to the Brain.* Biomacromolecules, 2014. 15(3): p. 1010-1018.

44. Huo, H., et al., *Polyion complex micelles composed of pegylated polyasparthydrazide derivatives for siRNA delivery to the brain.* Journal of colloid and interface science, 2015. 447: p. 8-15.
45. Liu, Y., et al., *Brain-targeting gene delivery and cellular internalization mechanisms for modified rabies virus glycoprotein RVG29 nanoparticles.* Biomaterials, 2009. 30(25): p. 4195-4202.
46. Beloor, J., et al., *Effective Gene Delivery into Human Stem Cells with a Cell-Targeting Peptide-Modified Bioreducible Polymer.* Small, 2015. 11(17): p. 2069-2079.
47. Kim, J.-Y., et al., *Brain-targeted delivery of protein using chitosan-and RVG peptide-conjugated, pluronic-based nano-carrier.* Biomaterials, 2013. 34(4): p. 1170-1178.
48. Kumar, P., et al., *Transvascular delivery of small interfering RNA to the central nervous system.* Nature, 2007. 448(7149): p. 39-43.
49. Kim, S.-S., et al., *Targeted delivery of siRNA to macrophages for anti-inflammatory treatment.* Molecular therapy, 2010. 18(5): p. 993-1001.
50. Ye, C., et al., *Human macrophage and dendritic cell-specific silencing of high-mobility group protein B1 ameliorates sepsis in a humanized mouse model.* Proceedings of the National Academy of Sciences, 2012. 109(51): p. 21052-21057.
51. Kuan, W.-L., et al., *A novel neuroprotective therapy for Parkinson's disease using a viral noncoding RNA that protects mitochondrial Complex I activity.* The Journal of experimental medicine, 2012. 209(1): p. 1-10.
52. Pulford, B., et al., *Liposome-siRNA-peptide complexes cross the blood-brain barrier and significantly decrease PrP C on neuronal cells and PrP RES in infected cell cultures.* PloS one, 2010. 5(6): p. e11085.
53. Conceição, M., et al., *Intravenous administration of brain-targeted stable nucleic acid lipid particles alleviates Machado-Joseph disease neurological phenotype.* Biomaterials, 2016. 82: p. 124-137.
54. Gong, C., et al., *Target delivery of a gene into the brain using the RVG29-oligoarginine peptide.* Biomaterials, 2012. 33(12): p. 3456-3463.
55. Yang, Y.-J., et al., *Production and characterization of a fusion peptide derived from the rabies virus glycoprotein (RVG29).* Protein expression and purification, 2014. 104: p. 7-13.
56. Ye, C., et al., *Targeting DNA vaccines to myeloid cells using a small peptide.* European journal of immunology, 2015. 45(1): p. 82-88.
57. Zeller, S., et al., *Attachment of cell-binding ligands to arginine-rich cell-penetrating peptides enables cytosolic translocation of complexed siRNA.* Chemistry & biology, 2015. 22(1): p. 50-62.
58. Cook, R.L., et al., *A critical evaluation of drug delivery from ligand modified nanoparticles: Confounding small molecule distribution and efficacy in the central nervous system.* Journal of Controlled Release, 2015. 220: p. 89-97.
59. Chen, W., et al., *Targeted brain delivery of itraconazole via RVG29 anchored nanoparticles.* Journal of drug targeting, 2011. 19(3): p. 228-234.
60. Pulford, B., et al., *Liposome-siRNA-Peptide Complexes Cross the Blood-Brain Barrier and Significantly Decrease PrP(C) on Neuronal Cells and PrP(RES) in Infected Cell Cultures.* PLoS One, 2010. 5(6): p. e11085.
61. Tugyi, R., et al., *Partial d-amino acid substitution: Improved enzymatic stability and preserved Ab recognition of a MUC2 epitope peptide.* Proceedings of the National Academy of Sciences of the United States of America, 2005. 102(2): p. 413-418.
62. Hermanson, G.T., *Chapter 3 - The Reactions of Bioconjugation*, in *Bioconjugate Techniques (Third edition)*. 2013, Academic Press: Boston. p. 229-258.
63. Kim, Y., et al., *Efficient Site-Specific Labeling of Proteins via Cysteines.* Bioconjugate chemistry, 2008. 19(3): p. 786-791.

64. Kim, J.Y., et al., *Brain-targeted delivery of protein using chitosan- and RVG peptide-conjugated, pluronic-based nano-carrier.* Biomaterials, 2013. 34(4): p. 1170-1178.
65. Gooding, M., et al., *Synthesis and characterization of rabies virus glycoprotein-tagged amphiphilic cyclodextrins for siRNA delivery in human glioblastoma cells: In vitro analysis.* European Journal of Pharmaceutical Sciences, 2015. 71: p. 80-92.
66. Tao, Y., J. Han, and H. Dou, *Brain-targeting gene delivery using a rabies virus glycoprotein peptide modulated hollow liposome: bio-behavioral study.* Journal of Materials Chemistry, 2012. 22(23): p. 11808-11815.
67. Hermanson, G.T., *Chapter 11 - (Strept)avidin–Biotin Systems*, in *Bioconjugate Techniques (Third edition)*. 2013, Academic Press: Boston. p. 465-505.
68. Immordino, M.L., F. Dosio, and L. Cattel, *Stealth liposomes: review of the basic science, rationale, and clinical applications, existing and potential.* International Journal of Nanomedicine, 2006. 1(3): p. 297-315.
69. Kirpotin, D., et al., *Sterically stabilized anti-HER2 immunoliposomes: design and targeting to human breast cancer cells in vitro.* Biochemistry, 1997. 36(1): p. 66-75.
70. Sawant, R.R. and V.P. Torchilin, *Challenges in development of targeted liposomal therapeutics.* The AAPS journal, 2012. 14(2): p. 303-315.
71. Conceição, M., et al., *Intravenous administration of brain-targeted stable nucleic acid lipid particles alleviates Machado-Joseph disease neurological phenotype.* Biomaterials, 2016. 82: p. 124-137.
72. Kamboj, V.K. and P.K. Verma, *Poloxamers based nanocarriers for drug delivery system.* Der Pharmacia Lettre, 2015. 7(2): p. 264-269.
73. El Andaloussi, S., et al., *Extracellular vesicles: biology and emerging therapeutic opportunities.* Nat Rev Drug Discov, 2013. 12(5): p. 347-357.
74. Tan, S., et al., *Cell or cell membrane-based drug delivery systems.* Theranostics, 2015. 5(8): p. 863.
75. Johnsen, K.B., et al., *A comprehensive overview of exosomes as drug delivery vehicles — Endogenous nanocarriers for targeted cancer therapy.* Biochimica et Biophysica Acta (BBA) - Reviews on Cancer, 2014. 1846(1): p. 75-87.
76. Korade, Z., et al., *Expression and p75 neurotrophin receptor dependence of cholesterol synthetic enzymes in adult mouse brain.* Neurobiology of aging, 2007. 28(10): p. 1522-1531.
77. Spindler, K.R. and T.-H. Hsu, *Viral disruption of the blood-brain barrier.* Trends in Microbiology, 2012. 20(6): p. 282-290.
78. Omidi, Y., et al., *Evaluation of the immortalised mouse brain capillary endothelial cell line, b.End3, as an in vitro blood–brain barrier model for drug uptake and transport studies.* Brain Research, 2003. 990(1–2): p. 95-112.
79. Shilo, M., et al., *The effect of nanoparticle size on the probability to cross the blood-brain barrier: an in-vitro endothelial cell model.* Journal of Nanobiotechnology, 2015. 13: p. 19.
80. Puchacz, E., et al., *Functional expression of nicotinic acetylcholine receptors containing rat α7 subunits in human SH-SY5Y neuroblastoma cells.* FEBS letters, 1994. 354(2): p. 155-159.
81. Xie, H.-r., L.-S. Hu, and G.-Y. Li, *SH-SY5Y human neuroblastoma cell line: in vitro cell model of dopaminergic neurons in Parkinson's disease.* Chinese medical journal, 2010. 123(8): p. 1086-1092.
82. Lukas, R.J., S.A. Norman, and L. Lucero, *Characterization of Nicotinic Acetylcholine Receptors Expressed by Cells of the SH-SY5Y Human Neuroblastoma Clonal Line.* Molecular and Cellular Neuroscience, 1993. 4(1): p. 1-12.
83. Peng, X., et al., *Human alpha 7 acetylcholine receptor: cloning of the alpha 7 subunit from the SH-SY5Y cell line and determination of pharmacological properties of native*

receptors and functional alpha 7 homomers expressed in Xenopus oocytes. Molecular Pharmacology, 1994. 45(3): p. 546-554.

Chapter 2

Goals of PhD thesis

The use of active targeting strategies for the delivery of active pharmaceutical ingredients (API) across the blood-brain barrier (BBB) is a common approach in nanoparticle formulation strategies. The approach introduced here is decorating particle surfaces with specific ligands that are able to interact with transporters or receptors located on brain endothelial cells. However, a successful active targeting is not only achieved through the "decoration" of nanoparticles. Although the selection of the targeting ligand is assumed to be the decisive factor in BBB-targeting strategies, the impact of the drug delivery system (DDS) itself on the fate of the whole system is completely neglected. This is particularly evident for virus-related CNS targeting strategies, which gained great popularity in brain-targeted delivery. DDS functionalized with virus peptide sequences are intended to follow the same pathway as the virus into the CNS. However, it is questionable whether the functionalized DDS follow exactly the same pathway. The introduction focusses on the fate of virus-functionalized DDS into the CNS. It is intended to deepen the understanding of the virus-related CNS targeting strategies by comparing the properties of rabies virus glycopeptide (RVG)-functionalized DDS with rabies virus (**chapter 1**).

The importance of tissue-specific properties for BBB-targeted DDS was further investigated by adjusting physiochemical properties of liposome formulations with respect to BBB requirements. Liposomes have a high versatility with respect to physicochemical properties and other sophisticated functionalization possibilities. Current preparation strategies and the knowledge about brain tissue specific requirements enable the formulation of tailor-made formulations with respect to size, surface charge or the use of the brain specific polyunsaturated fatty acid docosahexaenic acid (DHA) (**chapter 3**).

The analytical characterization is a *sine qua non* for the development of functionalized liposomes. The complex composition of functionalized liposomes in particular as well as their manufacturing, which is a multi-step process, requires extensive characterization. Although a variety of analytical techniques are available, quantitative data on the liposome composition and the targeting ligands density are often missing. This increased the motivation enormously to establish analytical methods for the quantification of all individual liposome components (**chapter 4**).

Maleimide-functionalized phospholipids play a key role in the functionalization of liposomes with targeting peptide sequences. The specificity for thiol-groups in combination with their fast reaction kinetics under mild and aqueous conditions explain their popularity. However, maleimides are prone to pH-dependent hydrolysis. This causes changes in the overall surface charge as well as the inability to react with thiols. To understand and control maleimide

intensity during functionalized liposomes manufacturing was, therefore, of key interest (**chapter 5**).

Finally, the targeting efficiency of BBB specific liposomes was investigated by the cell-binding studies using a brain endothelial cell line (bEnd.3). The cells were used to assess the tissue-specific requirements of BBB specific liposomes with respect to size, surface charge or the brain-specific polyunsaturated fatty acid DHA (**chapter 6**).

Chapter 3

Manufacturing of blood-brain barrier (BBB) specific liposomes: set up of a platform with favorable physicochemical characteristics

Abstract

While the majority of brain targeted drug delivery systems (DDS) uses active targeting strategies to reach their destination, physicochemical characteristics of these DDS are often neglected. This is surprising, since the passing of tailor-made DDS across the blood-brain barrier (BBB) requires more than an active targeting strategy. The presented work sheds light on important physicochemical characteristics focusing on size, charge, polyethylenglycole (PEG) amount and composition by the example of BBB-targeted liposomes. By the selection of different lipids and varying concentrations a screening platform was assembled for the analysis of BBB-specific physicochemical properties for liposomes. The setting of different sizes (from 50-405 nm) was feasible with a liposome composition of DOPC, CHO and DSPE-PEG-2000 in a molar ratio of 60:35:5 (mol%). The preparation of positively charged formulations was reached with liposomes composed of DMPC, CHO and DOTAP (20 ± 4 mV). The degree of PEGylation, which is of high importance for the functionalization of liposomes, could be increased up to 10% (mol/mol) of the total lipid concentration. Docasahexaenoic acid proposed as brain specific could successfully be incorporated into liposome formulation. The presented work provides important information in terms of BBB targeted delivery systems beyond the standard ligand coupling procedures.

1. Introduction

The targeted delivery across the blood-brain barrier (BBB) requires tailor made drug delivery systems (DDS). The published literature mainly deals with active targeting strategies [1, 2]. Whereby, the aim is to deliver DDS into the brain by attaching receptor-sensitive ligands on the surface of DDS. By this, the attached ligand is able to interact with receptors, located on the endothelial cells, and therefore induce receptor-mediated uptake into the brain [1]. While the uptake of these BBB targeted DDS is explained by the selection of the brain-specific ligand, the impact of physical and chemical DDS characteristics like size, charge and composition on brain uptake is completely overlooked. This is astonishing, as the biological characteristics and highly regulated uptake mechanisms of the BBB require tailor-made properties of BBB-targeted DDS [3-5]. Therefore, not only the selection of targeting ligand, but furthermore the precise setting of size, charge and composition are of high importance.

Several reviews, dealing with BBB-targeted DDS, state a particle diameter of less than 100 nm as ideal [1, 5, 6]. Such values are not only a matter of target tissue-specific requirements but can also result from the uptake mechanism. In the case of a clathrin-mediated endocytosis, the size of DDS is restricted to the size of vesicles, which are formed during the clathrin-mediated endocytosis, enabling entry into the cell. These vesicles have a diameter of 100-150 nm [7, 8]. In addition to that Sonavane et al. showed size-dependent uptake into the brain of different sized gold nanoparticles after intravenous administration. In this study, the uptake of 15 nm gold nanoparticles was 500 times higher than the uptake of 100 nm gold nanoparticles [9].

Furthermore, the uptake of DDS is affected by the cell membrane surface, which is negatively charged due to heparan sulphate proteoglycans [10, 11]. Therefore, the uptake of positively charged DDS is commonly facilitated probably due to ionic interaction between cell and nanoparticle membrane (adsorptive-mediated uptake) [11].

In addition, PEGylation of DDS plays an important role in the uptake into target cells. DDS are normally PEGylated to reduce opsonisation and the uptake by the reticuloendothelial system (RES), resulting in a prolonged blood circulation time [12]. In case of active targeting strategies, PEG-chains can be used for the functionalization of DDS with brain specific ligands that enable receptor-mediated transcytosis.

Liposomes are well suitable for BBB targeting strategies. As their physical (size, surface charge) and chemical characteristics (bilayer composition, degree of pegylation, bilayer rigidity) can be varied over a wide selection of lipids and preparation methods [13-15].

This allows to address questions such as which characteristics do liposomes need to be taken up into the brain and how are we obtain these characteristics?

Therefore, we wanted to establish a liposome formulation platform, which enables the setting of size, charge and target specific compositions to maximize BBB targeted uptake.

2. Materials and methods

2.1. Material

1,2-dioleoyl-sn-glycero-3-phosphocholine (DOPC), 1,2-dimyristoyl-sn-glycero-3-phosphocholine (DMPC) and 1,2-distearoyl-sn-glycero-3-phosphoethanolamine-N-[amino-2000] (DSPE-PEG-2000) were purchased from Lipoid GmbH (Ludwigshafen, Germany). Cholesterol (CHO), Docosahexaenoic acid (DHA) and Dulbecco´s phosphate buffered saline (PBS) (D1408) were obtained from Sigma-Aldrich (St. Louis, USA). R-DOTAP was obtained as chloride salt from Merck & Cie, Schaffhausen, Switzerland. Slide-A-LyzerTM Dialysis Cassettes (10kDa) were purchased from Thermo Fisher SCIENTIFIC Inc. (Waltham, USA). Ethanol was obtained from Merck KGaA (Darmstadt, Germany). Purified water was produced by a Millipore-Milli-Q integral water purification system (Merck KGaA, Darmstadt, Germany).

2.2. Solvent-injection method

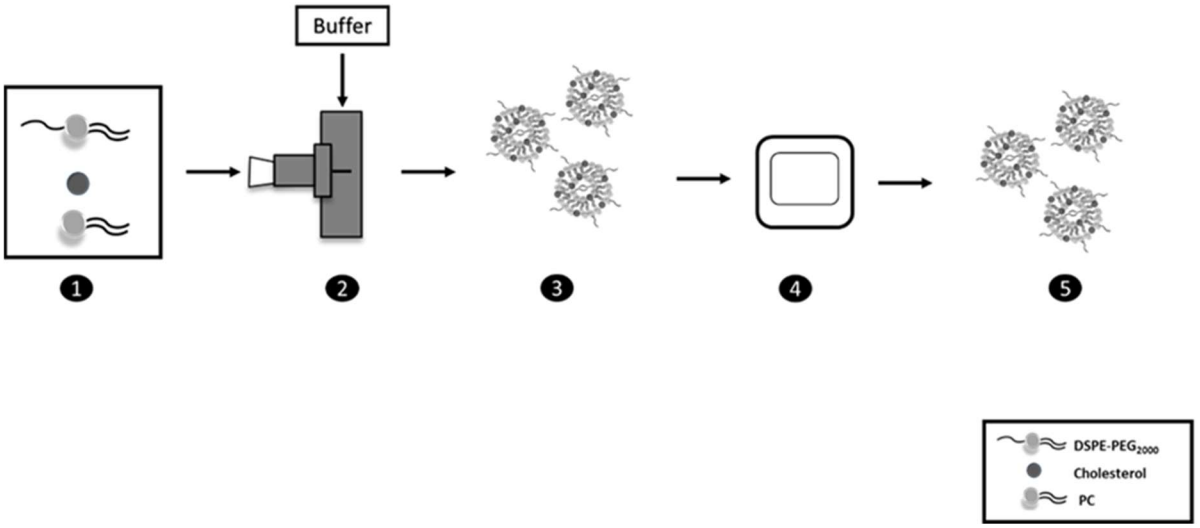

Figure 1: Illustration of the solvent injection method. The lipids and CHO were dissolved in ethanol (step 1). The ethanol solution was injected into phosphate buffered saline (pH 7.0 - 7.5) (step 2). The dilution of the ethanol led to the formation of liposomes (step 3). The sample was dialyzed against PBS (pH 7.0 - 7.5) with a 10.000 MWCO slide-a-lyzer over 5 h and three buffer changes (step 4, 5).

Liposomes were prepared using the solvent injection method [14]. The lipids and CHO were dissolved in ethanol (step 1). The ethanol solution was injected at a flow rate of 12 ml/min into PBS (pH 7.0 - 7.5) with a flow of 80 ml/min (step 2). The dilution of the ethanol led to a controlled precipitation of the lipids at the injection site, which were subsequently rearranged to form liposomes (step 3) [13, 14]. The size of liposomes was set by the initial total lipid concentration. Table 1 depicts the setting of initial and resultant final lipid concentration in dependency of the lipid- and buffer flow rate. The sample was dialyzed against PBS (pH 7.0 - 7.5) with a 10.000 MWCO slide-a-lyzer over 5 h and three buffer changes (step 4, 5). The final TLC was set to 10 mM. Step 5 represents the final formulation, which was analyzed by dynamic light scattering (DLS) and laser diffraction electrophoresis (LDE).

Table 1 shows the setting of final total concentration with a buffer to lipid flow ratio of 80 : 12 with increasing total lipid concentration (TLC).

Initial TLC [mM]	Flow rate: Buffer solution [ml/min]	Flow rate: Lipid solution [ml/min]	TLC [mM]
19.2	80	12	2.5
38.3			5
57.5			7.5
76.7			10
153.3			20

2.3. Size and zeta potential determination

Size distribution and zeta potential (ZP) were determined by dynamic light scattering (DLS) and Laser Doppler electrophoresis (LDE) using a Zetasizer Nano ZS Malvern Instruments (Worcestershire, UK), equipped with a helium neon laser (λ=633 nm). For size distribution analysis samples were measured undiluted at 25 ± 0.1°C with fixed position (4.65 nm) at a detection angle of 173° (back scatter). Data was analyzed via cumulants fit. For the determination of ZP, samples were diluted tenfold with Milli-Q-water and measured at 25°C. ZP was calculated by Smoluchowski's equation from the electrophoretic mobility of liposomes. All measurements were performed in triplicate.

3. Results and discussion

The main objective of the presented work was the formulation of BBB specific liposomes. While doing so, the ranges for the key parameters size, charge, PEGylation and composition of liposome were defined according to biological conditions of the BBB. Key parameters have been set by selection of phospholipid, total lipid concentration (TLC) and preparation method. Liposomes were analyzed by DLS and LDE.

3.1. Size

The aim was to cover a broad size range from 20–150 nm to analyze size-dependency of liposomes. The size of liposomes is highly dependent on selection of liposome composition [16] and preparation method [13]. As liposome composition, a mixture of DOPC or DMPC, CHO and DSPE-PEG-2000 in molar ratio of 60:35:5 was chosen. DOPC was selected due to its ability to form flexible liposomes [17, 18]. This natural phospholipid, is composed of unsaturated fatty acids and has a low transition temperature. In contrast DMPC was selected due to the length of fatty acid chain (C 14), resulting as well in a low transition temperature. In contrast to DOPC, it is a synthetic lipid with saturated fatty acids[18]. Cholesterol is used as stabilizer in liposome compositions and has a strong influence on liposome bilayer properties by interacting with fatty acid chains [19]. The incorporation of the PEGylated lipid DSPE-PEG-2000 ensured prolonged blood circulation time by reduced recognition of RES [12].
The second fact influencing the size of liposomes is the preparation method. Liposomes within this size range are usually unilamellar vesicles and depending on their size further classified as small unilamellar vesicles (SUV) with a size of <100 nm or large unilamellar vesicles (LUV) with a size of >100 nm [13]. These liposomes are composed of a single phospholipid bilayer [20]. Several methods have been described for the preparation of such liposomes [20, 21]. A major criterion of these methods is the generation of monodisperse populations. Unfortunately, most conventional preparation methods require additional homogenization to obtain monodispersed populations. This can be done by extrusion through a filter with defined pore size [22] or sonication [23]. In contrast liposomes with narrow size distribution can be obtained by injecting alcoholic lipid solution into the excess buffer [14]. In addition, this method allows the adjustment of defined size ranges by adjusting the lipid to buffer ratio [24] These facts highly motivated us to select this method.

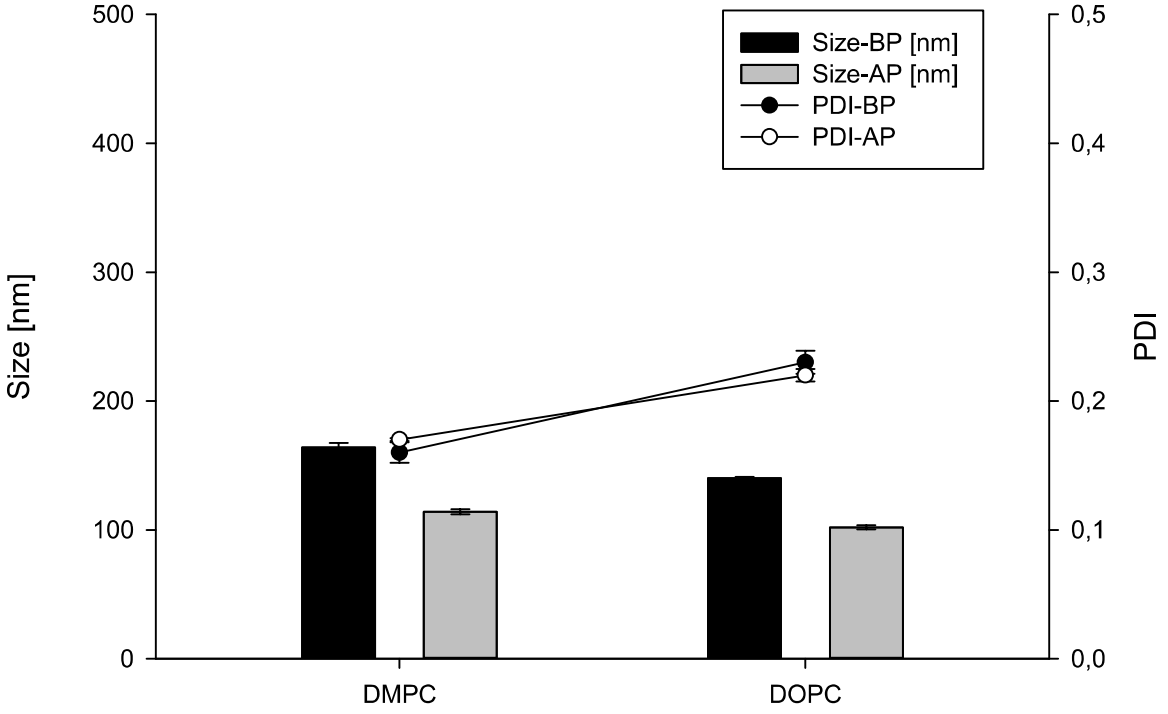

Figure 2: Physicochemical characterization of liposomes, before (BP) and after their purification (AP) composed of DMPC or DOPC, CHO and DSPE-PEG-2000 in a molar ratio of 60:35:5.The liposomes were prepared by the solvent injection method to a total final lipid concentration of 10 mM. (Mean ± SD of three individual batches, n=3).

Figure 2 depicts results of physicochemical characterization of both formulation composed of either DMPC or DOPC, CHO and DSPE-PEG-2000 in molar ratio of 60:35:5. Final TLC of 10 mM was defined according to common liposome preparation procedures [20]. DOPC liposomes had a size of 140 ± 1 nm (PDI: <0.25) before purification, which decreased thereafter to 102 ± 2 nm (PDI: <0.25). DMPC liposomes had a size of 164 ± 4 nm (PDI: <0.2) before purification, which decreased to 114 ± 2 nm (PDI: <0.2). The decrease in size can be explained by the removal of the ethanol. Ethanol interacts with phospholipid membranes [25], therefore, removal results in a reorganization of phospholipid membrane and causes a change in size. We were able to prepare SUV with both formulations. With a size of around 100 nm, both formulations provided liposomes at the upper size limit. Yet, both formulations were further analyzed with respect to size variation. Therefore, liposomes were prepared by increasing the initial TLC from 38.3 to 153.3 mM and a constant flow of buffer and lipid solution.

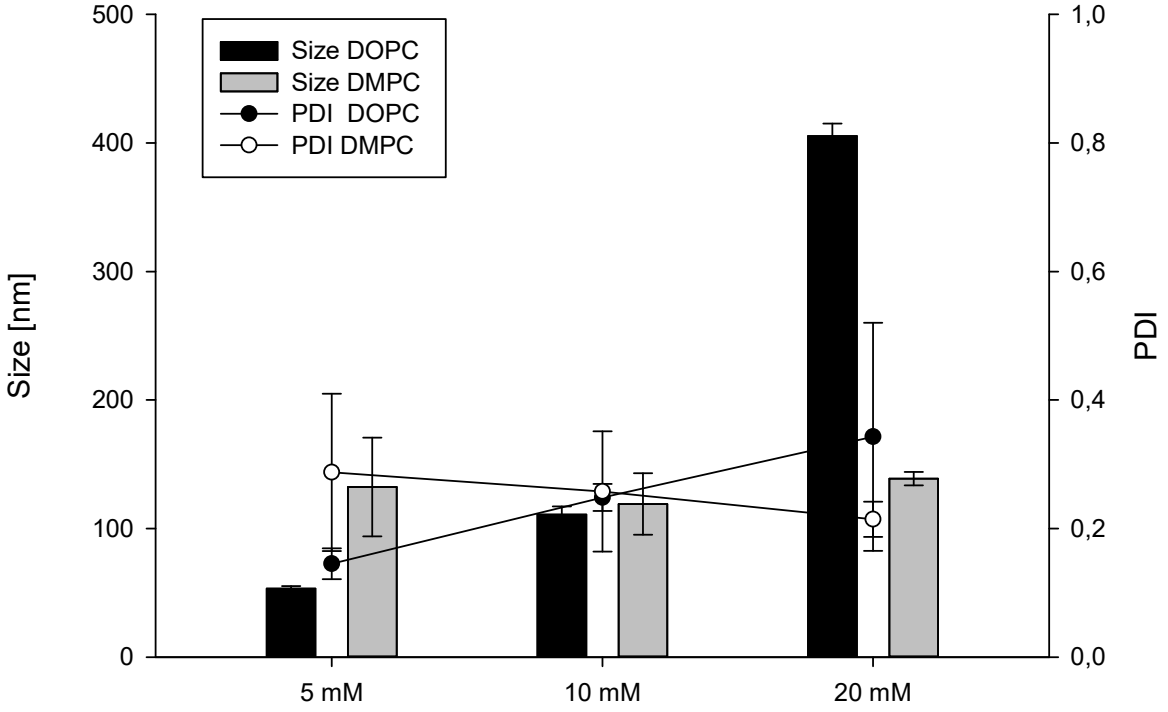

Figure 3: Physicochemical characterization of liposomes after purification, composed of DMPC or DOPC, CHO and DSPE-PEG-2000 in a molar ratio of 60:35:5 with increasing TLC. The liposomes were prepared by the solvent injection method to a total final lipid concentration of 10 mM. (Mean ± SD, n=3).

Figure 3 depicts the results of size titration of DOPC and DMPC liposomes. DOPC liposomes showed a size increase depending on the initial TLC from 46 ± 5 nm to 405 ± 10 nm. In contrast, the size of DMPC liposomes was not affected by increasing TLC and was approximately 130 nm. DOPC liposomes were much more sensitive to increasing TLC, resulting in a size increase, which was accompanied by an increase in PDI. In contrast, the size of DMPC liposomes was not affected by increasing TLC, resulting in a PDI decrease. These results could be explained by chemical properties of both phospholipids. DOPC is a natural, unsaturated phospholipid, which is much more flexible compared to the rigid structure of DMPC, which has saturated fatty acids [18]. The stability of DOPC formulations was proven over a time period of 4 weeks. Liposomes were stored at 2 - 8°C. No changes in size were observed (Figure 4).

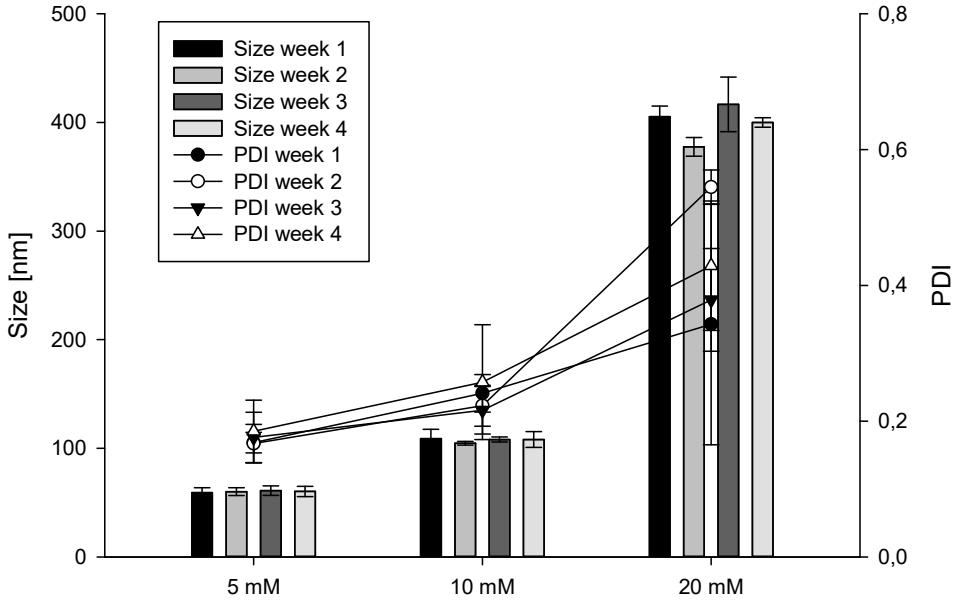

Figure 4: Stability of liposomes composed of DOPC, CHO and DSPE-PEG-2000 in a molar ratio of 60:35:5 with increasing TLC. Liposomes were stored at 2 - 8°C over a time period of 4 weeks Mean ± SD, n=3).

A further assessment of size titration is depicted in Figure 5. Size of DOPC increased depending on the TLC concentration in organic lipid stock, within the concentration range of 19.3 to 153.3 mM. The linear relationship between the TLC and size was shown for the concentration range of 5 to 10 mM, whereas the lowest and highest TLCs resulted in sizes which were not linear to concentration. Although the target size range of 20 – 150 nm could not completely be covered, these results verified that DOPC formulations are well suitable for the analysis of size dependent uptake in brain delivery in contrast to DMPC formulation.

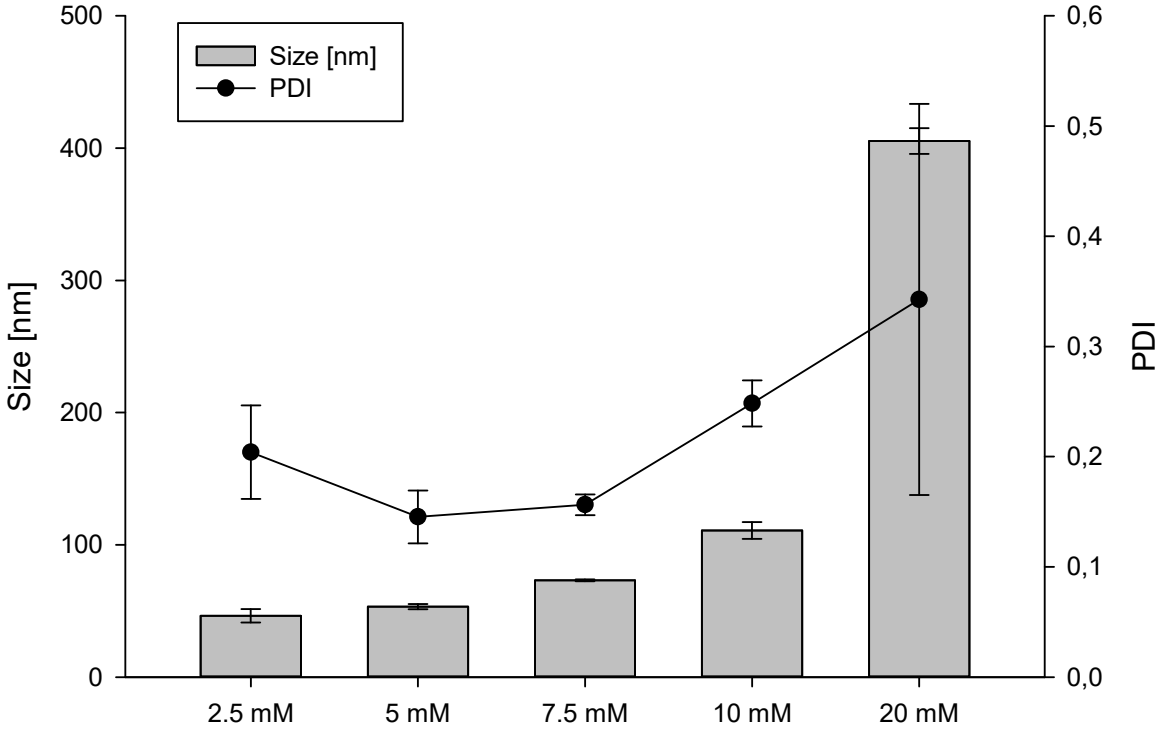

Figure 5: Physicochemical characterization of liposomes after dialysis prepared by the solvent injection method with an increasing TLC, starting from 2.5 mM up to 20 mM. The formulation was composed of DOPC, CHO and DSPE-PEG-2000 in a molar ratio of 60:35:5. (Mean ± SD, n=3).

3.2. Positively charged liposomes

Positive charge can be set by the modification of DDS with so-called cell-penetrating peptides (CPP), which consist of positively charged amino acids like arginine [26-28]. Another approach is the use of positively charged lipids like R-DOTAP. This lipid is normally applied as a transfection agent in gene delivery. The positive head group of lipid enables the interaction with DNA, forming stable lipoplexes [29]. For our platform DOTAP was chosen for the preparation of positively charged liposomes. By incorporation of DOTAP in liposome composition, the surface charge changes to positive values and, therefore, enables the electrostatic interaction of liposomes with a negatively charged cell membrane. The liposomes composed of DMPC, CHO and DOTAP in a molar ratio of 50:30:20 with a final TLC of 10 mM had a size of 183 ± 15 nm (PDI < 0.3) before dialysis and 152 ± 5 nm (PDI <0.37) after dialysis with a positive charge of + 20 ± 4 mV. Size and charge were in an acceptable range and met the desired criteria for the assessment of the uptake in brain endothelial cells with respect to adsorptive-mediated uptake [11]. The incorporation of DOTAP into the DMPC liposome formulation led to an increase in size and PDI. Figure 6 depicts the physicochemical characterization of positively charged

liposomes in comparison to DOPC and DMPC liposomes prepared by the solvent injection method. Such changes in physicochemical properties could be caused by the interactions of DOTAP with DMPC in the bilayer membrane and electrostatic interactions with the used buffer media. Campbell et al. showed that the physicochemical properties of PC-containing liposomes were impacted by increasing the amount of DOTAP. However, in contrast to our results, the incorporation of DOTAP into PC-liposomes resulted in a decrease in size with increasing amount of DOTAP [30].

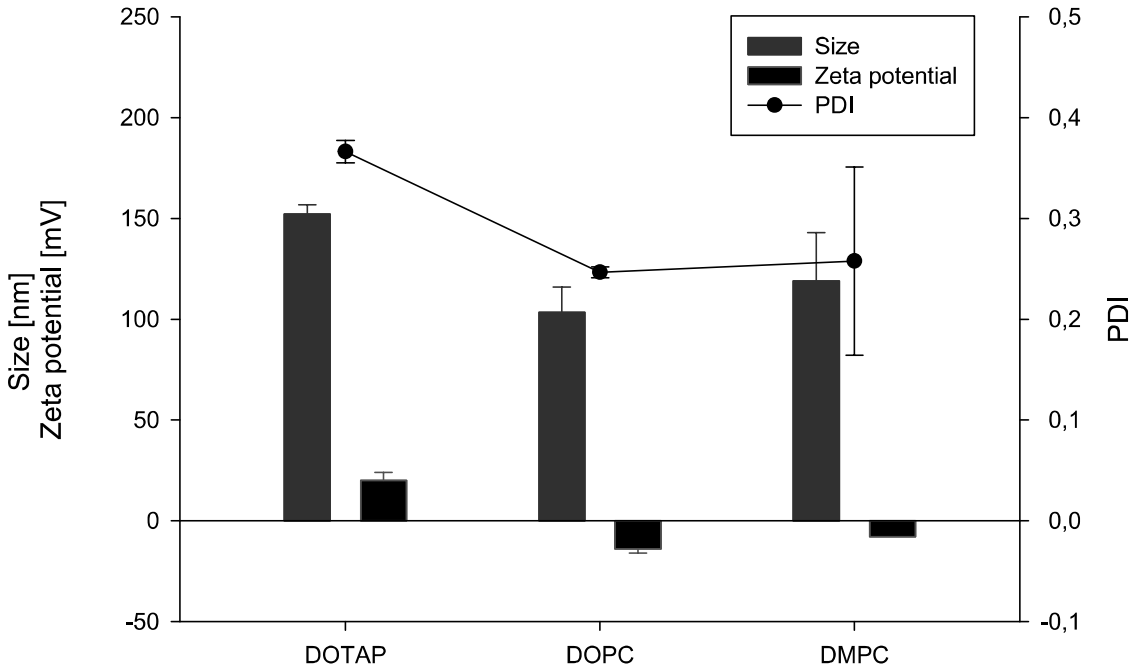

Figure 6: Physicochemical characterization of positively charged liposomes in comparison to DOPC and DMPC liposomes prepared by the solvent injection method. The DOTAP-formulation was composed of DMPC, CHO and DOTAP in a molar ratio of 50:30:20 with a final TLC of 10 mM. The DOPC and DMPC formulation were composed of DMPC or DOPC, CHO and DSPE-PEG-2000 in a molar ratio of 60:35:5 with a final TLC of 10 mM. (Mean ± SD, n=3).

3.3. PEG incorporation into liposomes

PEGylated lipids with functional groups bring two characteristics to the DDS. First, the PEGylation of liposomes enables a prolonged circulation lifetime due to reduced recognition by macrophages. Second, a functional group at the end of the PEG chain enables the attachment of specific ligands. A decisive factor for the uptake into the brain is the amount of PEG incorporated into the liposomes. While the amount of attached ligand might be highly dependent on the ligand and receptor of choice, it should be taken into account that a higher amount of PEG molecules on the DDS results, on the one hand, in reduced recognition by

macrophages, but also might affect the recognition of target cells [31]. The production of liposome with varying amounts of PEG are therefore, of utmost interest. DSPE-PEG-2000 was used as a model compound for the assessment of PEG incorporation. Figure 7 depicts the results of DSPE-PEG-2000 titration in a DOPC CHO liposome formulation, starting with 1 mol% up to 20 mol%. The formulations with 5 and 10 mol% showed the best results with regard to size and PDI. Overall size decreased with increasing PEG amount. After an increase of 10 mol%, DLS measurements are characterized by a decrease in size and an increase of PDI, indicating the disruption of lipid bilayer and formation of micelles [32, 33]. With increasing amount of PEG-lipids, PEG moieties concentrate on the surface of the liposome. While at lower PEG-lipid amounts the PEG moieties exist in a so-called mushroom regime, the increase in the PEG amount in the lipid bilayer causes a switch to the brush regime. The PEG moieties are now able to interact with each other on the surface of the lipid bilayer. This interaction causes the disruption of the lipid bilayer, resulting in the formation of micelles [32]. The results indicated an amount of 5 and 10 mol% of DSPE-PEG-2000 as feasible for the formulation composed of DOPC, CHO and DSPE-PEG-2000. The results could be also transferred to the formulation of liposomes containing DSPE-PEG-2000-Mal instead of DSPE-PEG-2000. The data with an amount of 5 mol% DSPE-PEG-2000-Mal is shown in chapter 3.

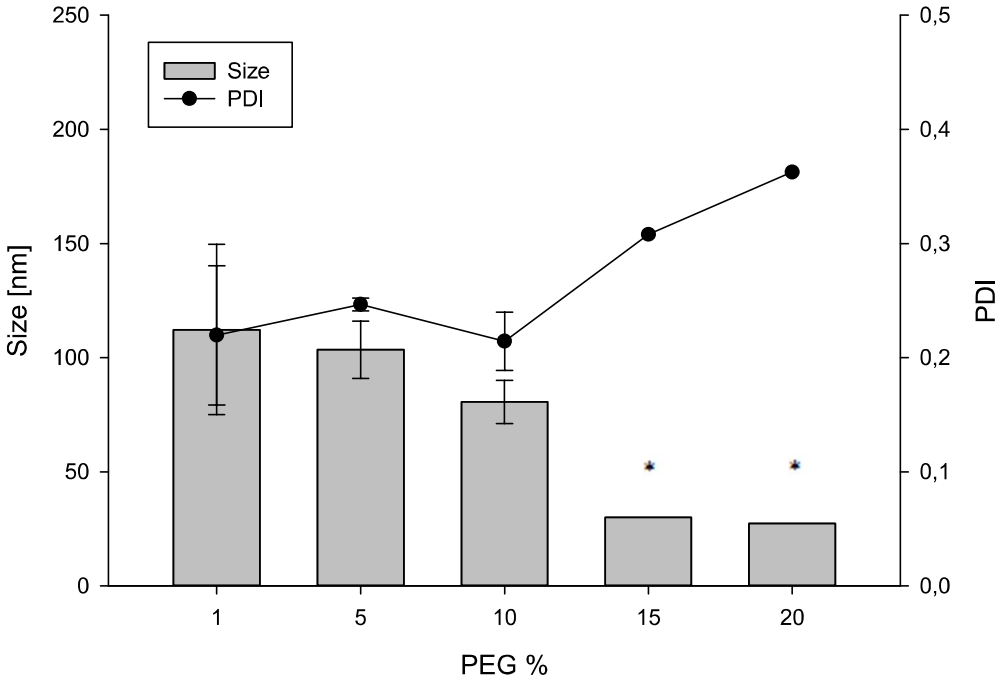

Figure 7: Physiochemical characterization of liposomes with increasing PEG-concentration starting from 1% up to 20% after dialysis (AD) prepared by the solvent injection method. The formulation is composed of DOPC, CHO and DSPE-PEG-2000 (Mean ± SD, n=3), *n=1.

3.4. Preparation of DHA-incorporated liposomes

Besides the size, charge and PEG-amount of a DDS, the composition might also have a decisive impact on the uptake into the brain. A frequently followed idea is to incorporate nutrients for the brain tissue into the liposome. The lipid bilayer structure of liposome enables the incorporation of brain specific lipophilic nutrients. DHA is an omega-3 fatty acid, which is important for brain development and function [34]. As DHA cannot be synthesized in the brain, the uptake is regulated by transporters into the brain. The Mfsd2, a member of the major facilitator superfamily, was recently identified as a DHA transporter, enabling transport across the BBB [35]. Using the neuroprotective effect of DHA, Eckert et al. formulated DHA-incorporated liposomes for the therapy of Alzheimer´s disease (AD) [36]. Therefore, DHA could not only be used as a neuroprotectant but, also facilitates the uptake of formulations by interacting with DHA receptors. Figure 8 depicts the results of the incorporation of DHA into liposomes. According to the liposome preparation by the solvent-injection, DHA was directly added to the alcoholic solution in a molar ratio of 50:33:17 (DOPC CHO:DHA). 0.05% 3,5-Di-tert-4-butylhydroxytoluene (BHT) was added as an antioxidant.

The liposomes had a size of 77 ± 5 nm with a PDI of <0.2 and a charge of -25 ± 3 mV before purification. The purification process did not influence size and charge characteristics (74 ± 2 nm with a PDI of <0.25 and charge of -25 ± 4 mV). With a size of <100 nm the liposomes are well suitable for the uptake into cells according to literature [8]. The increase of negative charge compared to the surface charge of PC liposomes can be explained by the incorporation of the DHA with a free carboxyl group.

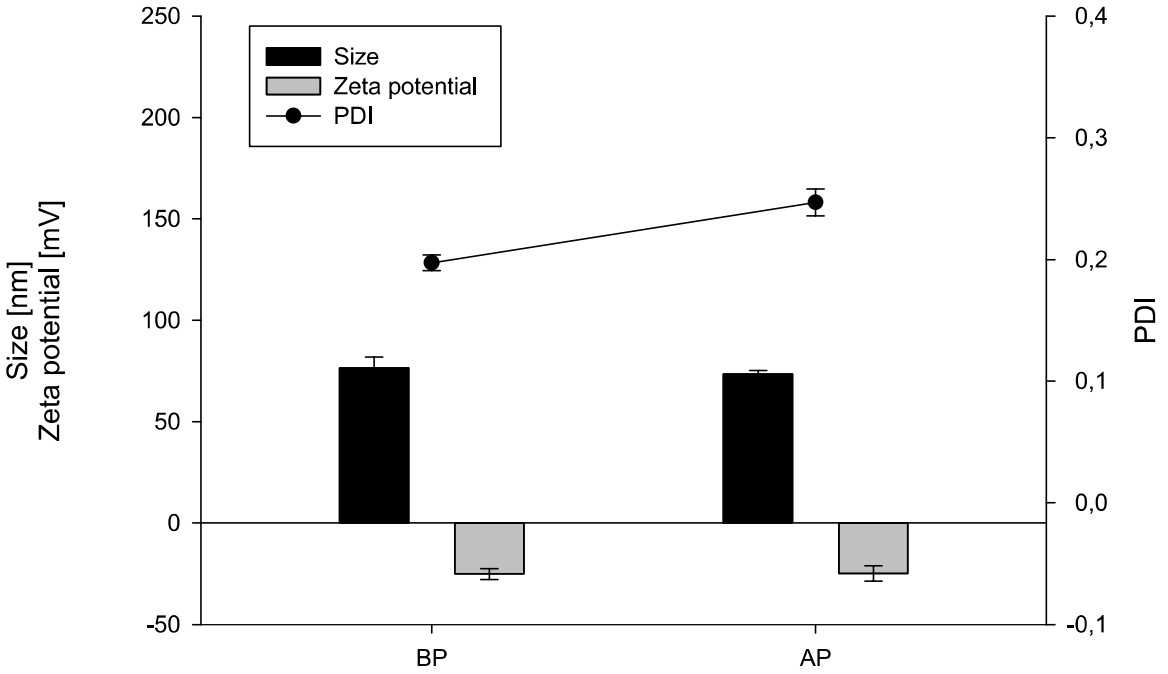

Figure 8: Physiochemical characterization of DHA-incorporated liposomes composed of DOPC, CHO and DHA with a molar ratio of 50:33:17, before (BP) and after purification (AP) prepared by the solvent injection method with a TLC of 10 mM. (Mean ± SD, n=3).

4. Conclusion

The presented work suggests important ways for the design of liposomes optimized for BBB targeting. Beside active targeting strategies, decisive factors like size, charge, PEG amount and brain-specific lipids were taken into account. Hence, the presented liposome formulations can be seen as screening platform for the decision of BBB targeted liposomes. The results underline the complexity and hence the necessity of careful parameter tuning in liposome formulation development.

Reference list

1. Chen, Y. and L. Liu, *Modern methods for delivery of drugs across the blood-brain barrier.* Advanced Drug Delivery ReviewsDelivery of Therapeutics to the Central Nervous System. 2012. p. 640-665.
2. Pardridge, W.M., *The Blood-Brain Barrier: Bottleneck in Brain Drug Development.* NeuroRx, 2005. 2(1): p. 3-14.
3. Shilo, M., et al., *The effect of nanoparticle size on the probability to cross the blood-brain barrier: an in-vitro endothelial cell model*. Journal of Nanobiotechnology, 2015. 13(1): p. 1-7.
4. Kulkarni, S.A. and S.-S. Feng, *Effects of Particle Size and Surface Modification on Cellular Uptake and Biodistribution of Polymeric Nanoparticles for Drug Delivery.* Pharmaceutical Research, 2013. 30(10): p. 2512-2522.
5. Masserini, M., *Nanoparticles for Brain Drug Delivery*. ISRN Biochemistry, 2013. 2013: p. 18.
6. Bhaskar, S., et al., *Multifunctional Nanocarriers for diagnostics, drug delivery and targeted treatment across blood-brain barrier: perspectives on tracking and neuroimaging*. Particle and Fibre Toxicology, 2010. 7: p. 3-3.
7. Papademetriou, J., et al., *Comparative binding, endocytosis, and biodistribution of antibodies and antibody-coated carriers for targeted delivery of lysosomal enzymes to ICAM-1 versus transferrin receptor*. Journal of inherited metabolic disease, 2013. 36(3): p. 467-477.
8. Shang, L., K. Nienhaus, and G.U. Nienhaus, *Engineered nanoparticles interacting with cells: size matters*. Journal of Nanobiotechnology, 2014. 12(1): p. 1-11.
9. Sonavane, G., K. Tomoda, and K. Makino, *Biodistribution of colloidal gold nanoparticles after intravenous administration: Effect of particle size*. Colloids and Surfaces B: Biointerfaces, 2008. 66(2): p. 274-280.
10. Cardoso, F.L., D. Brites, and M.A. Brito, *Looking at the blood–brain barrier: Molecular anatomy and possible investigation approaches*. Brain Research Reviews, 2010. 64(2): p. 328-363.
11. Chen, Y. and L. Liu, *Modern methods for delivery of drugs across the blood–brain barrier*. Advanced Drug Delivery Reviews, 2012. 64(7): p. 640-665.
12. Immordino, M.L., F. Dosio, and L. Cattel, *Stealth liposomes: review of the basic science, rationale, and clinical applications, existing and potential*. International Journal of Nanomedicine, 2006. 1(3): p. 297-315.
13. Akbarzadeh, A., et al., *Liposome: classification, preparation, and applications*. Nanoscale Research Letters, 2013. 8(1): p. 102-102
14. Batzri, S. and E.D. Korn, *Single bilayer liposomes prepared without sonication*. Biochimica et Biophysica Acta (BBA) - Biomembranes, 1973. 298(4): p. 1015-1019.
15. Lai, F., A.M. Fadda, and C. Sinico, *Liposomes for brain delivery*. Expert Opinion on Drug Delivery, 2013. 10(7): p. 1003-1022.
16. Rutherford, H., et al., *Dependence of liquid crystal morphology on phospholipid hydrocarbon length*. Colloids and Surfaces B: Biointerfaces, 2011. 87(1): p. 116-121.
17. Chang, H.-I. and M.-K. Yeh, *Clinical development of liposome-based drugs: formulation, characterization, and therapeutic efficacy*. International Journal of Nanomedicine, 2012. 7: p. 49-60.
18. Li, J., et al., *A review on phospholipids and their main applications in drug delivery systems*. Asian Journal of Pharmaceutical Sciences, 2015. 10(2): p. 81-98.
19. Briuglia, M.-L., et al., *Influence of cholesterol on liposome stability and on in vitro drug release*. Drug Delivery and Translational Research, 2015. 5(3): p. 231-242.

20. J.S. Dua, P.A.C.R., Dr. A.K. Bhandari, *LIPOSOME: METHODS OF PREPARATION AND APPLICATIONS*. International Journal of Pharmaceutical Studies and Research, 2012. 3(2): p. 14-20.
21. van Swaay, D. and A. deMello, *Microfluidic methods for forming liposomes*. Lab on a Chip, 2013. 13(5): p. 752-767.
22. Olson, F., et al., *Preparation of liposomes of defined size distribution by extrusion through polycarbonate membranes*. Biochimica et Biophysica Acta (BBA) - Biomembranes, 1979. 557(1): p. 9-23.
23. Patil, Y.P. and S. Jadhav, *Novel methods for liposome preparation*. Chemistry and Physics of Lipids, 2014. 177: p. 8-18.
24. Schubert, M.A. and C.C. Müller-Goymann, *Solvent injection as a new approach for manufacturing lipid nanoparticles-evaluation of the method and process parameters*. European journal of pharmaceutics and biopharmaceutics : official journal of Arbeitsgemeinschaft fur Pharmazeutische Verfahrenstechnik e.V, 2003. 55(1): p. 125-131.
25. Barry, J.A. and K. Gawrisch, *Direct NMR Evidence for Ethanol Binding to the Lipid-Water Interface of Phospholipid Bilayers. Biochemistry*, 1994. 33(26): p. 8082-8088.
26. Zeller, S., et al., *Attachment of Cell-Binding Ligands to Arginine-Rich Cell-Penetrating Peptides Enables Cytosolic Translocation of Complexed siRNA*. Chemistry & Biology, 2015. 22(1): p. 50-62.
27. Hervé, F., N. Ghinea, and J.-M. Scherrmann, *CNS Delivery Via Adsorptive Transcytosis*. The AAPS Journal, 2008. 10(3): p. 455-472.
28. Yuan, M., et al., *Targeted delivery of transferrin and TAT co-modified liposomes encapsulating both paclitaxel and doxorubicin for melanoma*. Drug Delivery, 2015: p. 1-13.
29. Balazs, D.A. and W. Godbey, *Liposomes for Use in Gene Delivery*. Journal of Drug Delivery, 2011. 2011.
30. Campbell, R.B., S.V. Balasubramanian, and R.M. Straubinger, *Phospholipid-cationic lipid interactions: influences on membrane and vesicle properties*. Biochimica et Biophysica Acta (BBA) - Biomembranes, 2001. 1512(1): p. 27-39.
31. Verhoef, J.J.F. and T.J. Anchordoquy, *Questioning the Use of PEGylation for Drug Delivery*. Drug delivery and translational research, 2013. 3(6): p. 499-503.
32. Garbuzenko, O., Y. Barenholz, and A. Priev, *Effect of grafted PEG on liposome size and on compressibility and packing of lipid bilayer*. Chemistry and Physics of Lipids, 2005. 135(2): p. 117-129.
33. Kastantin, M., et al., *Effect of the Lipid Chain Melting Transition on the Stability of DSPE-PEG(2000) Micelles*. Langmuir, 2009. 25(13): p. 7279-7286.
34. Campos-Bedolla, P., et al., *Role of the Blood–Brain Barrier in the Nutrition of the Central Nervous System*. Archives of Medical Research, 2014. 45(8): p. 610-638.
35. Nguyen, L.N., et al., *Mfsd2a is a transporter for the essential omega-3 fatty acid docosahexaenoic acid*. Nature, 2014. 509(7501): p. 503-506.
36. Eckert, G.P., et al., *Liposome-incorporated DHA increases neuronal survival by enhancing non-amyloidogenic APP processing*. Biochimica et Biophysica Acta (BBA) - Biomembranes, 2011. 1808(1): p. 236-243.

Chapter 4

HPLC analysis as a tool for assessing targeted liposome composition

This chapter was published as: Oswald, M.; Platscher, M.; Geissler, S.; Goepferich; A International Journal of Pharmaceutics 2016, 497 (1–2), 293-300.

Abstract

Functionalized phospholipids are indispensable materials for the design of targeted liposomes. Control over the quality and quantity of phospholipids is thereby key in the successful development and manufacture of such formulations. This was also the case for a complex liposomal preparation composed of 1,2-dioleoyl-sn-glycero-3-phosphocholine (DOPC), Cholesterol (CHO), 1,2-distearoyl-sn-glycero-3-phosphoethanolamine-N-[amino(polyethylene glycol)-2000] (ammonium salt) (DSPE-PEG-2000). To this end, an RP-HPLC method was developed. Detection was done via evaporative light scattering (ELS) for liposomal components. The method was validated for linearity, precision, accuracy, sensitivity and robustness. The liposomal compounds had a non-linear quadratic response in the concentration range of 0.012-0.42 mg/ml with a correlation coefficient greater than 0.99 with an accuracy of method confirmed with 95-105% of the theoretical concentration. Furthermore, degradation products from the liposomal formulation could be identified. The presented method was successfully implemented as a control tool during the preparation of functionalized liposomes. It underlined the benefit of HPLC analysis of phospholipids during liposome preparation as an easy and rapid control method for the functionalized lipid at each concentration step as well as for the quantification of all components.

1. Introduction

The analytical characterization is *a sine qua non* for the development of liposomes. While size distribution, surface charge and drug encapsulation efficiency are commonly determined for liposomal preparations, the quantification of phospholipids (PL) is often missing when it comes to their characterization. The PL content is usually assessed by analyzing the organic phosphates groups using the Barlett assay or via enzymatic reactions [1]. A significant disadvantage of these methods is that only a total lipid content is obtained rather than the specific composition of individual components. In addition, nowadays designed liposomes are often composed of functionalized lipids, such as PEGylated materials containing polyethylene glycol chains that are intended to support escape from the reticuloendothelial system [2]. These functional lipids could also provide functional groups that enable the coupling of targeting ligands [3, 4], the labeling with fluorescent dyes or the use in diagnostic applications [5-7]. DSPE-PEG-2000-Maleimide (DSPE-PEG-2000-Mal) is such a functionalized lipid, which combines the advantages of PEGylation with the possibility of coupling a ligand of choice for selective receptor binding. The use of a maleimide functionalized lipids is part of the classical ligation strategies. In the presence of thiol-reactive ligands stable thioether bonds are formed at the end of PEG-chain [8, 9]. Especially peptides are well suited for the maleimide-thiol coupling, as their sequence can be easily modified by the addition of cysteines or the creation of thiols by the use of chemical reagents, like N-succinimidyl S-acetylthioacetate (SATA) [10]. In the present work, a 29 amino acid glycopeptide (RVG-29) derived from rabies virus served as a model ligand. RVG-29 consists of the bioactive part of the glycoprotein relevant for cellular uptake of the whole virus into the CNS [11]. The peptide was modified with an additional cysteine on the C-terminal end to enable the coupling reaction to the DSPE-PEG-2000-Mal. Since it was our intention to control the amount of thiol-reactive lipid, there was an urgent need for a suitable analytical method, which allowed quantitative analysis of all individual liposome components during manufacturing. To our surprise the question of the quantification of such functionalized lipids is not raised. The principle of liquid chromatography offers as analytical method for the quantification of liposomes as it is well described for the analysis of phospholipids. The principal goal was to develop and implement a HPLC method for the manufacturing process of a liposomal formulation composed of DOPC, CHO and DSPE-PEG-2000 to control critical steps of preparation regarding loss of lipid or the formation of degradation products.

2. Materials and methods

2.1. Materials

1,2-dioleoyl-sn-glycero-3-phosphocholine (DOPC), 1,2-dimyristoyl-sn-glycero-3-phosphocholine (DMPC), 1,2-dioleoyl-sn-glycero-3-phosphoethanolamine (DOPE), 1,2-distearoyl-sn-glycero-3-phosphoethanolamine-N-[amino(polyethylene glycol)-2000] (ammonium salt) (DSPE-PEG-2000) and Lysophosphatidylcholine (Lipoid E LPC RS) were purchased from Lipoid GmbH (Ludwigshafen, Germany). Cholesterol and DPBS10x (D1408) were obtained from Sigma-Aldrich (St. Louis, USA). 1,2-distearoyl-sn-glycero-3-phosphoethanolamine-N-[maleimide(polyethylene glycol)-2000] (ammonium salt) (DSPE-PEG(2000) Maleimide) (DSPE-PEG-2000-Mal) was purchased from Avanti Polar Lipids (Alabaster, USA). The peptide RVG, derived from rabies virus, with an additional cysteine on the C-terminus (YTIWMPENPRPGTPCDIFTNSRGKRASNGC) was synthesized by Merck. Float-a-lyzer G2 (50kDa) were purchased from SPECTRUM® LABORATORIES Inc. (Rancho Dominguez, USA). Methanol, isopropanol, both HPLC grade, and ethanol and ammonium acetate were obtained from Merck KGaA (Darmstadt, Germany). Purified water was produced by a Millipore-Milli-Q integral water purification system (Merck KGaA, Darmstadt, Germany).

2.2. Methods

2.2.1 HPLC analysis

HPLC analysis was done using an Agilent 1260 Infinity (Agilent Technologies, Santa Clara, USA), equipped with a binary pump, mobile phase degasser, temperature-controlled autosampler, column thermostat, UV and evaporative light scattering detector (1260 ELSD). For separation a Kinetex Column (C18, 2.6u, 100Å, 100x3 mm) was used from Phenomenex (Torrance, Canada). The chromatograms were analyzed by EZ Chrom Elite Chromatography Data Systems Version 3.3.2. 1037 SP2 (Agilent technologies, Santa Clara, USA).

Eluent A was composed of methanol and water in a volume ratio of 40:60 with 10 mM ammonium acetate with a pH-value of 6.4, which was adjusted with 1 mM acetic acid. Eluent B was composed of methanol and isopropanol in a ratio of 10:90 with 10 mM ammonium acetate. The autosampler temperature was set to 20°C, the temperature of the column was set to 25°C. Temperature of evaporator and nebulizer was set to 55°C and 45°C with a gas flow of 1.50 standard liter per minute (slm) operated with 10.06 Hz. Stop run of sequence was after 20 min with a flow of 0.6 ml/min and an injection volume of 8 µl. The method was gradient based,

starting with first gradient phase from 0-2.6 min from 100% A to 20% A, followed by an isocratic phase from 2.6-5.3 min with 20% A and a second gradient phase from 5.3-10.6 min to 0% A, and followed by a second isocratic phase from 10.6-13.3 min (see Table 1). After that the column was flushed back to initial conditions.

Prior to HPLC analysis, the liposomal formulations were diluted with isopropanol according to the concentration range of calibration. Method validation included specificity, linearity, precision, accuracy, sensitivity and robustness. For specificity of method, a sample containing DOPC, CHO and DSPE-PEG-2000 was directly diluted with a isopropanol-water mixture in the ratio 9:1 and compared with respect to retention time and a resolution factor >2. A sample with known concentration, containing all three components, was diluted to at least 5 different concentrations to cover the entire working range. Each dilution was injected twice. The averaged peak area was plotted against the concentration. The correlation coefficient should be greater than 0.99. Recovery was tested at two different concentrations, the deviation should be less than +/- 5%. Furthermore, a liposomal formulation was diluted with isopropanol and injected six times on different days. The relative standard deviation of retention time, peak area of each compound as well as the total peak area should be smaller than 3%. The detection limit was visually determined by the analysis of samples with known concentrations of analyte and by establishing the minimum level at which the analyte can be reliably detected. For differentiation of degradation products, a liposomal formulation was exposed to 0.1N NaOH, 0.1N HCl, 3% H_2O_2 and at 50°C for 24 h.

Table 1: Conditions of HPLC method for the analysis of a liposomal formulation composed of DSPE-PEG-2000 (1,2-distearoyl-sn-glycero-3-phosphoethanolamine-N-(aminopolyethylene glycol)-2000), CHO (Cholesterol), and DOPC (1,2-dioleoyl-sn-glycero-3-phosphocholine detected via ELS.
MeOH (methanol), IPA (isopropanol), H_2O (water), $NH_4^+OAc^-$ (ammonium acetate).

Solvent	Solvent A: MeOH/H_2O (40/60),10 mM $NH^{4+}OAc^-$, 1 mM Acetic acid (yields pH 6.4)		
	Solvent B: IPA/MeOH (90/10), 10 mM $NH_4^+OAc^-$, 1 mM Acetic acid		
Column heater [°C]	25		
Flow [ml/min]	0.6		
Column	Kinetex 2,6u C18 100A		
Injection volume [µl]	8		
Stop time [min]	20		
Detector	ELS and UV		
ELSD - Evaporator Temperature [°C]	55		
ELSD - Nebulizer [°C]	45		
UV [nm]	220		
Compound	DSPE-PEG-2000	CHO	DOPC
Liposome concentration [mg/ml]	1,41	1,36	4,74
Diluent	IPA		

2.2.2 Preparation via ethanol injection method

The phospholipids and cholesterol were diluted in ethanol with a total lipid concentration of 77 mM. PBS was used as the aqueous phase. The ethanolic solution was injected with a flow rate of 12 ml/min into DPBS with a flow of 80 ml/min to afford a total lipid concentration of 10 mM. Purification of ethanol was done by dialysis over 5 h and three buffer changes. For the preparation of targeted liposomes, DSPE-PEG-2000-Mal was used instead of DSPE-PEG-2000.

2.2.3 Preparation via lipid-film-hydration

The phospholipids and cholesterol were diluted in dichloromethane with a total lipid concentration of 10 mM. The lipid-film was generated by rotary evaporation. Organic solvent was removed under vacuum overnight. The film was hydrated in DPBS for 1 h at 60°C. Sizing was performed by extrusion through a 200 nm-sized polycarbonate membrane, followed by a 100 nm sized-polycarbonate membrane with 21 extrusion steps per preparation.

2.2.4 Preparation of targeted liposomes

For the preparation of targeted liposomes DSPE-PEG-2000-Mal was used instead of DSPE-PEG-2000 (see above). In the present work, the rabies virus glycopeptide with 29 amino acid residues (RVG-29) derived from the rabies virus served as a model ligand [11]. Liposomes were reacted with RVG-29 in a molar ratio of 1:2 (1 µmol RVG per 0.544 µmol DSPE-PEG-2000-Mal) for 1 h at room temperature under inert conditions at a pH of 7.0. To remove unbound targeting ligand, liposomes were dialyzed overnight at 4°C with three buffer changes.

2.2.5 Statistical analysis

All values are expressed as means ± standard deviation (SD). Statistical data analyses were performed using the Student's t-test with $p < 0.001$ as level of significance. All tests were performed using the statistical software SigmaPlot (Systat Software, San Jose, CA).

3. Results and discussion

The implementation of HPLC analysis as a control tool during the preparation of functionalized liposomes was defined as our principal goal. Therefore, the work was divided into the development and validation of the method and the analytical application as proof of concept.

HPLC method development, optimization and validation

The physicochemical properties of PL, in particular of pegylated types, are challenging to characterize via HPLC analysis. Since they show poor UV absorption sensitivity, the analysis is limited to special detection methods [12]. Modification of PEG-chains with aromatic reagents is one method to overcome this problem. The use of detection methods that are independent of optical properties, like ELS is a common approach in the analysis of phospholipids. The ELS detects non-volatile particles by means of the scattered light [13, 14]. In contrast to UV detection, ELS detection is mass-dependent and not concentration-dependent [14]. Quantification is challenging due to the non-linearity of the response over a wide concentration range, the response variation with the composition of mobile phase, and the detector sensitivity [15, 16]. However, an advantage of ELS detection in the analysis of phospholipids is its greater sensitivity in comparison to UV detection. This leads to a reduction of concentration working range down to 0.1 mg/ml.

The use of ELS detection for the quantification of liposomal components was only described by a few groups [17, 18]. Thereof the work of Shibata et al. is the only one that describes a method for the determination of PEGylated lipids in a liposomal formulation. By using the lipid

composition of the liposome formulation of Doxil®, they were mainly interested in the detection of temperature induced degradation products via HPLC.

The simultaneous detection of DSPE-PEG-2000, CHO and DOPC was feasible with the described method. The optimal separation was achieved at a column temperature of 25°C and a flow rate of 0.6 ml/min. A further increase of column temperature led to a fusion of the peaks of CHO and DOPC.

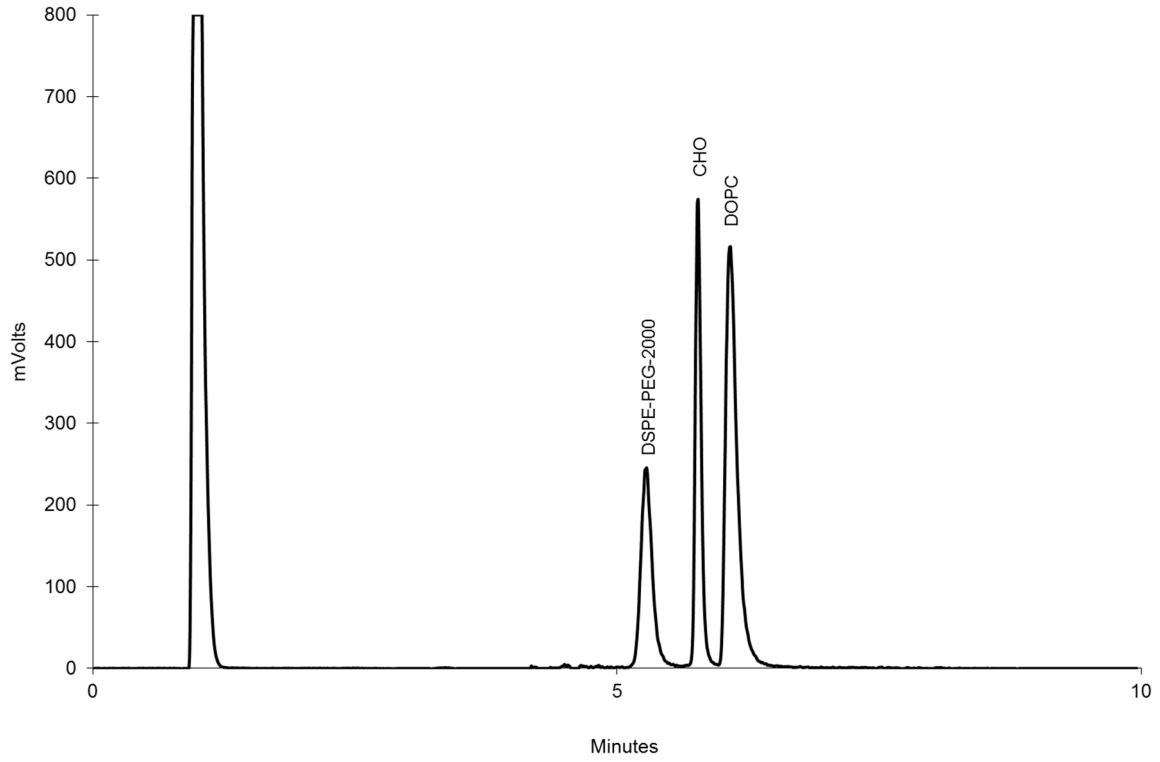

Figure 1: HPLC analysis of a liposomal formulation composed of DSPE-PEG-2000 (Rt= 5.2 min), CHO (Rt= 5.8 min)) and DOPC . The liposome formulation was diluted with isopropanol (IPA) prior to HPLC analysis. The injected amount was 1.1 µg for DSPE-PEG-2000, 1 µg for CHO, and 3,7 µg for DOPC (baseline subtracted).

Figure 1 depicts a typical chromatogram. All three liposomal compounds could be detected in the following order DSPE-PEG-2000 (RT= 5.2 min), CHO (RT= 5.8 min) and DOPC (RT= 6.1 min); peaks were not completely baseline separated according to ICH (International Conference on Harmonisation of Technical Requirements for Registration of Pharmaceuticals for Human Use) guidelines by a resolution factor of >2. The resolution factor between DSPE-PEG-2000 and CHO was 1.8 in contrast to that the resolution factor of 1.1 between CHO and DOPC, which indicated an incomplete baseline separation. Further optimization of flow rate was limited due to high backpressure, therefore the method validation was executed with the above mentioned settings. The linearity was tested in the following calibration ranges for 0.042-0.42 mg/ml for DSPE-PEG-2000, 0.012-0.12 mg/ml for CHO, and 0.03-0.31 mg/ml for DOPC (Table 2).

Table 2: Quantification was done via ESTD-calibration. The linearity was tested in the following calibration range: DSPE-PEG-2000 (0.042-0.42 mg/ml), CHO (0.012-0.1 mg/ml), and DOPC (0.03-0.3 mg/ml). In this concentration range, the ELSD response followed a non-linear quadratic relationship, indicated by a correlation coefficient greater than 0.99 for all three components. (Mean ± SD, n=3).

	DSPE-PEG-2000	**CHO**	**DOPC**
Calibration range [mg/ml]	0.042-0.42	0.012-0.12	0.03-0.31
y=ax2+bx+c r2 (±σ)	0.996 (± 0.002)	0.990 (± 0.005)	0.996 (± 0.001)

In this concentration range, the ELS detection response followed a non-linear quadratic relationship that had a correlation coefficient greater than 0.99 for all three components [19]. Each concentration was analyzed in triplicate. The recovery of the method was tested with samples with known concentration and should be within a deviation of 95-105% of the theoretical concentration (Table 3).

Table 3: A positive control consisting of DSPE-PEG-2000 , CHO and DOPC diluted in a mixture of water: isopropanol in a ratio of 10:90 with known concentration, was injected at two different concentrations. The deviation should be less than +/-5%.

Compound	**Theoretical concentration [mg/ml]**	**Measured concentration [mg/ml]**	**Recovery [%]**
DSPE-PEG-2000	0.314	0.327	104.1
	0.262	0.271	103.4
CHO	0.077	0.076	98.7
	0.039	0.038	97.4
DOPC	0.270	0.280	103.7
	0.135	0.132	97.7

The percentage residual standard deviation of the retention time, peak area of each compound as well as the total area was less than 3% for two liposomal formulations both composed of DSPE-PEG-2000, CHO, and DOPC (Table 4).

Table 4: Precision: A sample was injected six times on different days. The % relative standard deviation of retention time, peak area of each compound as well as the total peak area should be smaller than 3%.

			DSPE-PEG-2000	**CHO**	**DOPC**
Sample 1	**% relative standard deviation**	**Rt**	0.33	0.26	0.25
		Peak area	0.8	2.24	0.7
		Total Peak area	1.22		
Sample 2		**Rt**	0.101	0.088	0.082
		Peak area	0.376	1.044	0.314
		Total Peak area	0.482		

With regard to the non-linearity of the ELS detection response the LOD was determined visually: 144 ng for DSPE-PEG-2000, 56 ng for CHO, and 120 ng for DOPC. For the analysis of degradation products, aliquots of the placebo liposome formulation were each exposed to 0.1N NaOH, 0.1N HCl, 3% H_2O_2, or 50°C. The fact that HPLC analysis enabled the detection

of phospholipid degradation products showed the versatility of this analytical method. Phospholipids tend to degrade over time due to hydrolysis or oxidation. Both degradation pathways can be induced by oxygen, pH-shift, or increased temperature. Lysophospholipids and free fatty acids are generated. The hydrolysis of phospholipids was pH- and temperature-dependent. The pH-dependence was "V-shaped" with a minimum at a pH of 6.5. The effect of temperature can be described by the Arrhenius equation. In aqueous dispersions at a storage temperature of 4°C, the lyso-lipid formation is >20% per month [20]. For the used liposomal formulation expected degradation products of the phospholipids were free fatty acids like oleic and stearic acid, lyso-forms of DOPC and DSPE-PEG-2000 as well as glycerophospho-compounds. Lysophosphatidylcholin (Lyso-PC) as the main degradation product of liposomal formulations causes destabilization of the lipid bilayer due to enhanced permeability [17]. Besides active degradation induced by exposure to the aforementioned substances, a Lyso-PC standard could also be detected by the described method (Figure 2).

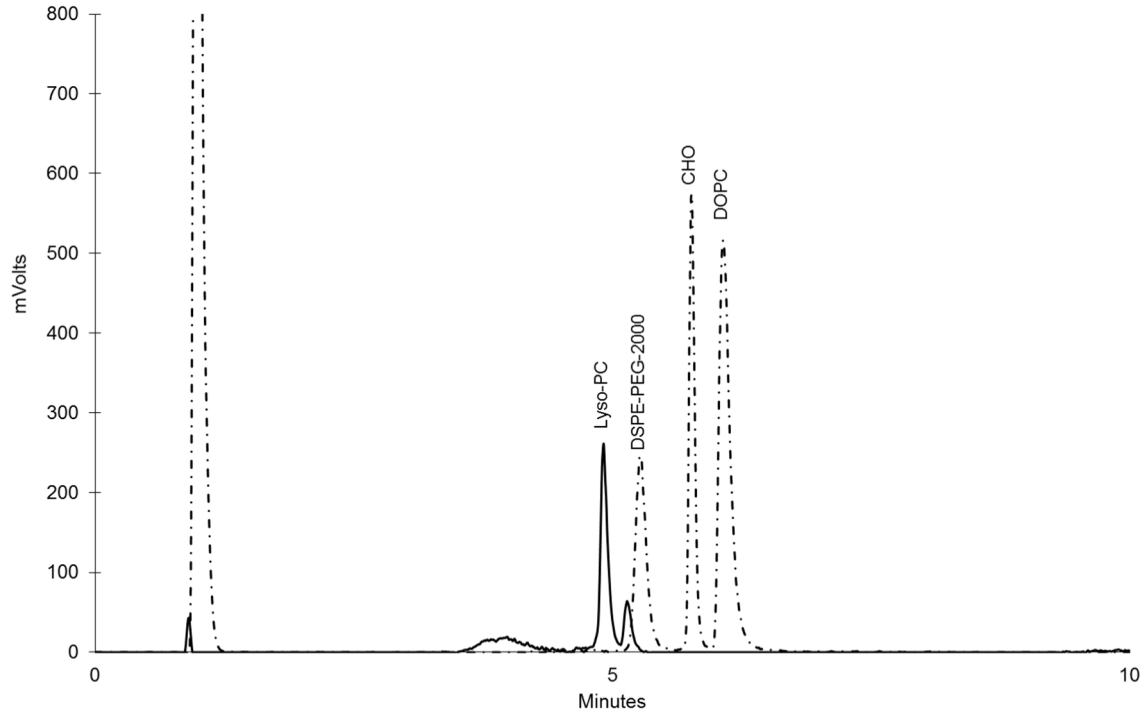

Figure 2: The chromatogram shows the detection of the Lysophosphatidylcholin (Lyso-PC) standard (solid line) in comparison to a normal liposomal formulation (dotted line) (Baseline subtracted).

The exposure of a liposomal formulation composed of DSPE-PEG-2000, CHO, and DOPC to 0.1N NaOH or 0.1N HCl induced a hydrolysis for both phospholipids. The exposure to 0.1N NaOH led to a complete hydrolysis of DOPC and DSPE-PEG-2000. In the HCl-stressed sample DOPC was still detectable, in addition to a new peak that appeared, which was not further analyzed. In contrast to that the exposure to 3% H_2O_2 or 50°C did not induce further degradation products within the time period of 24 h (Figure 3). A further differentiation of the degradation products was not analyzed.

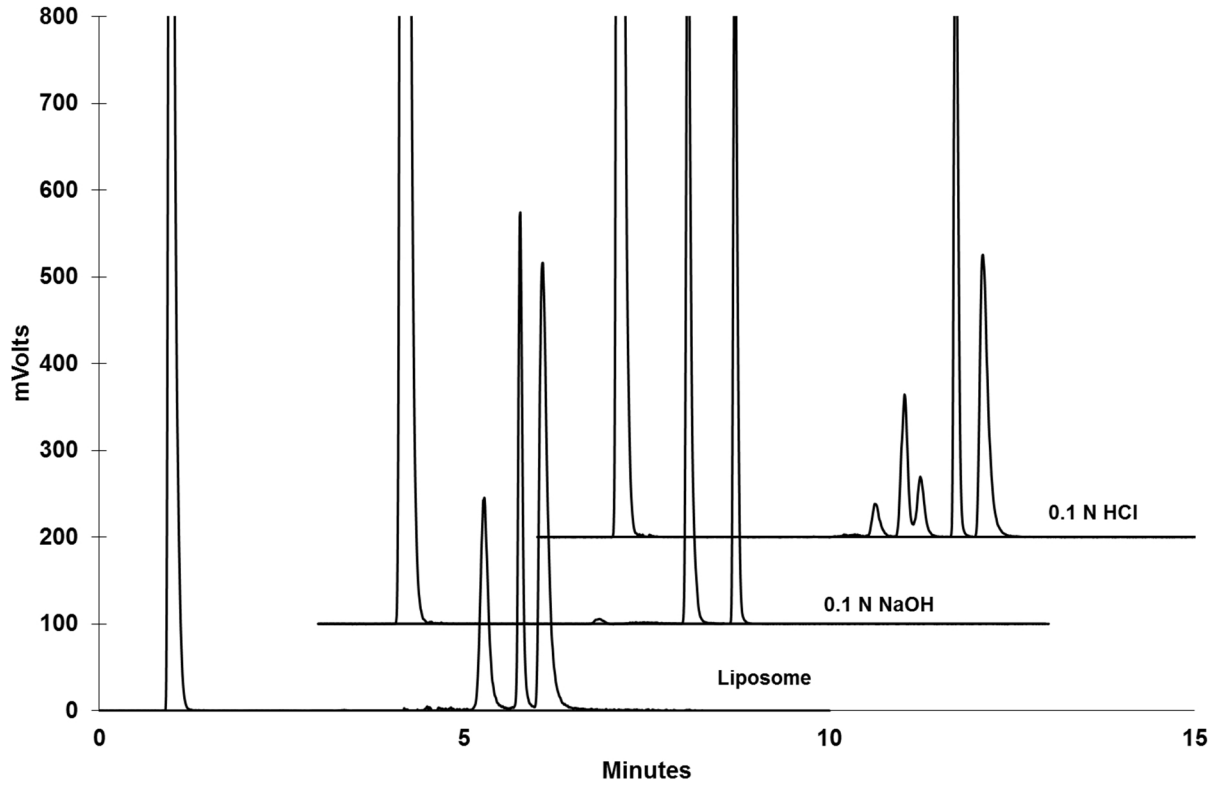

Figure 3: Liposomal formulations composed of DSPE-PEG-2000, CHO and DOPC (solid line) were exposed to 0.1N NaOH , 0.1N HCl , 3% H_2O_2, and 50°C (data not shown) for 24 h and compared with a non-stressed sample . The exposure to 0.1N NaOH led to a complete hydrolysis of DSPE-PEG-2000 and DOPC. The exposure to 0.1N HCl showed a new unknown peak, but DSPE-PEG-2000 and DOPC were not completely hydrolyzed to their lysoforms. Neither the exposure to with 3% H_2O_2 nor the exposure to 50°C for 24 h showed any degradation products.

Application to a liposomal preparation with surface immobilized peptide

The preparation of so called targeted formulations was a multistep process. These multi-step processes required control on the concentrations of desired functionalized PEG lipid and the ligand immobilized to it over the sequence of operations. In the ethanol injection method, a phospholipid solution was injected into a perpendicularly flowing aqueous phase applied by a T-shaped stainless steel device with defined geometry. The dilution of the ethanol led to a controlled precipitation of the lipids at the injection site, which subsequently rearranged to form liposomes [21, 22]. The removal of ethanol followed directly after the preparation and was

performed mostly by dialysis. Critical steps of lipid loss could be due to adsorption effects on material surfaces during the ethanol injection step. In addition to that the dialysis process might especially change the concentration of a component. Either due to adsorption to the dialysis membrane, by simple removal of lipids, which were not completely incorporated into the lipid bilayer, or due to dilution effects. To control these preparation steps, different placebo formulations were screened regarding the retention of the PEGylated component during the whole preparation process.

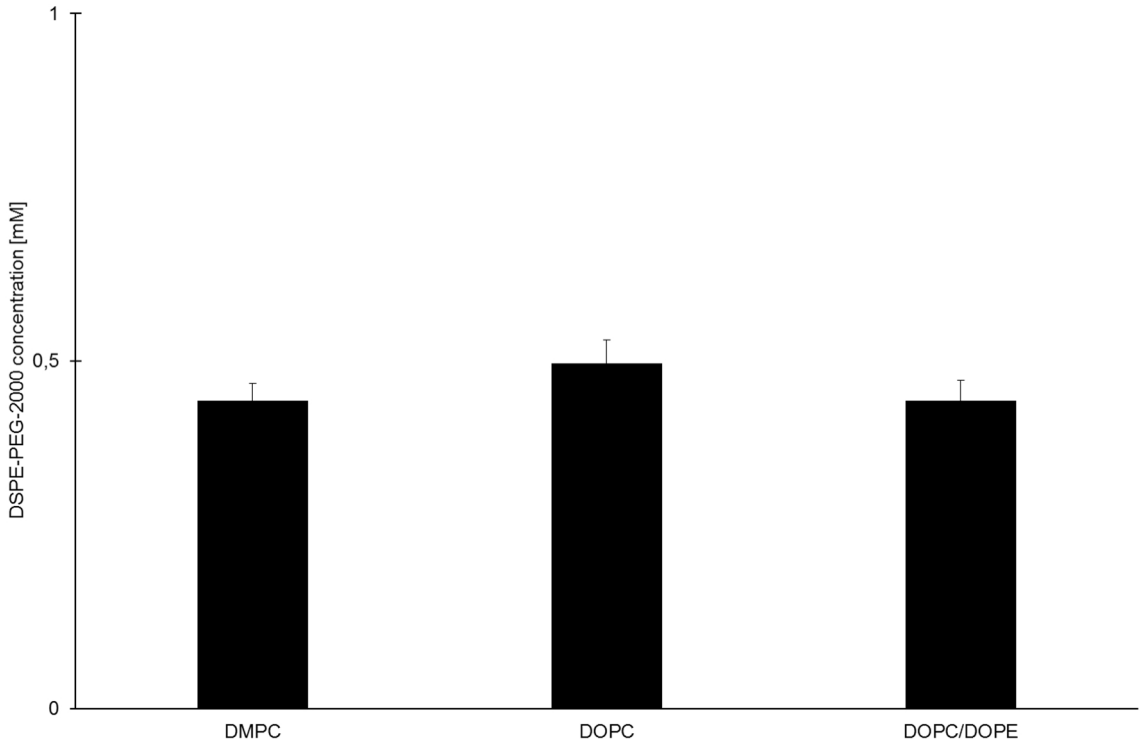

Figure 4: The graph showed the concentration of DSPE-PEG-2000 in three different liposomal placebo formulations after dialysis, which were performed with a cutoff of 50 kDa and three buffer changes over a time period of 5 hours. All formulations were composed of the main phospholipid or phospholipid mixture DMPC , DOPC or DOPC and DOPE, cholesterol, and the PEGylated lipid (DSPE-PEG-2000) with the molar ratio of 60:35:5 for the DMPC and DOPC liposomes and with a molar ratio of 30:30:35:5 for the phospholipid mixture of DOPC and DOPE.
(Mean ± standard deviation (SD), n=3).

Figure 4 displays the measured concentration of the DSPE-PEG-2000 after dialysis. The formulation composed of DOPC, CHO, and DSPE-PEG-2000 could maintain the initial content of the PEGylated component over the purification process, whereas the two other formulations showed a minimal loss of lipid. The formulation composed of DOPC as the main phospholipid was chosen for further analysis. The described method was applied to two different preparation processes for such targeted formulation. Besides the ethanol injection method, the lipid-film-hydration was used as it is an approved method for the preparation of liposomes [23, 24].

In both cases the formation of targeted liposomal formulations required additional steps compared to the "regular" preparation procedure. The addition of ligand could lead to further changes in lipid composition.

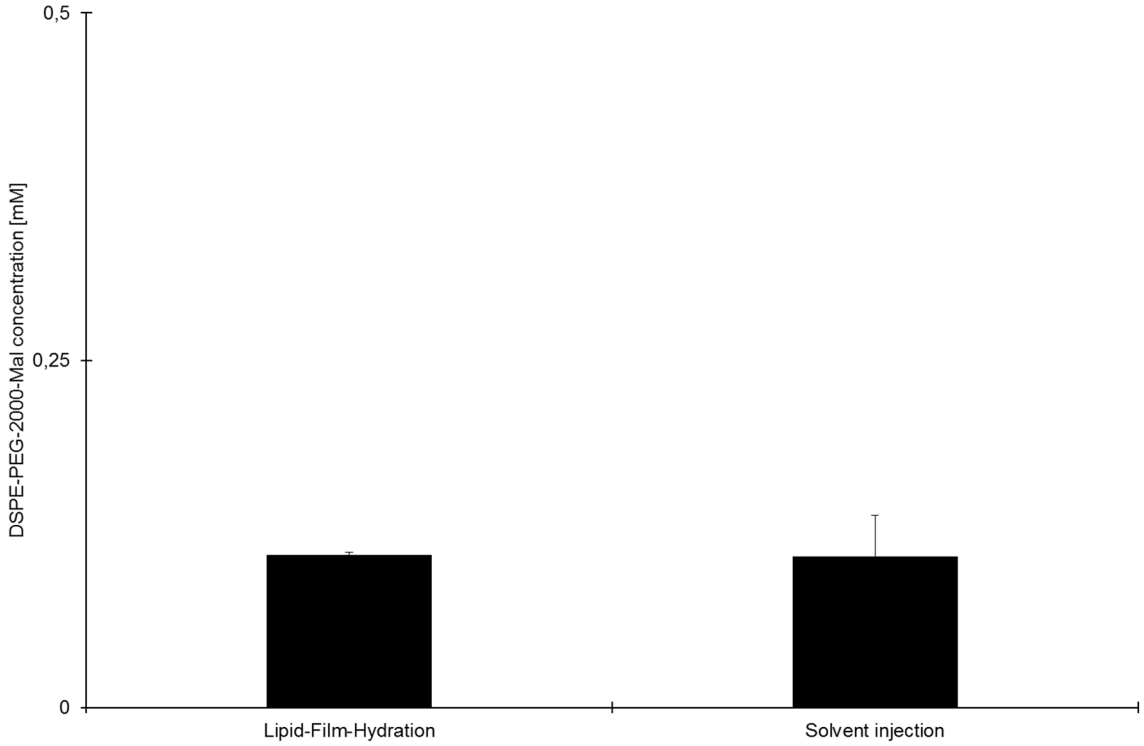

Figure 5 depicts the comparison of two preparation methods for targeted liposomal formulations, regarding the amount of DSPE-PEG-2000-Mal in the final formulation of a liposome composed of DOPC, CHO and DSPE-PEG-2000-Mal. Statistical data analyses were performed using the Student's t-test with $p < 0.001$ as level of significance. (Mean ± SD, n=3), ns= not significant.

Figure 5 depicts the comparison of both preparation methods regarding the amount of DSPE-PEG-2000-Mal in the final formulation of a liposome composed of DOPC, CHO and DSPE-PEG-2000-Mal. In both formulations only an amount of 0.1 mM DSPE-PEG-2000-Mal could be detected from an initial amount of 0.5 mM. The performed t-test indicated no statistically significant difference in the results of the two preparation methods. In contrast the results of the non-functionalized liposomes were different to the functionalized liposomes ($p<0.001$). Surprisingly, the functionalized formulations could not maintain the initial concentration of DSPE-PEG-2000-Mal. As both preparation methods yielded similar results, we hypothesized that the dramatic loss of lipid could be due to the interaction of the targeting ligand with the liposomal formulation. With the aid of this HPLC method different phospholipids and preparation methods could be analyzed regarding their usage in the field of functionalized liposomal formulations. The ligand density could be calculated with the actual amount of functional lipid and was not based on theoretical considerations.

4. Conclusion

The described method allowed direct tracking of all compounds during each step of liposome preparation. It provided information about the actual composition of liposomes. Especially during the purification as well as during the coupling of ligands, the individual loss of lipids could change the composition of liposomes. With regard to functionalized lipids where the concentration of lipid is important for further coupling reactions, the described method gave evidence about the correct concentration. The loss of lipid during preparation could be due to a variety of reasons. The method provided a qualitative statement of the actual amount in final formulations and allowed a deeper insight into peptide-functionalized liposomes.

Reference list

1. Edwards, K.A. and A.J. Baeumner, *Analysis of liposomes.* Talanta, 2006. 68(5): p. 1432-1441.
2. Immordino, M.L., F. Dosio, and L. Cattel, *Stealth liposomes: review of the basic science, rationale, and clinical applications, existing and potential.* International Journal of Nanomedicine, 2006. 1(3): p. 297-315.
3. Knudsen, N.Ø., et al., *Design of cyclic RKKH peptide-conjugated PEG liposomes targeting the integrin α2β1 receptor.* International Journal of Pharmaceutics, 2012. 428(1–2): p. 171-177.
4. Tao, Y., J. Han, and H. Dou, *Brain-targeting gene delivery using a rabies virus glycoprotein peptide modulated hollow liposome: bio-behavioral study.* Journal of Materials Chemistry, 2012. 22(23): p. 11808-11815.
5. Berchel, M., et al., *Functionalized phospholipid molecular platform: use for production of cationic fluorescent lipids.* European Journal of Organic Chemistry, 2014. 2014(5): p. 1076-1083.
6. Mulder, W.J.M., et al., *Lipid-based nanoparticles for contrast-enhanced MRI and molecular imaging.* NMR in Biomedicine, 2006. 19(1): p. 142-164.
7. Park, S. and R.A. Durst, *Immunoliposome sandwich assay for the detection of Escherichia coli O157: H7.* Analytical biochemistry, 2000. 280(1): p. 151-158.
8. Nobs, L., et al., *Current methods for attaching targeting ligands to liposomes and nanoparticles.* Journal of pharmaceutical sciences, 2004. 93(8): p. 1980-1992.
9. Marqués-Gallego, P. and A.I.P.M. de Kroon, *Ligation strategies for targeting liposomal nanocarriers.* BioMed research international, 2014. 2014.
10. Hermanson, G.T., *Chapter 3 - The Reactions of Bioconjugation*, in *Bioconjugate Techniques (Third edition)*. 2013, Academic Press: Boston. p. 229-258.
11. Kumar, P., et al., *Transvascular delivery of small interfering RNA to the central nervous system.* Nature, 2007. 448(7149): p. 39-43.
12. Cheng, T.-L., et al., *Analytical measurement of PEGylated molecules.* Bioconjugate chemistry, 2012. 23(5): p. 881-899.
13. Megoulas, N.C. and M.A. Koupparis, *Twenty years of evaporative light scattering detection.* Critical reviews in analytical chemistry, 2005. 35(4): p. 301-316.
14. Aruda, W.O., S. Walfish, and I.S. Krull, *Review and optimization of linearity and precision in quantitative HPLC-ELSD with chemometrics.* LC GC North America, 2008. 26(10).
15. Fox, C.B., et al., *Charged aerosol detection to characterize components of dispersed-phase formulations.* Advances in colloid and interface science, 2013. 199: p. 59-65.
16. Mathews, B.T., et al., *Improving quantitative measurements for the evaporative light scattering detector.* Chromatographia, 2004. 60(11-12): p. 625-633.
17. Shibata, H., C. Yomota, and H. Okuda, *Simultaneous Determination of Polyethylene Glycol-Conjugated Liposome Components by Using Reversed-Phase High-Performance Liquid Chromatography with UV and Evaporative Light Scattering Detection.* AAPS PharmSciTech, 2013. 14(2): p. 811-817.
18. Zhong, Z., Q. Ji, and J.A. Zhang, *Analysis of cationic liposomes by reversed-phase HPLC with evaporative light-scattering detection.* Journal of pharmaceutical and biomedical analysis, 2010. 51(4): p. 947-951.
19. Eom, H.Y., et al., *Comparison between evaporative light scattering detection and charged aerosol detection for the analysis of saikosaponins.* Journal of Chromatography A, 2010. 1217(26): p. 4347-4354.
20. Bergstrand, N., *Liposomes for Drug Delivery: from Physico-chemical Studies to Applications*. 2003, Uppsala University.

21. Batzri, S. and E.D. Korn, *Single bilayer liposomes prepared without sonication.* Biochimica et Biophysica Acta (BBA) - Biomembranes, 1973. 298(4): p. 1015-1019.
22. Schubert, M.A. and C.C. Müller-Goymann, *Solvent injection as a new approach for manufacturing lipid nanoparticles-evaluation of the method and process parameters.* European journal of pharmaceutics and biopharmaceutics : official journal of Arbeitsgemeinschaft fur Pharmazeutische Verfahrenstechnik e.V, 2003. 55(1): p. 125-131.
23. J.S. Dua, P.A.C.R., Dr. A.K. Bhandari, *LIPOSOME: METHODS OF PREPARATION AND APPLICATIONS.* International Journal of Pharmaceutical Studies and Research, 2012. 3(2): p. 14-20.
24. Torchilin, V. and V. Weissig, *Liposomes: a practical approach*. 2003: Oxford University Press.

Chapter 5

Determination of the activity of maleimide-functionalized phospholipids during preparation of liposomes

This chapter was published as: Oswald, M.; Geissler, S.; Goepferich, A., International Journal of Pharmaceutics 2016, 514 (1), 93-102.

Abstract

Numerous examples exist in the literature for the use of maleimide-thiol-reactions in the area of functionalized nanoparticles. Although the hydrolysis tendency of maleimides is well-known, qualitative and quantitative information on the stability and reactivity of maleimide groups during preparation and in final formulations are missing. This is surprising, since hydrolysis of maleimides prevents nanoparticle functionalization and results in an increase of negative surface charge due to the hydrolysis product maleic acid. In this study we investigated the stability of 1,2-distearoyl-sn-glycero-3-phosphoethanolamine-N-[maleimide-2000] (DSPE-PEG-2000-Mal) during the preparation of liposomes via two common preparation methods, which can be distinguished by the insertion of DSPE-PEG-2000-Mal during or after the liposome formation process (pre-insertion and post-insertion process). The liposomes prepared by the pre-insertion method had 63% active maleimide groups remaining on their surface. The activity decreased dramatically during the purification process down to 32%. The preparation by post-insertion showed minimal effects with regard to maleimide activity. 76% of maleimide groups were active and therefore available for coupling reaction. By identifying active maleimide groups on the surface of the final formulations, the presented work revealed the dramatic impact of preparation methods on the activity of maleimide groups.

1. Introduction

The maleimide-thiol reaction gained great popularity in the field of surface modification of drug delivery systems (DDS) [1, 2] and bioconjugation of drugs to antibodies [3]. Maleimides react with thiols resulting in the formation of stable thioether bonds. The specificity to thiols, fast aqueous reaction kinetics and mild reaction conditions explain their broad pharmaceutical application in DDS functionalization [4, 5]. A great pitfall however is the pH-dependent hydrolysis of maleimides, which is often neglected. With increasing pH (pH >8), maleimide groups are hydrolyzed to maleic acid, a ring-open hydrolysis product that lacks an electrophile carbon and is, therefore, unable to react with nucleophile thiols [4, 6-8]. This hydrolysis carries two inherent risks for functionalized DDS, as the DDS does not obtain the desired functionalization but furthermore, resulting in an increase of free carboxyl groups on the outer surface. This fact becomes especially critical in active targeting strategies, where the functionalization should enable a controlled and specific uptake into cells. The absence of ligands and increase of negative charge on the outer surface can result in unspecific uptake pattern of nanoparticles [9, 10]. Although the risk of the hydrolysis of final functionalized DDS is intensively discussed in the literature, the impact of the preparation on maleimide activity is completely overlooked [11, 12]. Facing the risk of maleimide hydrolysis during preparation, the use of maleimide functionality for liposome functionalization is an interesting example. The complex composition of liposomal formulations as well as the multi-step character of the preparation are critical parameters with potential impact on the activity of maleimides. In that regard, we had a closer look at two common functionalization methods for liposomes modified with maleimide-containing PEGylated phospholipid 1,2-distearoyl-sn-glycero-3-phosphoethanolamine-N-[maleimide-2000] (DSPE-PEG-2000-Mal). We investigated the maleimide acitivty of DSPE-PEG-2000-Mal during preparation of liposomes by solvent-injection and their functionalization via pre-insertion or post-insertion. The distinct difference feature between both methods is the insertion of DSPE-PEG-2000-Mal, which is either during (pre-insertion) or after liposome formation (post-insertion) [13]. Both methods have potential risks with respect to maleimide activity. Therefore, tracking maleimide activity during the complex preparation processes was the main purpose of our studies.

2. Material and methods

2.1. Material

1,2-dioleoyl-sn-glycero-3-phosphocholine (DOPC), 1,2-dimyristoyl-sn-glycero-3-phosphocholine (DMPC), 1,2-distearoyl-sn-glycero-3-phosphoethanolamine-N-[amino-2000] (DSPE-PEG-2000) were purchased from Lipoid GmbH (Ludwigshafen, Germany). Cholesterol (CHO), Ethylenediaminetetraacetic acid (EDTA) and Dulbecco´s phosphate buffered saline (PBS) (D1408) were obtained from Sigma-Aldrich (St. Louis, USA). 1,2-distearoyl-sn-glycero-3-phosphoethanolamine-N-[maleimide-2000] (DSPE-PEG-2000-Mal) was purchased from Avanti Polar Lipids (Alabaster, USA). Tris(2-carboxyethyl)phosphine hydrochloride (TCEP) was purchased from AMRESCO LLC (Solon, USA). Rabies virus glycopeptide (RVG) and EPRNEEK peptide, both modified with terminal sulfhydryl-groups and supposed to enable blood-brain barrier targeting, were used as model ligands (Kumar, Wu et al., 2007; Liu, He et al., 2014). The peptides were modified with an additional cysteine on the C-terminus and were synthesized by Novo Nordisk A/S (Bagsvaerd, Denmark). Float-a-lyzer G2 (50kDa) was purchased from SPECTRUM® LABORATORIES Inc. (Rancho Dominguez, USA). Methanol, isopropanol (HPLC grade), ethanol, dichloromethane, ammonium acetate, L-cysteine, disodium hydrogen phosphate, sodium dihydrogen phosphate and 2,2´Dinitro-5,5´-dithio-dibenzoic acid (DTNB), also referred to as Ellman´s reagent, were obtained from Merck KGaA (Darmstadt, Germany). Purified water was produced by a Millipore-Milli-Q integral water purification system (Merck KGaA, Darmstadt, Germany).

2.2. Methods

2.2.1 Preparation of functionalized liposomes by pre-insertion method

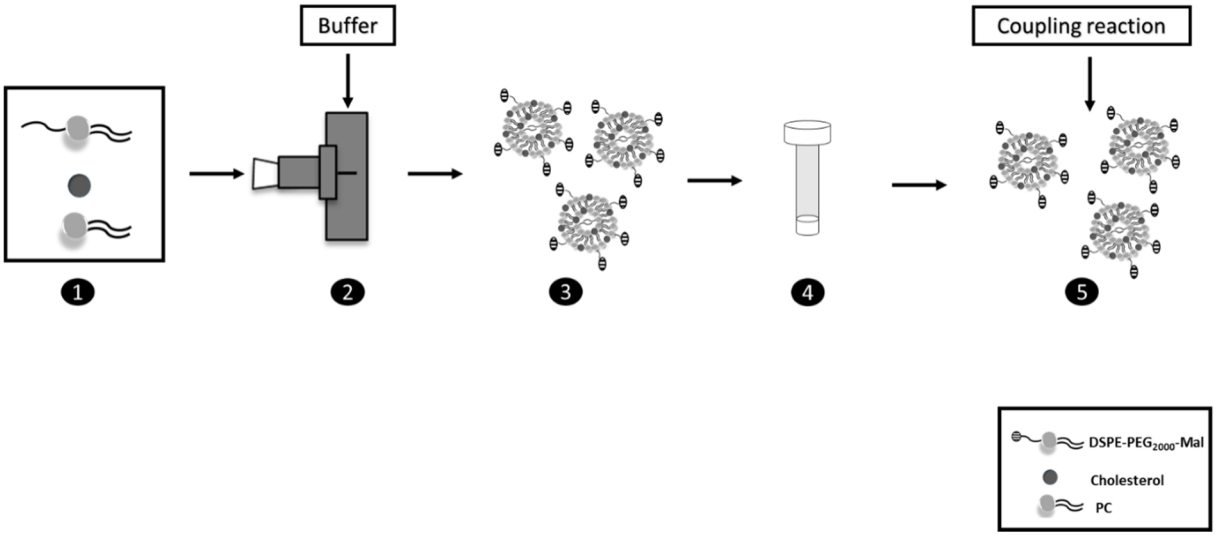

Figure 1: Graphic illustration of the pre-insertion method. Liposomes were prepared by solvent injection method. DSPE-PEG-2000-Mal, DMPC and CHO were dissolved in ethanol with a total lipid concentration of 77 mM (step 1). The ethanol solution was injected at a flow rate of 12 ml/min into a stream of PBS (pH 7.0-7.5) with a flow of 80 ml/min (step 2), resulting in a total lipid concentration of 10 mM. The dilution of the ethanol led to a controlled precipitation of the lipids at the injection site, which were subsequently rearranged to form liposomes (step 3). Removal of solvent was carried out directly after preparation with a cut-off of 50.000 MWCO over 5 h and three buffer changes (step 4). The coupling of ligand was performed after a purification step (step 5).

The preparation of ligand-functionalized liposomal formulations was a multistep process (Figure 1, Table 1). Liposomes were prepared using a solvent injection method [14]. DSPE-PEG-2000-Mal, DMPC and CHO were diluted in ethanol with a total lipid concentration of 77 mM (step 1). The ethanol solution was injected at a flow rate of 12 ml/min into PBS (pH 7.0 - 7.5) with a flow of 80 ml/min and resulting in a total lipid concentration of 10 mM (step 2). Dilution with ethanol led to a controlled precipitation of the lipids at the injection site, which were subsequently rearranged to form liposomes (step 3) [14, 15]. According to the common protocol for the preparation of plain liposomes, the removal of solvent was carried out directly after preparation with a cut-off of 50.000 MWCO over 5 h and three buffer changes (step 4). The coupling reaction was performed with a molar ratio of 2:1 peptide to DSPE-PEG-2000-Mal for 1 h at room temperature under nitrogen atmosphere at pH of 7.0 (step 5). The model peptide RVG was reduced prior to the coupling reaction with TCEP (10-fold molar excess).

Table 1: Theoretical composition of functionalized liposome formulation, prepared by pre-insertion.

Compound	Molar ratio (mol/mol %)	Initial total lipid concentration [mM]	Final total lipid concentration [mM]	Final peptide concentration [mM]
DMPC	0.6	46.2	6	
CHO	0.35	26.95	3.5	
DSPE-PEG-2000-Mal	0.05	3.85	0.5	
Peptide	0.05			0.5

2.2.2 Preparation of functionalized liposomes by post-insertion method

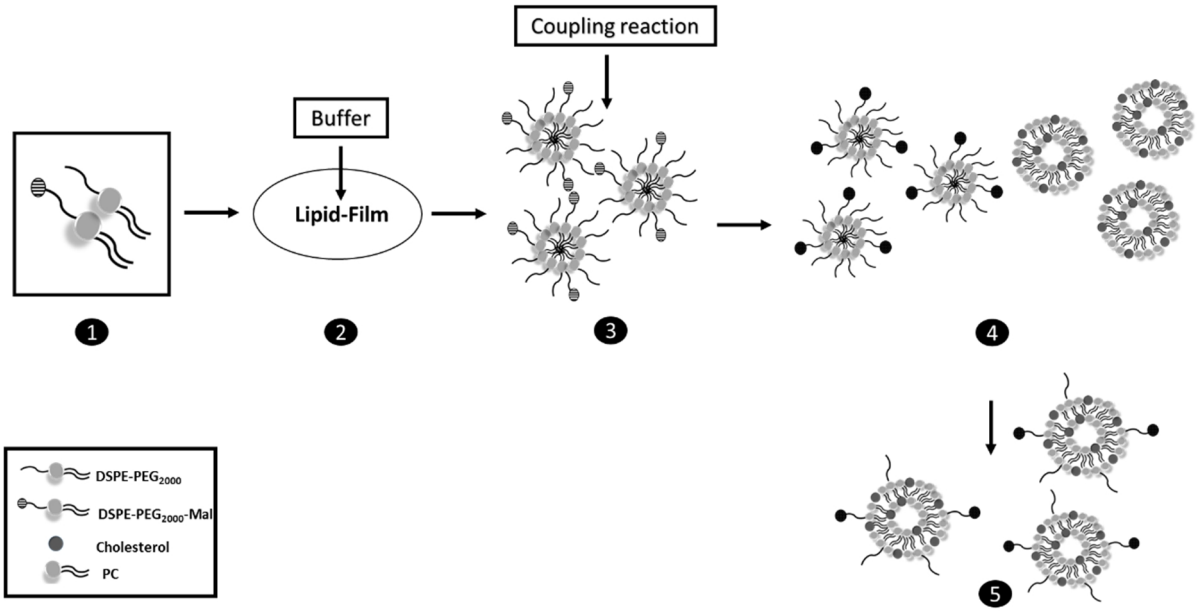

Figure 2: Graphic illustration of the post-insertion method. DSPE-PEG-2000-Mal and DSPE-PEG-2000 were dissolved in methylene chloride in a molar ratio of 1:4 with total lipid concentration of 2 mM (step 1). A lipid-film was generated under nitrogen stream by the removal of solvent (step 2). The micelles were formed by the hydration of the lipid-film with PBS to 2 mM at 40°C for 5 minutes in a water bath. Peptide was dissolved in PBS and reduced with TCEP prior to coupling reaction (10-fold molar excess). Peptide solution was added to the micellar solution and incubated for 1h at room temperature at pH 7.00 with a molar ratio of 2:1 peptide to DSPE-PEG-2000-Mal (step 3). The micelles were inserted into preformed liposomes composed of DOPC and CHO for one hour at 65°C in a water bath (step 4, 5).

Liposomes composed of DOPC and CHO were prepared according to the protocol described in 2.2.1 by solvent injection method and concentrated to a final total lipid concentration of 20 mM by centrifugal filtration (Figure 2, Table 2). DSPE-PEG-2000-Mal and DSPE-PEG-2000 were dissolved in methylene chloride in a molar ratio of 1:4 with total lipid concentration of 2 mM (step 1). A lipid-film was generated under nitrogen stream by the removal of solvent (step 2). The micelles were formed by hydration of the lipid-film with PBS to a concentration of 2 mM

at 40°C for 5 minutes in a water bath. The model peptide EPRNEEK was dissolved in PBS and reduced with TCEP prior to coupling (10-fold molar excess). Peptide solution was added to the micellar solution and incubated for 1 h at room temperature at pH 7.00 with a molar ratio of 2:1 peptide to DSPE-PEG-2000-Mal (step 3). The micelles were finally inserted into preformed liposomes composed of DOPC and CHO for 1 h at 65°C in a water bath (step 4, 5) [16].

Table 2: Theoretical composition of targeted liposome formulation, prepared by post-insertion.

Compound	Molar ratio (mol/mol %)	Initial total lipid concentration [mM]	Final total lipid concentration [mM]	Final peptide concentration [mM]
DOPC	0.6	23.1	6	
CHO	0.4	15.4	4	
DSPE-PEG-2000-Mal	0.01	0.4	0.1	
DSPE-PEG-2000	0.04	1.6	0.4	
Peptide	0.01			0.1

2.2.3 Size and zeta potential determination

Size distribution and zeta potential (ZP) were determined by dynamic light scattering (DLS) and Laser Doppler electrophoresis (LDE) using a Zetasizer Nano ZS Malvern Instruments (Worcestershire, UK), equipped with a helium neon laser (λ= 633 nm). To determine size distribution, samples were measured undiluted three times at 25 ± 0.1°C with fixed position (4.65 nm) at a detection angle of 173° (back scatter). Data was analyzed via cumulants fit. For the determination of ZP, samples were diluted 1:10 with Milli-Q-water and measured three times at 25°C. ZP was calculated by Smoluchowski's equation from the electrophoretic mobility of liposomes.

2.2.4 Quantification of maleimide functionalized phospholipids: DSPE-PEG-2000-Mal

To determine the impact of the purification process with regard to the amount of active maleimide groups the formulation was analyzed by HPLC and indirect Ellman´s assay during preparation. The total amount of DSPE-PEG-2000-Mal, the sum of active and inactive DSPE-PEG-2000-Mal molecules was obtained by HPLC analysis (see 2.2.4.1), whereas active amount was determined by indirect Ellman´s assay (see 2.2.4.2).

2.2.4.1 Total amount of maleimide functionalized phospholipid (DSPE-PEG-2000-Mal)

Samples of each preparation step were analyzed by RP-ELSD-HPLC using a recently published method [17]. In brief, the micellar and liposomal samples were dissolved in a mixture of isopropanol and water then analyzed on an Agilent 1260 HPLC system equipped with an ELSD. Eluent A was composed of methanol and water in a volume ratio of 40:60 with 10 mM ammonium acetate and pH-value of 6.4, which was adjusted with 1 mM acetic acid. Eluent B was composed of methanol and isopropanol in a ratio of 10:90 with 10 mM ammonium acetate. Separation was performed on a Kinetex Core shell column (C18, 2.6 u, 100Å, 100 x 3 mm, Phenomenex, Aschaffenburg).

2.2.4.2 Active amount of maleimide functionalized phospholipid (DSPE-PEG-2000-Mal)

The active maleimide groups were analyzed by an indirect Ellman´s assay [18]. The reagent solution was prepared by dissolving Ellman´s reagent in reaction buffer, 0.1 M sodium phosphate containing 1 mM EDTA with pH 8.00, to 4 mg/ml. The maleimide-containing samples were incubated with a cysteine solution of known concentration (5-fold molar excess) at room temperature and pH 7.00. Free thiol-groups reacted with maleimides to form a stable thioether-linkages. After 30 minutes the amount of non-reacted thiol groups were analyzed by Ellman´s assay. 250 µl of the sample were added to 50 µl Ellman´s reagent (4 mg/ml) diluted in 2.5 ml reaction buffer and incubated for 15 minutes at room temperature at pH 8.00. Ellman´s reagent forms a mixed disulfide and a colored product with free thiol-groups of unreacted cysteine (Figure 3). The reaction was followed spectrophotometrically at 412 nm. The amount of active maleimides was calculated from the amount of unreacted cysteine.

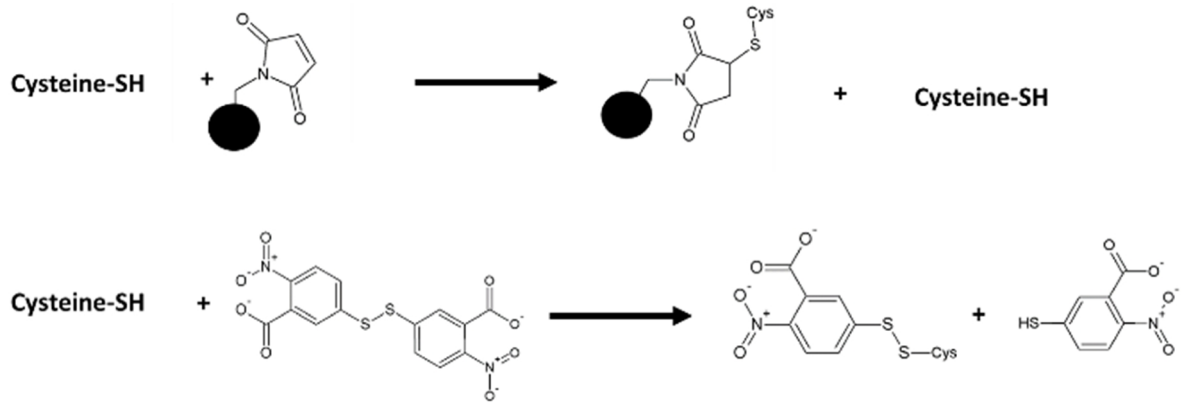

Figure 3: Maleimide activity was determined by an indirect Ellman´s assay. The sample was incubated with a known amount of cysteine. Free thiol-groups reacted with maleimides to form a stable thio-ether linkage. The amount of active maleimide was calculated from the amount of unreacted cysteines, which were determined by the incubation with Ellman´s reagent, forming a mixed disulfide and the colored product. The reaction can be followed spectrophotometrically at 412 nm.

2.2.5 Activity of DSPE-PEG-2000-Mal at different pH values

As proof of concept, DSPE-PEG-2000-Mal was dissolved in PBS (0.5 mM). The pH values were set to pH 7.0 and 9.5. Maleimide activity was analyzed over a time period of 24 h at room temperature. Sampling was carried out after 5 and 24 h. The time-point directly after the setting of the pH-values was defined as t= 0 h. For analysis, samples of the two solutions were treated according to the above mentioned instructions.

2.2.6 Statistical analysis

All values are expressed as means ± standard deviation of three individual performed experiments. Statistical data analyses were performed using Student's t-test with $p < 0.05$ as level of significance. All tests were performed using the statistical software SigmaPlot (Systat Software, San Jose, CA).

3. Results and discussion

The unmasking of inherent risks during preparation of maleimide functionalized liposomes with respect to maleimide activity was the main objective of the presented work. Declared goals were the development of a quick and easy method for the determination of active maleimide groups, as well as the application of this method during the preparation of liposomes. RP-HPLC was used for the determination of the total lipid content. In addition to that the formation process and the integrity of liposomes were followed by changes in size and surface potential.

3.1. Evaluation of maleimide activity

The identification of an assay for the quick and reliable assessment of maleimide activity was of high interest. Several methods were investigated for their suitability. The coupling reaction could be directly monitored spectrophotometrically by assessing the decrease in absorbance at 300 nm, which is due to the disappearance of the double bond upon the nucleophile addition of thiols [4]. However, this approach was not further followed since high quantities of thiols are needed and the monitoring might be interfered by the double bonds of CHO and DOPC that are also part of the liposomal composition. Using the reactivity of maleimide towards thiol-containing compounds at neutral pH-values is another strategy to quantify maleimide activity. Instead of the thiol-containing peptide of choice, thiol-containing fluorophores, like SAMSA (5-((2-(and-3)-S-(acetylmercapto)succinoyl)amino)fluorescein), can be used as reaction partner. A drawback however, are the compulsory washing steps to guarantee that only coupled fluorophores are detected. M. Dreher and H. Hirsch described the indirect Ellman´s reaction [19], where the maleimide-containing sample was incubated with a thiol-containing compound. Since the reaction stoichiometry is 1:1, the amount of active maleimides can be calculated from the amount of non-reacted thiols, which can be detected spectrophotometrically upon reaction with Ellman´s reagent. In contrast to the other methods, this approach is ideal for fast in-process controls during preparation. In addition to that the indirect Ellman´s assay was successfully used for the assessment of coupling efficiencies on polystyrene nanoparticles [20]. Therefore, there was a tremendous motivation to apply it to the liposomal preparation process. As proof of concept 0.5 mM DSPE-PEG-2000-Mal solutions were incubated at pH 7.0 and pH 9.5 over 24 h (Figure 4). This time period was chosen in accordance to published protocols for maleimide-thiol-reactions [2]. Hydrolysis to the unreactive maleic acid is pH-dependent and occurs preferably at higher pH values [4]. The DSPE-PEG-2000-Mal solution at pH 7.0 showed an activity of 100 ± 0.6% after 24 h. As expected all maleimide groups remained stable under these

conditions. In contrast to that the DSPE-PEG-2000-Mal solution with pH 9.5 showed a decrease of the activity down to 18 ± 0.8% ($p \leq 0.001$) and 26 ± 4.5% ($p \leq 0.001$) after 5 and 24 h respectively. This reflects the fact that under alkaline conditions, maleimides undergo hydrolysis to the unreactive, ring-open form [4].

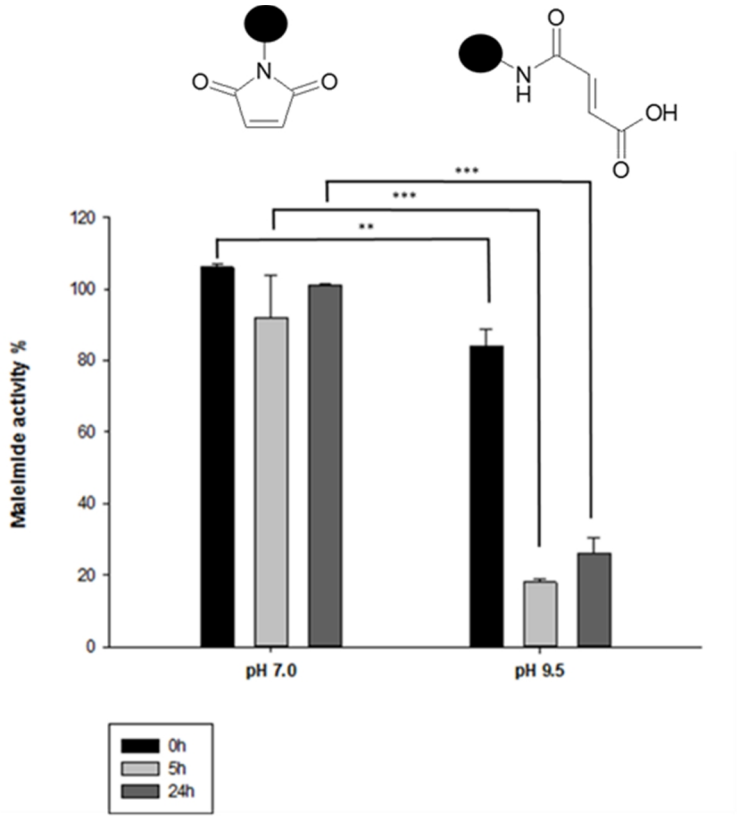

Figure 4: Maleimide activity of a DSPE-PEG-2000-Mal solution in PBS at different pH-values (7 and 9.5) analyzed by the indirect Ellman´s assay. The solution at pH 7.0 showed only minor decrease of activity whereas the solution at pH 9.5 showed a massive loss of activity due to hydrolysis of the maleimide group. (Mean ± SD, n=3). Statistical difference indicated by: *$p \leq 0.05$, ** $p \leq 0.01$, *** $p \leq 0.001$.

3.2 Application to different preparation methods of functionalized liposomes

3.2.1 Functionalized liposomes prepared by pre-insertion method

The preparation of functionalized liposomes by pre-insertion is depicted in Figure 1. The solvent-injection is an approved method for the preparation of liposomes [14]. The liposomes are directly formed by the injection of a lipid solution into an excess of buffer. The results are summarized in Table 3. The unmasking of the critical steps with regard to maleimide activity were achieved by analysis of size, surface charge, total amount of DSPE-PEG-2000-Mal and maleimide activity before (step 3) and after purification (step 4). The liposomes composed of DMPC, CHO and DSPE-PEG-2000-Mal had a size of 192 ± 5 nm with PDI of 0.20 before

purification (step 3) and 139 ± 5 nm with PDI of <0.25 after purification (step 4). The purification of liposomes was characterized by a decrease in size due to the removal of ethanol. Ethanol interacts with phospholipid membranes [21] and its removal results in a reorganization of the phospholipid membrane and causes the change in size. The surface charge was -12.8 ± 0.3 mV before purification (step 3) and -14.7 ± 1.3 mV after purification (step 4). The monitoring of surface charge plays a significant role for maleimide functionalized DDS. The hydrolysis causes a change of surface functionalization due to the formation of free carboxyl groups. This was shown by Pereira et al., who analyzed surface functionalized quantum dots by capillary electrophoresis. The migration time of quantum dots carrying hydrolyzed maleimide groups on the outer surface was similar to the migration time of quantum dots carrying free carboxyl groups [22]. Therefore, the increase of negative charge during the purification can provide a first hint of hydrolyzed maleimide groups on the outer surface. Nevertheless, further analysis was needed, as surface charge of pre-inserted liposomes can also be affected by changes in buffer system. The formulation was further analyzed by HPLC and indirect Ellman´s assay, to determine the impact of the purification process with regard of the amount of active maleimide groups during preparation (Figure 5). The total amount of the DSPE-PEG-2000-Mal decreased during the purification process from 0.49 ± 0.05 mM down to 0.44 ± 0.04 mM. The loss of lipid during purification could be explained by adsorption effects of the dialysis membrane, removal of incompletely incorporated lipids which were not completely incorporated or due to dilution effects [17]. A specific focus was on the active amount of maleimides determined by indirect Ellman´s assay, which was 63% of the total amount ($p \leq 0.01$). In contrast to HPLC analysis, where the liposomal bilayer is destroyed prior to analysis, the investigation of active maleimide groups by indirect Ellman´s assay is directly examined on the surface of the intact liposome. Therefore, this result could provide insights into the orientation of functionalized PEG-chains at the liposomal bilayer. The PEGylated phospholipids are part of the organic lipid phase, which is injected into the aqueous phase. During this process the PEG-chain ends carrying the maleimide groups can be oriented towards the liposome core as well as towards the outside [13]. The indirect Ellman´s assay detected 63% of the initial maleimide groups. These results reveal a maleimide distribution of approximately two-thirds on the surface, available for conjugation, and one-third towards the inner liposome´s core. Although the analysis was performed with intact liposomes, the diffusion of Ellman´s reagent into the inner core could cause false-positive results. However, since Ellman´s reagent is hydrophilic and is negatively charged at pH 8.00 its diffusion rate across the liposomal wall was assumed to be negligible.

The further decrease of activity during purification to 32% ($p \leq 0.01$) impressively showed the impact of manufacturing with respect to maleimide activity. According to the common protocol, the purification was done by dialysis over a time period of 5 h. The maleimide groups protruded from the liposomal surface and were in close contact to aqueous media, which could cause the loss of activity. In case of the pre-insertion method the purification was identified as the most critical step with respect to maleimide activity. As a consequence the coupling reaction could be performed prior to the purification step. Performing the coupling reaction prior to purification might be beneficial with regard to maleimide activity, but may enhance the creation of undesired coupling products. This fact becomes especially critical for liposomal formulations that carry a cargo. Hydrophilic cargos are encapsulated during the liposome formation process (step 3) [23]. Free and non-encapsulated cargo could compete with a ligand intended for being immobilized on the surface for targeting purposes for maleimide-thiol coupling. Therefore prior purification is of high importance. In case of the preparation of maleimide-functionalized liposomes by pre-insertion method, dialysis is not the purification method of choice due to its impact on maleimide activity and should be replaced by other purification techniques like tangential flow filtration (TFF) or gel filtration [24, 25]. Nevertheless, the impact on maleimide activity of these techniques still needs to be investigated and was not part of the presented work.

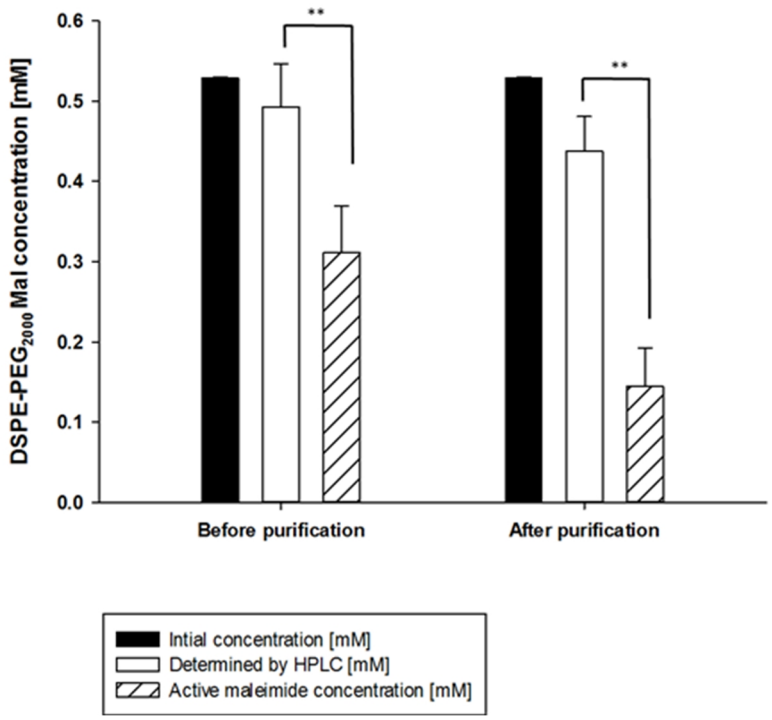

Figure 5: Comparison of theoretical amount, total amount and active amount of DSPE-PEG-2000-Mal before and after purification during liposomal preparation by pre-insertion method. Liposome was composed of DMPC, CHO and DSPE-PEG-2000 Mal. (Mean ± SD, n=3) Statistical difference indicated by: *$p \leq 0.05$, ** $p \leq 0.01$, *** $p \leq 0.001$.

Table 3: Summary of physicochemical characterization of maleimide-functionalized liposomal formulations prepared by pre-insertion method. (Mean ± SD, n=3). Determined by DLS[1], LDE[2], RP-ELSD-HPLC[3], Indirect Ellman´s assay[4].

Preparation method	Preparation step	Liposome composition	Size[1] [nm]	PDI[1]	Zeta potential[2] [mV]	Total amount of DSPE-PEG-2000-Mal[3] [mM]	Maleimide activity[4] [%]
Pre-insertion	Before purification	DMPC:CHO:DSPE-PEG-2000-Mal	192 ± 5	0.200 ± 0.003	-12.8 ± 0.3	0.49 ± 0.05	63
	After purification		139 ± 5	0.220 ± 0.006	-14.7 ± 1.3	0.44 ± 0.04	32

3.2.2 Functionalized liposomes by the post-insertion method

As an alternative to the pre-insertion method, functionalized liposomes were prepared by the post-insertion method. In contrast to the pre-insertion method, post-insertion comprises two consecutive reactions. First, micelles are formed with DSPE-PEG-2000-Mal in the presence of aqueous phase and subsequently model peptide EPRNEEK was coupled to the PEG ends. These ligand-modified micelles were then inserted in preformed liposomes [13, 26, 27]. The preparation steps are depicted in Figure 2. Micelles, composed of DSPE-PEG-2000 and DSPE-PEG-2000-Mal, were prepared prior to the coupling reaction (step 1, 2, 3). The peptide-functionalized micelles were then inserted into preformed liposomes (step 4, 5). Liposomes prepared post-insertion were again analyzed by the assessment of size, charge, total and active DSPE-PEG-2000-Mal amount to identify the critical steps of preparation (Table 4 and Figure 6-8). The liposomes, composed of DOPC and CHO, had a size of 62 ± 4 nm with PDI <0.19. These size ranges could be achieved with an initial lower total lipid concentration of 38.5 mM in the ethanol solution. The micelles had a size of 16.0 ± 0.2 nm with a PDI of <0.13 (step 3), which increased after the coupling reaction with the model peptide EPRNEEK in size to 20 ± 3 nm with a PDI <0.25 (step 4). The narrow size distribution was achieved by addition of DSPE-PEG-2000 to the micellar composition. Finally, when the peptide-functionalized micelles were incubated with the preformed liposomes, particles with a size of 65 ± 3 nm and PDI of <0.2 (step 4, 5) were obtained. Figure 7 shows that the zeta potential measurements proved the insertion of micelles into the liposomes. While the preformed liposomes had a neutral charge (-0.7 ± 3.5 mV), the incorporation of peptide-functionalized micelles (-17.3 ± 4.5 mV) into the liposomes resulted in the negatively charged liposomes after post-insertion (-18.53 ± 0.8 mV) [28]. DSPE-PEG-2000 and DSPE-PEG-2000-Mal lose their zwitterionic property due to the linking of PEG-chain to free primary amino group via carbamoyl linkages [28], resulting in a

negative charge. Surface charge of peptide-functionalized micelles and post-inserted liposomes was within the same range. An increase of negative surface charge due to the formation of free carboxyl groups of hydrolysis product was not observed.

Directly after the micelle formation (step 3), samples were analyzed with respect to total amount of DSPE-PEG-2000 and DSPE-PEG-2000-Mal and maleimide activity (Figure 8). Contrary to the liposomes prepared by pre-insertion method, the formulations also contained DSPE-PEG-2000. The HPLC analysis provided information about the total amount of both PEG-lipids but was not able to distinguish between them. The micelles had a concentration of 1.71 ± 0.02 mM. The amount of active maleimide groups was determined by indirect Ellman´s assay. 76% of the maleimide groups were available for coupling reaction directly after the micelle preparation. Although the post-insertion process avoided long contact to the aqueous phase, the results revealed that the solvent removal as well as the hydration of lipid-film for the generation of micelles already had measurable effects on maleimide activity. After the coupling of the model peptide, the micelles were inserted into preformed liposomes with an amount of 0.42 ± 0.03 mM. The samples were finally purified by centrifugal filtration. The purified sample showed no change in liposome composition after the purification, indicating the complete insertion of PEGylated lipids (data not shown).

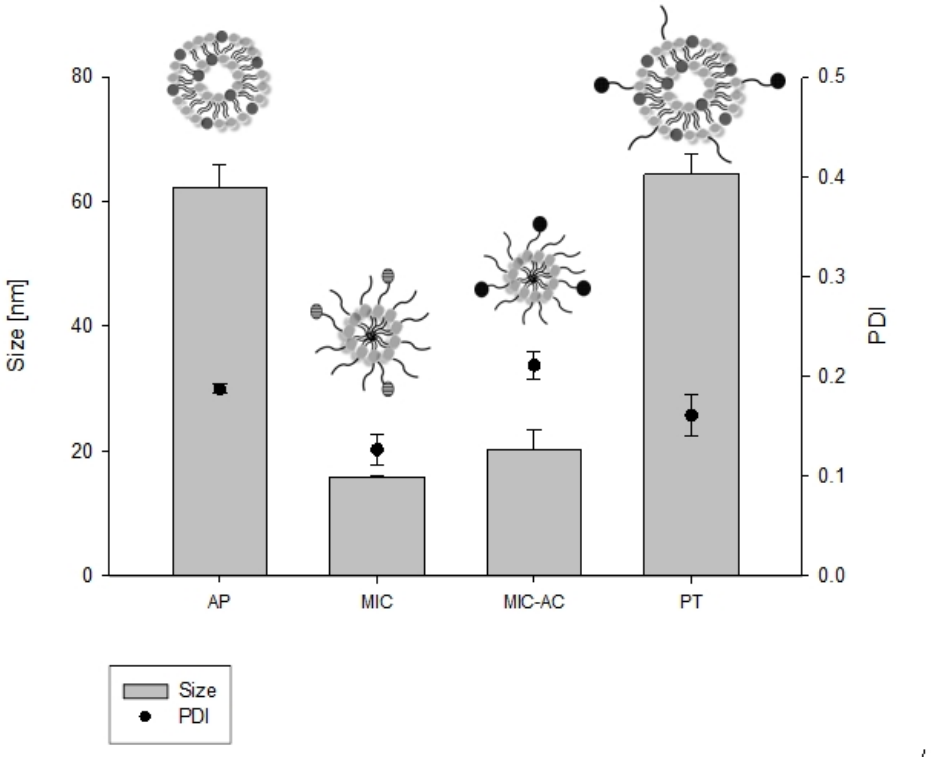

Figure 6: Size of liposomes prepared by the post-insertion method by DLS. The preformed liposomes were composed of CHO and DOPC with a molar ratio of 0.6:0.4 (AP). The micelles were composed of DSPE-PEG-2000 and DSPE-PEG-2000-Mal with a molar ratio of 0.04:0.01 (Mic). Mic-Ac showed the DLS results, after the coupling of model peptide. Finally, peptide-functionalized peptides were inserted into preformed liposomes (PT). (Mean ± SD, n=3) AP: after purification; MIC: micelle; MIC-AC: micelle after coupling; PT: post insertion.

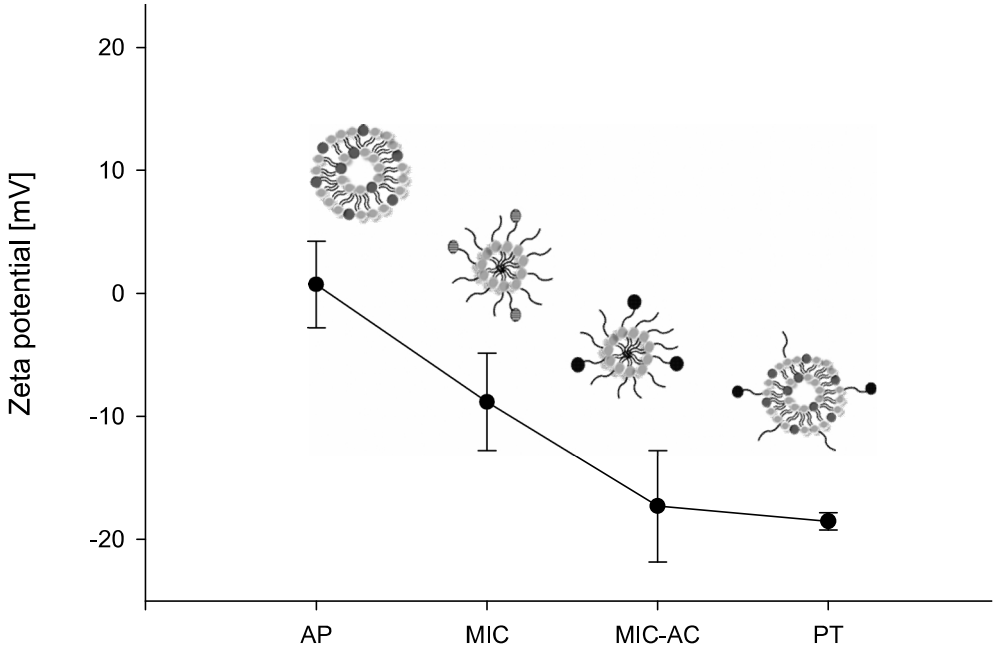

Figure 7: Zeta potential of prepared liposomes by the post-insertion method. The preformed liposomes were composed of CHO and DOPC with a molar ratio of 0.6:0.4 (AP). The micelles were composed of DSPE-PEG-2000 and DSPE-PEG-2000 Mal with a molar ratio of 0.04:0.01 (Mic). Mic-Ac showed the surface charge after the coupling of model peptide. Finally peptide-functionalized peptides were inserted into preformed liposomes (PT).(Mean ± SD,n=3)AP: after purification; MIC: micelle; MIC-AC: micelle after coupling; PT: post insertion.

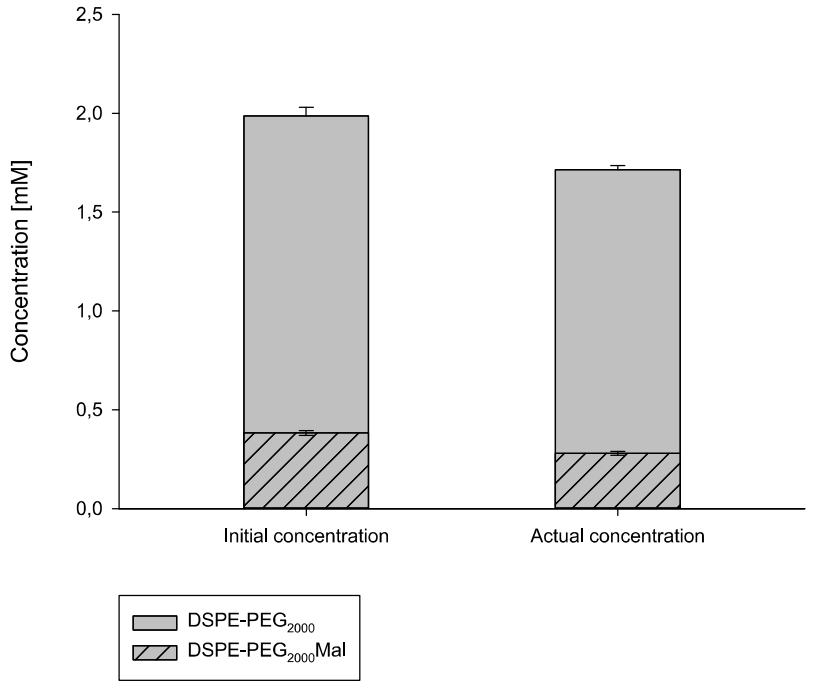

Figure 8: Amount of DSPE-PEG-2000 and DSPE-PEG-2000-Mal, determined by HPLC, and the active amount of DSPE-PEG-2000-Mal, determined by indirect Ellman´s assay, in the micelle sample directly after hydration compared to the initial concentration of both PEG-lipids.(Mean ± SD, n=3).

Table 4: Summary of physicochemical characterization of maleimide-functionalized liposomal formulations prepared by post-insertion method. (Mean ± SD, n=3). Determined by DLS[1], LDE[2], RP-ELSD-HPLC[3], Indirect Ellman´s assay[4].

Preparation method	Preparation step	Composition	Size[1] [nm]	PDI[1]	Zeta potential[2] [mV]	Total amount of DSPE-PEG-2000+DSPE-PEG-2000-Mal[3] [mM]	Maleimide activity[4] [%]
Post-insertion	After purification	DOPC:CHO	62 ± 4	0.187 ± 0.004	-0.7 ± 3.5	-	-
	Micelle	DSPE-PEG-2000:DSPE-PEG-2000-Mal	16.0 ± 0.2	0.13 ± 0.02	-8.8 ± 3.9	1.71 ± 0.02	76
	Micelle-After coupling	DSPE-PEG-2000:DSPE-PEG-2000-Mal+EPRNEEK	20 ± 3	0.211 ± 0.014	-17.3 ± 4.5	1.71 ± 0.02	-
	After post-insertion	DOPC:CHO: DSPE-PEG-2000:DSPE-PEG-2000-Mal+EPRNEEK	65 ± 3	0.161 ± 0.021	-18.53 ± 0.8	0.42 ± 0.03	-

4. Conclusion

The hydrolysis of maleimide groups is a crucial factor during the preparation of maleimide-functionalized liposomes. The loss of reactivity against thiol-containing peptides and increase of negative charge due to the formation of free carboxyl groups, changes dramatically the uptake of DDS by cells. Our proposed indirect Ellman´s assay unmasked critical preparation steps of two common methods for the preparation of DSPE-PEG-2000-Mal functionalized liposomes. By this, the method can not only be used for the stability assessment of preparation methods with regard to maleimide activity, but furthermore reveal the number of active maleimide groups located on the outer surface of liposome or micelle prior to the coupling reaction.

Reference List

1. Kim, J.-Y., et al., *Brain-targeted delivery of protein using chitosan-and RVG peptide-conjugated, pluronic-based nano-carrier.* Biomaterials, 2013. 34(4): p. 1170-1178.
2. Tao, Y., J. Han, and H. Dou, *Brain-targeting gene delivery using a rabies virus glycoprotein peptide modulated hollow liposome: bio-behavioral study.* Journal of Materials Chemistry, 2012. 22(23): p. 11808-11815.
3. Christie, R.J., et al., *Stabilization of cysteine-linked antibody drug conjugates with N-aryl maleimides.* Journal of Controlled Release, 2015. 220, Part B: p. 660-670.
4. Hermanson, G.T., *Chapter 3 - The Reactions of Bioconjugation*, in *Bioconjugate Techniques (Third edition)*. 2013, Academic Press: Boston. p. 229-258.
5. Nair, D.P., et al., *The thiol-Michael addition click reaction: a powerful and widely used tool in materials chemistry.* Chemistry of Materials, 2013. 26(1): p. 724-744.
6. Brinkley, M., *A brief survey of methods for preparing protein conjugates with dyes, haptens, and cross-linking reagents.* Bioconjugate chemistry, 1991. 3(1): p. 2-13.
7. Khan, M.N., *Kinetics and Mechanism of the Alkaline Hydrolysis of Maleimide.* Journal of Pharmaceutical Sciences, 1984. 73(12): p. 1767-1771.
8. Mattson, G., et al., *A practical approach to crosslinking.* Molecular biology reports, 1993. 17(3): p. 167-183.
9. Fröhlich, E., *The role of surface charge in cellular uptake and cytotoxicity of medical nanoparticles.* Int J Nanomedicine, 2012. 7(1): p. 5577-91.
10. Kelf, T.A., et al., *Non-specific cellular uptake of surface-functionalized quantum dots.* Nanotechnology, 2010. 21(28): p. 285105.
11. Patterson, J.T., et al., *Improving the serum stability of site-specific antibody conjugates with sulfone linkers.* Bioconjugate chemistry, 2014. 25(8): p. 1402-1407.
12. Tumey, L.N., et al., *Mild method for succinimide hydrolysis on ADCs: impact on ADC potency, stability, exposure, and efficacy.* Bioconjugate chemistry, 2014. 25(10): p. 1871-1880.
13. Nag, O.K. and V. Awasthi, *Surface engineering of liposomes for stealth behavior.* Pharmaceutics, 2013. 5(4): p. 542-569.
14. Batzri, S. and E.D. Korn, *Single bilayer liposomes prepared without sonication.* Biochimica et Biophysica Acta (BBA) - Biomembranes, 1973. 298(4): p. 1015-1019.
15. J.S. Dua, P.A.C.R., Dr. A.K. Bhandari, *LIPOSOME: METHODS OF PREPARATION AND APPLICATIONS.* International Journal of Pharmaceutical Studies and Research, 2012. 3(2): p. 14-20.
16. Marqués-Gallego, P. and A.I.P.M. de Kroon, *Ligation strategies for targeting liposomal nanocarriers.* BioMed research international, 2014. 2014.
17. Oswald, M., et al., *HPLC analysis as a tool for assessing targeted liposome composition.* International Journal of Pharmaceutics, 2016. 497(1–2): p. 293-300.
18. Ellman, G.L., *A colorimetric method for determining low concentrations of mercaptans.* Archives of biochemistry and Biophysics, 1958. 74(2): p. 443-450.
19. Dreher, M. and H. Hirsch, *Method for the determination of maleimide groups*. 1992, Google Patents.
20. Moser, M., et al., *Quantification of PEG-maleimide ligands and coupling efficiencies on nanoparticles with Ellman's reagent.* Analytical chemistry, 2015. 87(18): p. 9376-9383.
21. Barry, J.A. and K. Gawrisch, *Direct NMR Evidence for Ethanol Binding to the Lipid-Water Interface of Phospholipid Bilayers.* Biochemistry, 1994. 33(26): p. 8082-8088.
22. Pereira, M. and E.P.C. Lai, *Capillary electrophoresis for the characterization of quantum dots after non-selective or selective bioconjugation with antibodies for immunoassay.* Journal of Nanobiotechnology, 2008. 6(1): p. 10.

23. Akbarzadeh, A., et al., *Liposome: classification, preparation, and applications.* Nanoscale Research Letters, 2013. 8(1): p. 102-102.
24. Guichardon, P., et al., *Comparative study of semi-solid liposome purification by different separation methods.* Separation and purification technology, 2005. 41(2): p. 123-131.
25. Torchilin, V. and V. Weissig, *Liposomes: a practical approach*. 2003: Oxford University Press.
26. Iden, D.L. and T.M. Allen, *In vitro and in vivo comparison of immunoliposomes made by conventional coupling techniques with those made by a new post-insertion approach.* Biochimica et Biophysica Acta (BBA)-Biomembranes, 2001. 1513(2): p. 207-216.
27. Uster, P.S., et al., *Insertion of poly (ethylene glycol) derivatized phospholipid into pre-formed liposomes results in prolonged in vivo circulation time.* FEBS letters, 1996. 386(2): p. 243-246.
28. Garbuzenko, O., et al., *Electrostatics of PEGylated Micelles and Liposomes Containing Charged and Neutral Lipopolymers.* Langmuir, 2005. 21(6): p. 2560-2568.

Supplementary material

Post insertion of micelles – Dynamic light scattering

Size distribution was determined by dynamic light scattering (DLS) using a Zetasizer Nano ZS Malvern Instruments (Worcestershire, UK), equipped with a helium neon laser (λ= 633 nm). Samples were measured undiluted three times at 25 ± 0.1°C with fixed position (4.65 nm) at a detection angle of 173° (back scatter). Data was analyzed via cumulants fit. Figure 1 depicts the overlay of the size distribution graph of a micelle sample (red) and a final liposome preparation after post insertion (green). A single symmetrical peak indicating the existence of a homogeneous population that is larger than the micelles characterizes the size distribution graph of the liposome formulation.

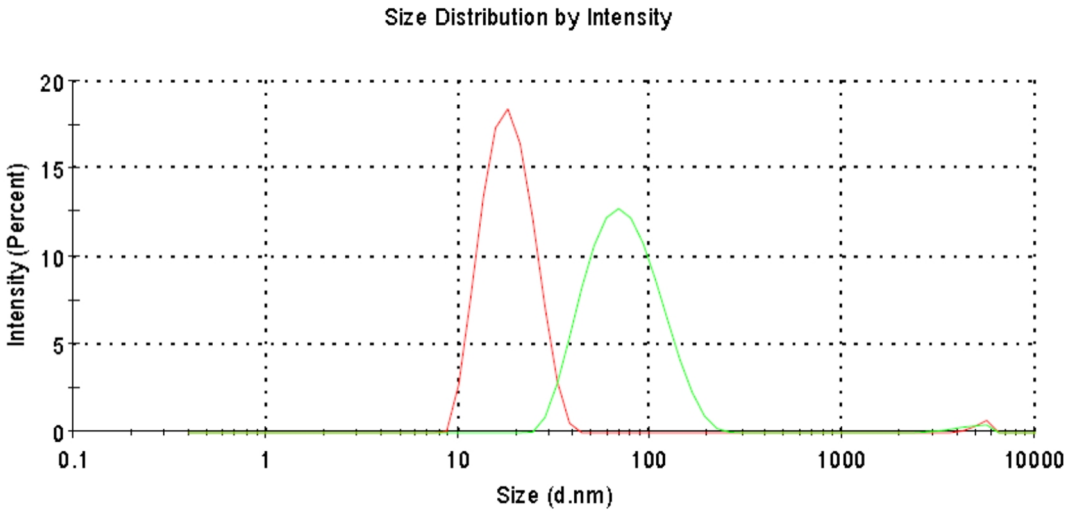

Figure 1: Overlay of a micelle sample (red) and liposome after post insertion (green).

SEC analysis

Post-insertion of micelles into liposomes was also followed by size exclusion chromatography (SEC) analysis. Micelles, liposomes and the final liposome formulation after post-insertion were injected into a HPLC system (Agilent 1260) quipped with diode array detector (DAD). Phosphate buffered saline (PBS) was used as eluent. Size exclusion chromatography was performed on a TSKgel 4000 PWxl column (7.8 mm x30 cm; 10 µm particle size; exclusion limit dextran: 1000 kDa), with a flow rate of 0.6 ml/min over 30 minutes.

Chromatograms obtained for each of the three preparations (micelles, liposomes and liposomes after the post-insertion) nicely confirm the integration of micelle material into the liposomes (Figure 2). Preformed liposomes eluted first due to their large size followed by the micelles and the free peptide. The chromatogram of the final liposome formulation confirmed the success of micelle 'insertion' by the disappearance of the micelle peak.

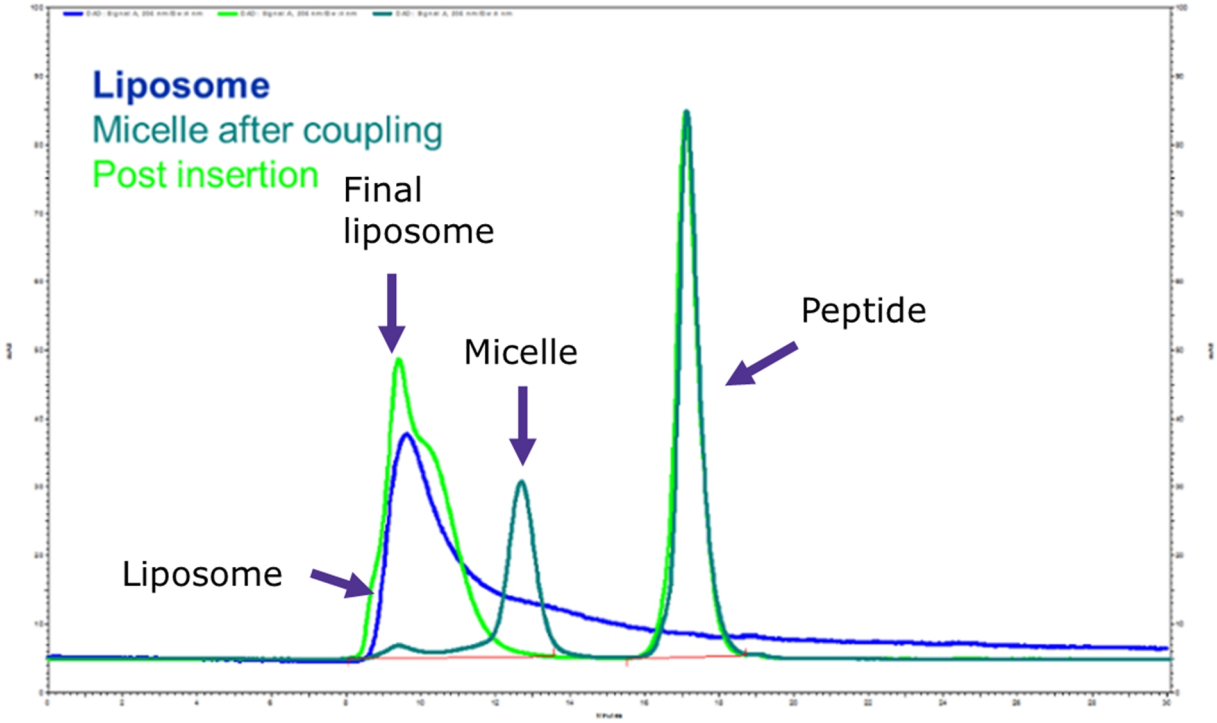

Figure 2: Results of SEC analysis. The preformed liposomes (blue line) were made of DOPC and CHO with a molar ratio of 0.6:0.4. The micelles (petrol blue) contained DSPE-PEG-2000 and DSPE-PEG-2000-Mal with a molar ratio of 0.04:0.01 (Mic). Finally, peptide-functionalized phospholipids were inserted into preformed liposomes (green).

Chapter 6

In vitro analysis of blood-brain barrier (BBB) specific liposomes: understanding the impact of tailoring formulation properties

Abstract

The purpose of the presented work was the analysis of the fundamental characteristics of liposomal formulations for brain endothelial cell uptake. Aside from the functionalization of liposomes with special recognition motifs for blood-brain barrier (BBB) targeting, other factors may support particle internalization. The presented work depicts the impact of size, charge, degree of PEGylation and the addition of the brain-specific polyunsaturated fatty acid docosahexaenoic acid (DHA) of liposomal formulations on the binding to the brain endothelial cell line bEND.3. Flow cytometry analysis revealed enhanced binding for positively charged, non-PEGylated liposomes. In contrast, size and PEG density showed only minor effects on cell binding. The findings have important implications for providing guidance on the formulation development of BBB-targeted liposomes. They underline the importance of adjusting physicochemical properties for targeted drug delivery.

1. Introduction

The blood-brain barrier (BBB) is a highly regulated and controlled barrier of our body [1–3]. Therefore, it is not surprising that the development of BBB-targeted formulations require tailor-made properties with respect to their physicochemical properties and active targeting strategies. While most of the published data focusses on active targeting strategies making use of ligands such as transferrin [4–6], apolipoprotein E [7, 8] or rabies virus glycoprotein [9–11], physicochemical properties of drug delivery systems (DDS) are often neglected. This is astonishing as defined settings for size, charge and liposome composition could directly impact the uptake of actively targeted liposomes [12]. As a consequence, a careful analysis of the physicochemical properties of DDS is highly required to determine particle-inherent passive targeting effects.

A major characteristic of the BBB is its selective uptake of molecules [13]. A lack of fenestrations and the existence of tight junction proteins between endothelial cells ensure that molecules with a molecular weight above 500 Da are not able to use paracellular pathways [13]. Consequently, the uptake of BBB-specific liposomes is controlled by endocytotic mechanisms [14]. The underlying mechanisms are strongly related to the physiochemical properties of the compound. For example, in the case of clathrin-mediated endocytosis, endocytosed vesicles have a diameter of 100–150 nm, which is a typical size of DDS prior to it being endocytosed [15, 16]. Furthermore, the charge or the composition of the liposome can also impact the unspecific uptake behaviour. Electrostatic and hydrophobic interactions between the liposome and the cell membrane have been reported to result in an adsorptive-mediated uptake of liposomes [12]. What is more, the PEGylation of liposomes, which is highly required for a reduced recognition by macrophages, could also cause a reduced unspecific uptake on target cells [17]. The impact of physicochemical properties should accordingly always be addressed in the context of delivering liposomes across the BBB.

The brain endothelial cell line bEnd.3 is well suited as a cellular uptake model, since it has important blood-brain barrier (BBB) characteristics [18]. Figure 1 depicts a microscopic picture of a bEND.3 cell line monolayer.

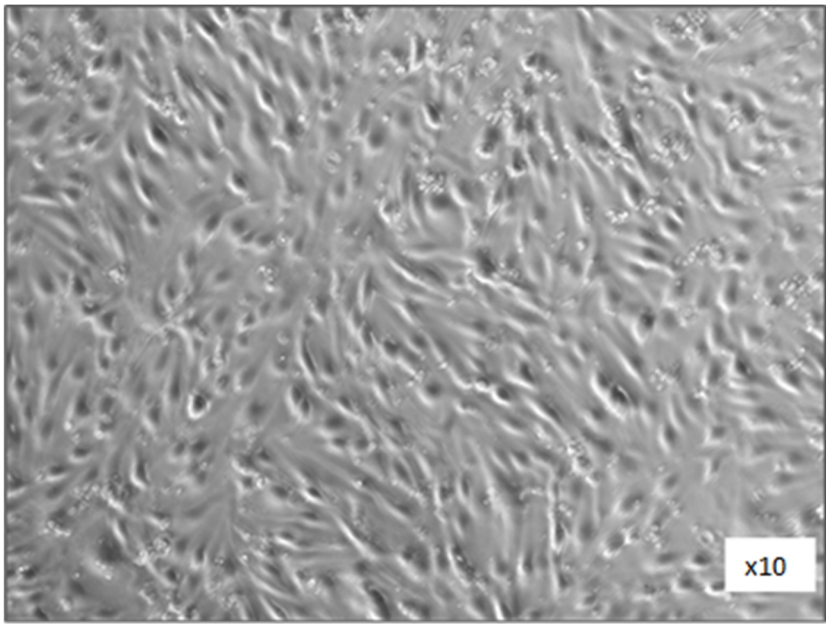

Figure 1 depicts the microscopic picture of bEND.3 cells after day three of seeding. The cells were seeded in a 24-well plate with a density of 12x105 per well. The image shows the characteristic spindle shaped morphology.

Omidi et al. characterized the bEND.3 cell line regarding its use as an in vitro BBB model for drug uptake and transport studies [18]. They showed that the cells express several vesicle-associated proteins and important transporters and receptors of the BBB such as glucose and amino acid carriers and P-glycoprotein. It is, therefore, not surprising that the bEnd.3 cell line is a popular in vitro model for studying interactions of DDS with the BBB [7, 10, 19, 20].

The aim of the presented work was to identify beneficial physicochemical properties for BBB-specific liposomes by applying different liposomal formulations to a well-established in vitro model for BBB-targeting effects [18]. By doing so, the present work gives a deeper insight into the tailor-made development of BBB-specific liposomes.

2. Materials and methods

2.1. Materials

Cells were cultured in Dulbecco's Modified Eagle Medium (DMEM) (InvitrogenTM, Carlsbad (USA), Cat.No: 41965) with 10% fetal bovine serum (FBS) (PAN-Biotech, Aidenbach (Germany), Cat.Nr.: 1502-P121511) and 1 mM Sodium-Pyruvate (InvitrogenTM, Carlsbad (USA), Cat.No.:11360). Penetratin 5-FAM was used as positive control and was obtained from Innovagen (Innovagen AB, Lund [Sweden]). Phosphate buffered saline (PBS) (1x) was obtained from Gibco (Life technologiesTM, Carlsbad [USA]). Accutase was used for the detachment of cells and bought from Innovative cell technologies (San Diego, USA). 1,2-dioleoyl-sn-glycero-3-phosphoethanolamine-N-(carboxyfluorescein) (ammonium salt) (Avanti Polar Lipids, Inc., Alabaster [USA]) and Dextran, Fluorescein, 10,000 MW, Anionic (Thermo Fisher Scientific, Inc. Waltham [USA]) was used for the labelling of liposomal formulations.

2.2. Methods

2.2.1 Liposome preparation and characterization

The preparation and characterisation of liposomes are described in chapter 2. Table 1 gives an overview of the liposome formulations used.

2.2.2 Labeling of liposomes

Fluorescein dextran with a molecular weight of 10.000 Da dissolved in PBS (0.05 mM) was encapsulated into the liposomes for analytical purposes. Purification of liposomal samples was performed via dialysis against PBS with a 50.000 MWCO slide-a-lyzer. Final total lipid concentration was adjusted to 10 mM. Particle size and charge were analyzed by dynamic light scattering (DLS) and laser diffraction electrophoresis (LDE) using a Zetasizer Nano ZS from Malvern Instruments (Worcestershire, UK), equipped with a helium neon laser (λ= 633 nm). For size-distribution analysis samples were measured undiluted at 25 ± 0.1°C with fixed position (4.65 nm) at a detection angle of 173° (back scatter). The data was analyzed via cumulants fit. For the determination of zeta potential, samples were diluted tenfold with Milli-Q-water and measured at 25°C. ZP was calculated using Smoluchowski's equation, which describes the electrophoretic mobility of liposomes. All measurements were performed in triplicate.

2.2.3 Endotoxin level

Endotoxin level of all formulations were assessed prior to in vitro testing by using the Endosafe®-PTSTM (Charles River Laboratories International, Inc, Wilmingtion [USA]). Endotoxin level was below 0.1 EU/ml for all formulations.

2.2.4 Cell culture media stability of liposomes

The physical stability of liposomes was analyzed after the incubation with cell culture media. To this end, liposome dispersions were diluted with culture media in a ratio of 1:10. Aggregation was analyzed by DLS, after an incubation time of 1h at room temperature.

2.2.5 Cell viability

The cell viability test was kindly performed by Mie Kristensen (Department of pharmacy, University of Copenhagen). The cytotoxicity of prepared liposome formulations was conducted by MTS ([3-(4,5-dimethylthiazol-2-yl]-5-[3-carboxymethoxyphenyl]-2-[4-sulfophenyl]-2H-tetrazolium)/PMS (phenazine methosulfate) assay. Mouse brain endothelial cell line bEND.3 was chosen for the assessment of cytotoxicity. Cells were seeded in growth medium at 37°C in a CO_2 humidified atmosphere in 96-well plates 24 h before the cell viability assay. Cytotoxicity was assessed over a concentration range of 0.125-2 mM total lipid. As positive toxic control, 0.2% SDS was used and buffer-treated cells as negative control. All formulations and controls were prepared as solution in Hanks balanced salt solution (HBSS) with 10 mM HEPES (hHBSS) at pH 7.4 immediately before the application to the cells. Cells were incubated with 100 µl of sample or control solution for 4 h (50 rpm, 37°C). After 4 h of incubation, the samples and controls were discarded and the cells were washed twice with 200 µl hHBSS. Then, 100 µl of MTS/PMS solution was added to the cells and incubated for 1.5 h (50 rpm, 37°C) under light protection. After incubation, absorbance (492 nm) was measured on a plate reader system. The relative cell viability was calculated as follows. The dehydrogenase activity in untreated cells was set to 100%.

$$viability\ (\%) = \frac{A-S}{C-S} \times 100$$

Where A is the absorbance obtained for each of the concentrations of the test substance, S is the absorbance obtained for the 0.2% SDS and CM is the absorbance obtained for untreated cells (incubated with buffer). All experiments were performed in triplicate.

2.2.6 Cellular uptake assay

Cellular uptake studies were performed using again bEnd.3 cells. The cells were seeded at a density of 100.000 cells per well in 24 flat-bottom-well plates for 72 h at 37°C and 10% CO_2 humidified atmosphere. DMEM supplemented with 10% FBS, 1 mM Sodium-Pyruvate was used as uptake buffer. Liposomes were diluted with uptake medium to a total lipid concentration of 0.1 mM labelled with 0.05 mM Fluorescein-Dextran. A 5 µM solution of cell-penetrating peptide (CPP) Penetratin-5-FAM was used as positive control. For control of cell barrier integrity a solution of free Fluorescein-Dextran (5 µM) was analyzed. Untreated cells served as negative control. After 72 hours, cells were removed and washed twice with PBS. Thereupon, cells were incubated with 500 µl of sample solution for 1 h at 37°C and 10% CO_2. All samples were prepared in triplicate. After the incubation time, the uptake medium was removed and the cells were washed twice with PBS. For the flow cytometry analysis, the cells were incubated with 100 µl accutase. After cell detachment, they were transferred in a V-bottom shaped 96-well-plate. Cellular uptake was analyzed by flow cytometry (iQueScreener; IntelliCyt Corporation; San Mateo [USA]). Samples were pulled out for 8 seconds (sip time) of each well. The data consisted of sideward scatter, forward scatter and fluorescence emission at 530/30 nm (FL-1). The data was analyzed with the ForeCyt Software (San Mateo, [USA]). Only the cell events of the single, viable cell population were used for analysis.

3. Results and discussion

The aim of the presented work was to determine key characteristics of brain-targeted liposomes. As a first step, the stability of liposomes in cell culture medium and the potential cytotoxic effects on bEND.3 cells were assessed. The CPP penetratin and fluorescein-dextran-loaded liposomes were used to investigate binding to bEnd.3 cells. Finally, the cell model was used to assess different potential key characteristics of liposomes like size, charge, PEGylation amount or the addition of the brain-specific polyunsaturated fatty acid DHA in the liposome composition.

3.1. Physicochemical characterization

Table 1 gives an overview of the liposome formulations used, as well as liposome composition and physicochemical properties.

Table 1: Summary of used liposome formulations. The table provides information on liposome composition, total lipid concentration (TLC) and physicochemical characteristics, like size distribution and surface charge. All liposome formulations were prepared and analyzed in triplicate. (*=n=1,).

Liposome formulation	**Liposome composition (molar ratio)**						
Cell viability	DOPC	CHO	DSPE-PEG$_{2000}$	TLC [mM]	Size [nm]	PDI	Zeta potential [mV]
	60	35	5	10	104	<0.25	-15
Size	DOPC	CHO	DSPE-PEG$_{2000}$	TLC [mM]	Size [nm]	PDI	Zeta potential [mV]
	60	35	5	20	489 ± 84	< 0.67	-12 ± 2
				10	103 ± 13	< 0.25	-14 ± 2
				5	70 ± 5	< 0.20	-15 *
Charge	DMPC	CHO	DOTAP	TLC [mM]	Size [nm]	PDI	Zeta potential [mV]
	50	30	20	10	152 ± 5	< 0.37	+ 20 ± 4
PEG-Amount	DOPC	CHO	DSPE-PEG$_{2000}$	TLC [mM]	Size [nm]	PDI	Zeta potential [mV]
	62	37	1	10	112 ± 37	<0.23	n.a
	60	35	5		104 ± 13	<0.25	n.a
	57.5	32.5	10		81 ± 9	<0.25	-11*
DHA	DOPC	CHO	DHA	TLC [mM]	Size [nm]	PDI	Zeta potential [mV]
	50	33	17	10	74 ± 2	<0.25	-25 ± 4

3.2. Cell culture media stability of liposomes

One important step prior to the contact of drug delivery systems (DDS) with cells is the stability testing of the used formulations with the used culture media. In interaction with biological fluids, nanoparticle adsorb proteins on their surface [21]. This adsorption of proteins is known as the protein corona [22]. As the protein corona can massively affect the properties of DDS [22, 23], all formulations should be tested with respect to their stability in cell culture media.

This is illustrated in Figure 1 for a placebo liposome formulation composed of DOPC, CHO and DSPE-PEG-2000. The formulation was incubated with DMEM supplemented with 10%.

FBS in a ratio of 1: 10, over a 1-h time period at room temperature. Size analysis was performed prior to the incubation (0 minutes) and after 10, 30 and 60 minutes. The incubation of the placebo liposomes with DMEM + 10% FBS results in a decrease of size from 102 ± 6 nm to less than 90 nm after 10 minutes and in an increase of PDI (<0.30). No aggregation of liposomes or adsorption of FBS was observed, which would have resulted in an increase in size.

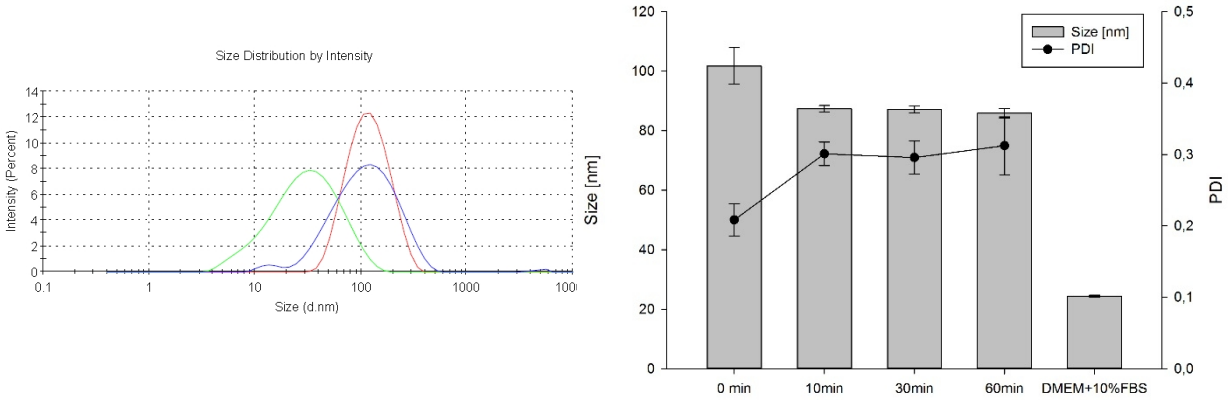

Figure 2 depicts the media stability testing of liposome formulations. A placebo liposome formulation composed of DOPC, CHO and DSPE-PEG-2000 in a molar ratio of 60:35:5 and final lipid concentration of 10 mM was incubated with DMEM supplemented with 10% FBS in a ratio of 1:10. Left: The graph shows an overlay of the size distribution by intensity of DMEM+10% FBS (green), the placebo liposome formulation (red) and after the incubation of DMEM+10% FBS (blue). Right: Samples were incubated with cell culture media over 1h at room temperature. Size analysis was assessed before (0 min) and after 10, 30 and 60 minutes of incubation (Mean ± SD, n=3 samples).

3.3. Cell viability

Cell viability was assessed by using the MTS/PMS assay with bEND.3 cells (Figure 2). Cells were incubated with the phosphatidylcholine (PC) liposome formulation. The PC liposome formulation was composed of 1,2-dioleoyl-sn-glycero-3-phosphocholine (DOPC), cholesterol (CHO) and 1,2-distearoyl-sn-glycero-3-phosphoethanolamine-N-[amino-2000] (DSPE-PEG-2000) in a molar ratio of 60:35:5. The reagent solution MTS/PMS was added to all cells. The metabolic activity of viable cells results in the reduction of MTS to the coloured formazan product. The liposome formulation showed no cytotoxic effects over a concentration range of 0.125–1 mM. Cell viability decreased at a concentration of 2 mM to 84 ± 18% for the DOPC formulation. The high standard deviation could be explained by a difference in the metabolic activity of the cells. The metabolic activity of viable cells is used to convert MTS to the coloured

formazan product. The differences in metabolic activity have been reported to have an impact on the intensity of the signal [24].

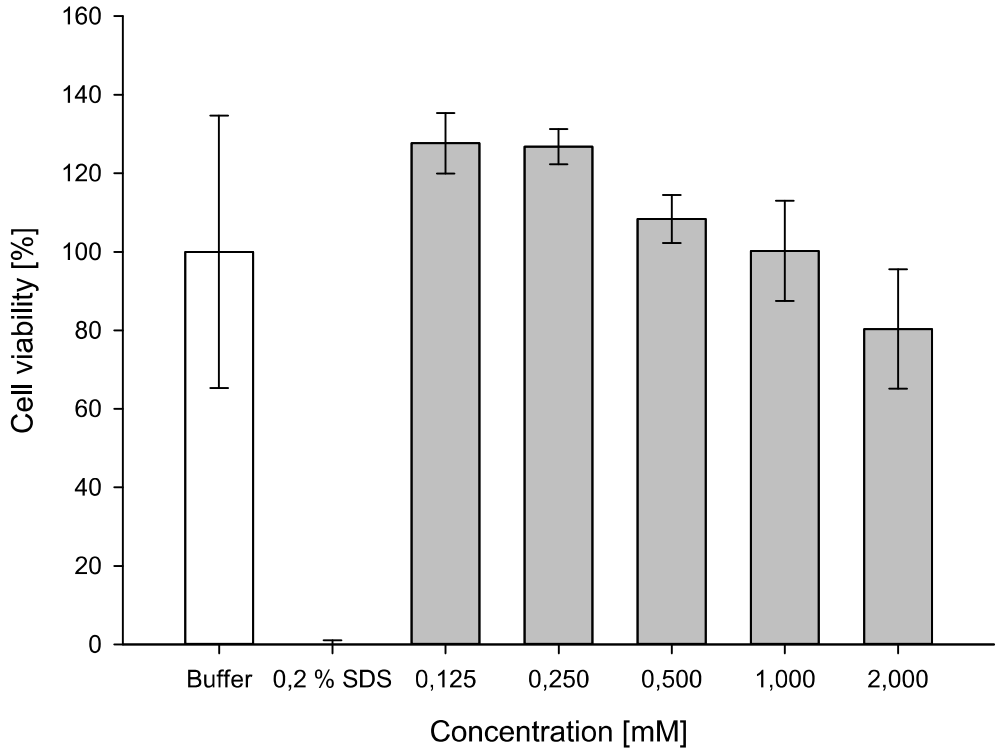

Figure 3 depicts the assessment of cell viability after the incubation of bEND.3 cells with a DOPC liposome formulation. Cell viability was assessed over a concentration range of 0.125–2 mM. Buffer-treated cells were used as negative control. Cells treated with 0.2% SDS served as positive control. Each sample was measured in triplicate (Mean ± SD, n=3).

3.4. Cell binding studies

Cellular binding studies employed the analysis by flow cytometry. A decisive factor in such studies is the application of controls to ensure the functionality. Consequently, two controls were selected. The cell-penetrating peptide (CPP) penetratin showed cellular uptake on brain endothelial cells [25] and was, therefore, used as positive control. Penetratin is derived from amphiphilic Drosophila Antennapedia homeodomain and is a 16 amino acid peptide. It belongs to the arginine-rich CPPs [26]. A possible uptake could be due to electrostatic and hydrophobic interactions between the residues of penetratin and the cell membrane (e.g. heparan sulphate proteoglycans, phospholipids) [26]. Fluorescein dextran (10.000 Da) served two purposes in this study: as label for the aqueous compartment of the liposomes and as control of cell barrier integrity. Due to their hydrophilic nature and high molecular weight (10.000 Da), dextrans are not able to pass an intact BBB via the paracellular or transcellular pathway nor the bilayers of

liposomes. Therefore, a control group of cells treated with F-Dextran solution was used for checking barrier integrity [27].

As a first step, the two controls, penetratin (5 µM) and F-Dextran (5 µM), were applied to the in vitro model over 5 h (Figure 4). The aim was to prove the functionality of the designated controls and to define an appropriate incubation time. The results are given as the mean fluorescence intensity. Cells incubated with penetratin showed a high fluorescence signal at all three time points. The increase of the fluorescence signal for dextran-treated cells after 5 h indicated a loss of cell barrier integrity. This was further underlined by a decrease of the fluorescence signal of penetratin-treated cells. This decrease could be the result of toxicological effects and it was also accompanied with a decrease in cell counts (data not shown). Due to the decrease of fluorescence intensity of penetratin and the increase of fluorescence intensity of fluorescein dextran, we decided to perform further experiments with an incubation time of 1 hour.

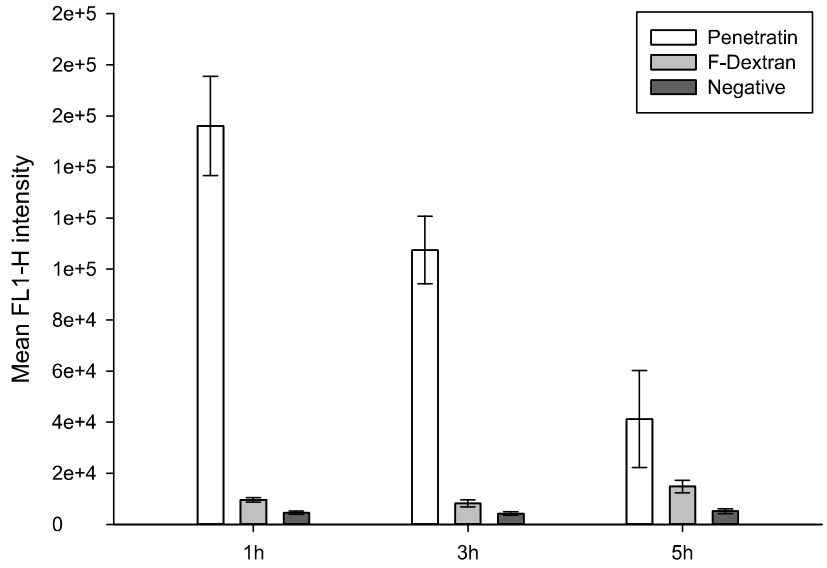

Figure 4: Cellular binding of positive control penetratin (5 µM) in bEND.3 cell line after 1,3 and 5h. Results are given as the mean fluorescence intensity. Cell barrier integrity was checked with fluorescein dextran (5 µM). Buffer treated cells were used as negative control (Mean ± SD, n= 3).

After it had been established, the in vitro model was applied to several liposome formulations. Figure 5a depicts the cell binding of different sized liposomes. The liposomes were composed of DOPC, CHO and DSPE-PEG-2000 in a molar ratio of 60:35:5 and were manufactured in three different size ranges of 70 ± 5 nm (PDI: <0.20), 103 ± 13 nm (PDI: <0.25) and 489 ± 84 nm (PDI:<0.67). All liposome formulations were negatively charged with a zeta potential around -15 mV. After an incubation time of 1 h, the liposomes with the smallest size showed

some higher values compared to untreated cells with 2.1 ± 0.5% compared to 1.4 ± 0.2%, however, it was still below the signal of free fluorescein dextran control with 2.3 ± 0.4%.

As discussed above in chapter 2, the particle diameters of less than 100 nm were considered to be ideal for the uptake by brain endothelial cells [13, 28, 29]. The results reported by Sonavane et al. showed that after intravenous injection of different-sized gold nanoparticles into mice, the uptake of 15 nm gold nanoparticles was 500 times higher than the uptake of 100 nm gold nanoparticles [30]. The lowest particle size of liposomes formulation in this study was limited to 50 nm and could be, therefore, a likely reason for the missing uptake of the liposomes.

Another factor, which can also impact the cell uptake, is the PEG density on the liposomes. PEGylated lipids are widely used in liposome formulations for reducing the recognition by reticuloendothelial system [31]. However, the amount of PEG on the liposome surface might also effect the recognition of target cells [17]. Therefore, we applied DOPC liposomes with different PEG amount, respectively 1, 5 and 10% (Figure 5b) to the in vitro model. Interestingly, none of the PEGylated formulations showed an uptake in the bEnd.3 cell line. These results were in accordance with those of Shilo et al., who analyzed barbiturate conjugated gold nanoparticles with different sizes from 20–110 nm and used PEGylated gold nanoparticles as control. While the 70 nm barbiturate gold nanoparticle showed the highest uptake, the PEGylated ones showed no uptake in the bEND.3 cell line [19].

In the next step, non-PEGylated liposomes with a positive charge were applied to the cell-culture model (Figure 5c). The liposomes had a positive charge of +20 ± 4 mV and were composed of DMPC, CHO and DOTAP with a molar ratio of 50:30:20. In contrast to the other liposome formulations, the DOTAP liposomes showed a somewhat higher uptake of 4.9 ± 0.1% compared to 1.4 ± 0.1% of the negatively charged liposomes or 2.3 ± 0.4% of the FITC-Dextran-treated cells. These results showed that the uptake of liposomes in bEND.3 cells is impacted by their surface charge. The influence of the charge was further underlined by the positive control penetratin, whose uptake can also be explained by electrostatic interactions. To our surprise, even the brain-specific DHA liposomes showed no uptake in bEND.3 cells (Figure 5d).

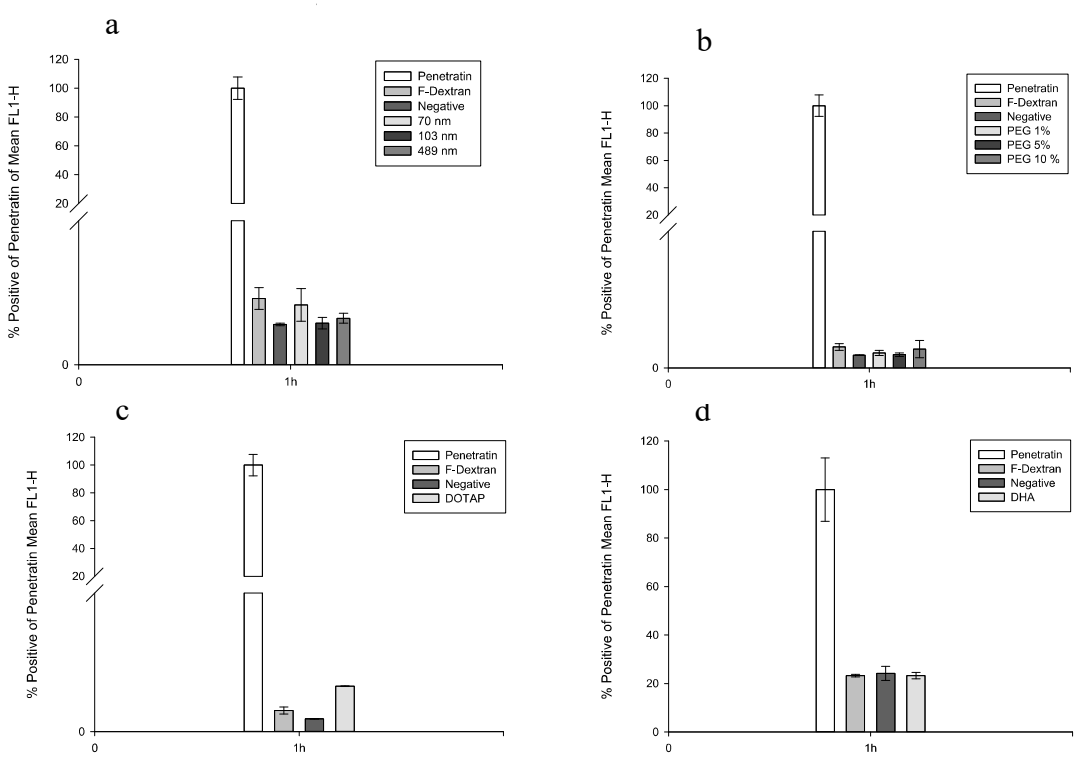

Figure 5: Cellular uptake of liposome formulations by brain endothelial bEnd.3 cells. Liposome uptake was investigated as a function of size (a), PEGylation degree (b), charge (c) or the addition of the brain-specific DHA (d). Penetratin was used as positive control (5 µM) in bEnd.3. Results are given as the percentage of the mean fluorescence intensity of the positive control of penetratin. Cell barrier integrity was checked with fluorescein dextran (5 µM). Buffer-treated cells served as negative control (Mean ± SD, n=3).

These results show that the unspecific uptake of liposomes in brain endothelial cells can be clearly impacted by a positive charge. To our surprise, neither the size nor the PEGylation degree affected the uptake of the liposomes. Hence, for BBB-targeted liposomes positive charge seems to be a key characteristic. However, positive charge alone will not be sufficient for the BBB penetration by liposomes. The presented results rather emphasize the need for an additional functionalization of BBB-specific liposomes with targeting ligands.

4. Conclusion

A well suitable in vitro model for the investigation of BBB-targeted nanomaterials was established. The influence of several physicochemical properties of liposomes on the brain endothelial cell uptake could be assessed. The presented results give direction on relevant factors for BBB specific liposomes with positive charge as an important characteristic.

Reference list

1. Chen, Y. and L. Liu, *Modern methods for delivery of drugs across the blood–brain barrier*. Advanced Drug Delivery Reviews, 2012. 64(7): p. 640-665.
2. Cardoso, F.L., D. Brites, and M.A. Brito, *Looking at the blood–brain barrier: Molecular anatomy and possible investigation approaches*. Brain Research Reviews, 2010. 64(2): p. 328-363.
3. Pardridge, W.M., *The Blood-Brain Barrier: Bottleneck in Brain Drug Development*. NeuroRx, 2005. 2(1): p. 3-14.
4. Ulbrich, K., et al., *Transferrin- and transferrin-receptor-antibody-modified nanoparticles enable drug delivery across the blood–brain barrier (BBB)*. European Journal of Pharmaceutics and Biopharmaceutics, 2009. 71(2): p. 251-256.
5. Georgieva, J.V., D. Hoekstra, and I.S. Zuhorn, *Smuggling Drugs into the Brain: An Overview of Ligands Targeting Transcytosis for Drug Delivery across the Blood–Brain Barrier*. Pharmaceutics, 2014. 6(4): p. 557-583.
6. Qian, Z.M., et al., *Targeted Drug Delivery via the Transferrin Receptor-Mediated Endocytosis Pathway*. Pharmacological Reviews, 2002. 54(4): p. 561.
7. Wagner, S., et al., *Uptake mechanism of ApoE-modified nanoparticles on brain capillary endothelial cells as a blood-brain barrier model*. PloS one, 2012. 7(3): p. e32568.
8. Sauer, I., et al., *An Apolipoprotein E-Derived Peptide Mediates Uptake of Sterically Stabilized Liposomes into Brain Capillary Endothelial Cells*. Biochemistry, 2005. 44(6): p. 2021-2029.
9. Kumar, P., et al., *Transvascular delivery of small interfering RNA to the central nervous system*. Nature, 2007. 448(7149): p. 39-43.
10. Tao, Y., J. Han, and H. Dou, *Brain-targeting gene delivery using a rabies virus glycoprotein peptide modulated hollow liposome: bio-behavioral study*. Journal of Materials Chemistry, 2012. 22(23): p. 11808-11815.
11. Soddu, E., et al., *From naturally-occurring neurotoxic agents to CNS shuttles for drug delivery*. European Journal of Pharmaceutical Sciences, 2015. 74: p. 63-76.
12. Georgieva, J.V., et al., *Surface Characteristics of Nanoparticles Determine Their Intracellular Fate in and Processing by Human Blood-Brain Barrier Endothelial Cells In Vitro*. Mol Ther, 2011. 19(2): p. 318-325.
13. Chen, W., et al., *Targeted brain delivery of itraconazole via RVG29 anchored nanoparticles*. Journal of drug targeting, 2011. 19(3): p. 228-234.
14. Oller-Salvia, B., et al., *Blood–brain barrier shuttle peptides: an emerging paradigm for brain delivery*. Chemical Society Reviews, 2016.
15. Papademetriou, J., et al., *Comparative binding, endocytosis, and biodistribution of antibodies and antibody-coated carriers for targeted delivery of lysosomal enzymes to ICAM-1 versus transferrin receptor*. Journal of inherited metabolic disease, 2013. 36(3): p. 467-477.
16. Shang, L., K. Nienhaus, and G.U. Nienhaus, *Engineered nanoparticles interacting with cells: size matters*. Journal of Nanobiotechnology, 2014. 12(1): p. 1-11.
17. Verhoef, J.J.F. and T.J. Anchordoquy, *Questioning the Use of PEGylation for Drug Delivery*. Drug delivery and translational research, 2013. 3(6): p. 499-503.
18. Omidi, Y., et al., *Evaluation of the immortalised mouse brain capillary endothelial cell line, b.End3, as an in vitro blood–brain barrier model for drug uptake and transport studies*. Brain Research, 2003. 990(1–2): p. 95-112.
19. Shilo, M., et al., *The effect of nanoparticle size on the probability to cross the blood-brain barrier: an in-vitro endothelial cell model*. Journal of Nanobiotechnology, 2015. 13: p. 19.

20. Helms, H.C., et al., *In vitro models of the blood–brain barrier: An overview of commonly used brain endothelial cell culture models and guidelines for their use*. Journal of Cerebral Blood Flow & Metabolism, 2016. 36(5): p. 862-890.
21. Maiorano, G., et al., *Effects of Cell Culture Media on the Dynamic Formation of Protein−Nanoparticle Complexes and Influence on the Cellular Response*. ACS Nano, 2010. 4(12): p. 7481-7491.
22. Karmali, P.P. and D. Simberg, *Interactions of nanoparticles with plasma proteins: implication on clearance and toxicity of drug delivery systems*. Expert Opinion on Drug Delivery, 2011. 8(3): p. 343-357.
23. Tenzer, S., et al., *Rapid formation of plasma protein corona critically affects nanoparticle pathophysiology*. Nat Nano, 2013. 8(10): p. 772-781.
24. Riss, T.L., et al., *Cell viability assays*. 2015.
25. Zou, L.-L., et al., *Cell-Penetrating Peptide-Mediated Therapeutic Molecule Delivery into the Central Nervous System*. Current Neuropharmacology, 2013. 11(2): p. 197-208.
26. Madani, F., et al., *Mechanisms of Cellular Uptake of Cell-Penetrating Peptides*. Journal of Biophysics, 2011. 2011.
27. Saunders, N.R., et al., *Markers for blood-brain barrier integrity: how appropriate is Evans blue in the twenty-first century and what are the alternatives?* Frontiers in Neuroscience, 2015. 9: p. 385.
28. Masserini, M., *Nanoparticles for Brain Drug Delivery*. ISRN biochemistry, 2013. 2013: p. 238428.
29. Bhaskar, S., et al., Multifunctional *Nanocarriers for diagnostics, drug delivery and targeted treatment across blood-brain barrier: perspectives on tracking and neuroimaging*. Particle and Fibre Toxicology, 2010. 7: p. 3-3.
30. Sonavane, G., K. Tomoda, and K. Makino, *Biodistribution of colloidal gold nanoparticles after intravenous administration: Effect of particle size. Colloids and Surfaces* B: Biointerfaces, 2008. 66(2): p. 274-280.
31. Immordino, M.L., F. Dosio, and L. Cattel, *Stealth liposomes: review of the basic science, rationale, and clinical applications, existing and potential*. International Journal of Nanomedicine, 2006. 1(3): p. 297-315.

Chapter 7

Summary and conclusion

Summary

The blood-brain barrier (BBB) is an extremely selective barrier that prevents undesired entry of xenobiotics and noxae into the human body. While essential for many physiological processes, this function is a major drawback in brain drug delivery [1]. The fact that viruses are able to pass the BBB accounts for why research tries to mimic their structure to enable the targeted delivery of drugs into the brain [2]. By doing so, uptake-relevant virus peptide sequences are coupled to the surface of nanoparticulate systems. The fate of virus peptide functionalized drug delivery systems (DDS) is an exciting focal point. Despite the immobilization of virus-related uptake information on the surface of the DDS, it is questionable whether such functionalized DDS follow the fate of the virus into the central nervous system (CNS). The rabies virus glycopeptide (RVG), an external peptide sequence derived from rabies virus, is said to have a CNS tropism [3]. Therefore, RVG is widely used as ligand for CNS targeting strategies. However, its use as targeting ligand on DDS requires the modification of the RVG peptide sequence. Furthermore, the DDS itself has certain characteristics that may differ from the original rabies virus. The comparison of the rabies virus with RVG-functionalized DDS with respect to peptide modifications and physicochemical properties allows an invaluable insight into BBB-targeting strategies (**chapter 1**).

However, a delivery to the brain is not only a matter of decorating nanoparticulate systems with specific peptide sequences. The knowledge about tissue-specific requirements of the BBB together with cutting-edge manufacturing techniques allow for the preparation of tailor-made nanoparticulate systems with respect to size, surface charge and BBB-penetrating molecules with enhanced brain uptake. Liposomes were selected as promising candidates for BBB delivery. By selecting various phospholipids and using a solvent-injection technique [4], several liposome formulations were prepared to assess the impact of size, surface charge, PEG density and the usage of the brain specific polyunsaturated fatty acid docosahexaenic acid (DHA) on the cellular binding of brain endothelial cells (**chapter 3**).

To our surprise, the analytical characterization of these elaborate formulations is often overlooked. Although, there are no boundaries set with regard to formulation development of functionalized liposomes, the analytical characterization of such DDS often lacks the use of recent analytical techniques such as HPLC. This is a drawback as the manufacturing of functionalized liposomes is a multi-step process, which requires the analytical tracking of functionalized phospholipids during manufacturing. Therefore, an HPLC method using evaporative light scattering detection (ELSD) was developed to simultaneously determine all

compounds of a PEG containing liposome formulation. The presented method emphasized HPLC analysis as a powerful technique for the tracking of functionalized phospholipids during manufacturing. Furthermore, the developed HPLC method allowed the detection of degradation products (**chapter 4**).

The functionalization of a liposome requires the use of phospholipids carrying reactive groups for the covalent coupling of targeting ligands such as virus peptide sequences. The reactivity of the functional group is hence a prerequisite for the successful binding of the targeting ligand. Another important factor is that functionalization strategies of liposomes often demand multiple preparation steps, which may result in delay of the final reaction. This is especially critical for functional groups, which suffer from activity loss during this process. A prominent example is the maleimide functionality, which is prone to activity loss due to hydrolysis during manufacturing. By using an indirect Ellman's assay, two common preparation methods for functionalized liposomes, namely pre- and post-insertion method, were analysed with regard to maleimide stability. The severe impact on maleimide activity was shown with 63% active maleimide groups for the pre-insertion method and 76% active maleimide groups for the post-insertion method (**chapter 5**).

Finally, brain endothelial cells were used to establish a cellular binding model for BBB-specific liposomes. The physiology of the BBB necessitate specific requirements with regard to size, surface charge or the use of brain-specific lipids for liposomes. bEnd.3 cells were used to assess such requirements with respect to physicochemical properties of liposomes. A positive charge was identified as an important key characteristic for BBB-specific liposomes, while size, PEG density and the use of the brain-specific polyunsaturated fatty acid DHA had no impact on the cellular binding of bEnd.3 cells (**chapter 6**).

Conclusion

On the whole, the presented work addressed neglected points of BBB-targeted delivery. The direct confrontation of RVG-functionalized DDS with rabies virus clearly revealed the impact of physicochemical properties on the native fate into the CNS. This unveils the common assumption of an exclusive uptake due to receptor-ligand interactions and emphasizes the relevance of the tracking of virus-functionalized DDS under the perspective of a combined virus-peptide and DDS related uptake strategy. Besides the deep dive into virus-related CNS targeting strategies, the missing quantitative characterization of such formulations turned out to be a weak point. Analytical methods need to be established considering how sophisticated these formulations are and how complex their manufacturing is.

The application of quantitative methods such as HPLC analysis as well as the determination of maleimide functionality enable profound process understanding and fulfil the requirement of today's standards to DDS. All in all, this work contributes significantly to a better understanding of the manufacturing and the analysis of BBB-targeted DDS.

Reference list

1. Pardridge, W.M., *Molecular Trojan horses for blood–brain barrier drug delivery.* Current Opinion in Pharmacology, 2006. 6(5): p. 494-500.
2. Avila-Olias, M., et al., *Inspired by nature: fundamentals in nanotechnology design to overcome biological barriers.* Therapeutic Delivery, 2012. 4(1): p. 27-43.
3. Kumar, P., et al., *Transvascular delivery of small interfering RNA to the central nervous system.* Nature, 2007. 448(7149): p. 39-43.
4. Batzri, S. and E.D. Korn, *Single bilayer liposomes prepared without sonication.* Biochimica et Biophysica Acta (BBA) - Biomembranes, 1973. 298(4): p. 1015-1019.

Appendices

AA	Amino acid
AD	Alzheimer disease
AD	After dialysis
AP	After purification
API	Active pharmaceutical ingredient
BBB	Blood-brain barrier
BCECs	Brain capillary endothelial cells
BD	Before dialysis
bEND3	Mouse brain endothelical cell line
BHT	Butylhydroxy toluene
CNS	Central nervous system
CRD	Cystein rich domain
CPP	Cell penetrating peptide
CHO	Cholesterol
DMPC	1,2-Dimyristoyl-sn-glycero-3-phosphocholine
DOPC	1,2-Dioleoyl-sn-glycero-3-phosphocholine
DOPE	1,2-Dioleoyl-sn-glycero-3-phosphoethanolamine
DSPE	1,2-Distearoyl-sn-glycero-3-phosphoethanolamine
DSPE-PEG-2000	1,2-Distearoyl-*sn*-glycero-3-phosphoethanolamine-N-[methoxy(polyethylene glycol)-2000] (ammonium salt)
DSPE-PEG-2000-Mal	1,2-Distearoyl-*sn*-glycero-3-phosphoethanolamine-N-[maleimide(polyethylene glycol)-2000] (ammonium salt)
DTNB	5,5-Dithio-bis-(2-nitrobenzoic acid)
DHA	Docosa hexaenic acid
DMEM	Dulbecco´s modified eagle medium
DDS	Drug delivery system
DLS	Dynamic light scattering
EDTA	Ethylendiamintetra acetic acid

ELSD	Evaporative light scattering detection
F´Ab	Fragment antigen binding
HBSS	Hank's Balanced Salt Solution
H_2O	Water
HPLC	High performance liquid chromatography
IG	Immunoglobulin
IPA	Isopropanol
JEV	Japanese encephalitis virus
LUV	Large unilamellar vesicle
LDE	Laser Doppler Electrophoresis
Lyso-PC	Lyso- phosphatidylcholin
MetOH	Methanol
MIC	Micelle
NCAM	Neural cell adhesion molecule
NMJ	Neuromuscular junction
NTR	Neutrophin receptor
nAchR	Nicotinic acetylcholine receptor
p75NTR	p75 neutrophin receptor
pDNA	Plasma Desoxy ribonucleic acid
PNS	Peripheral nervous system
PBS	Phosphate buffered saline
PL	Phospholipid
PEG	Polyethylenglycole
PT	Post insertion
RVG	Rabies virus glycopeptide
RV-Mat	Rabies virus marix protein
RES	Reticular endothelial system
SAMSA	5-((2-(and-3)-*S*-(acetylmercapto) succinoyl) amino) Fluorescein

SUV	Small unilamellar vesicle
SUV	Small unilamellar vesicle
SATA	N-succinimidyl S-acetylthioacetate
SD	Standard deviation
TFF	Tangential flow filtration
TLC	Total lipid concentration
TCEP	Tris(2-carboxyethyl)-phosphin
ZP	Zeta potential

Name	Mira Oswald
Date of birth	20th of December 1984
Place of birth	64807 Dieburg

Scientific education

Since March 2016	Principal Scientist, Analytical Development, Merck KGaA
January 2013- March 2016	PhD student, Department for Pharmaceutical Technology, University of Regensburg in cooperation with Merck KGaA
November 2012	Third State Examination Licensed as pharmacist
May 2012- November 2012	Second part of the practical year, pharmacist in internship, Apfelapotheke, Münster
November 2011- April 2012	First part of the practical year, pharmacist in internship, Merck KGaA
October 2011	Second State Examination
March 2011	Internship at a public pharmacy in Edmonton (Alberta, Kanada) Student Exchange Program (IPSF)
August 2010	Internship, Department of Pharmaceutical Biology (J. Gutenberg-University, Mainz) „Antiangiogenic and cytotoxic effects of Korean substances"

Wahl, O.; **Oswald, M.**; Tretzel, L.; Herres, E.; Arend, J.; Efferth, T., Inhibition of tumor angiogenesis by antibodies, synthetic small molecules and natural products. Current medicinal chemistry 2011, 18 (21), 3136-3155.

Kuete, V.; Seo, E.-J.; Krusche, B.; **Oswald, M**.; Wiench, B.; Schröder, S.; Greten, H. J.; Lee, I.-S.; Efferth, T., Cytotoxicity and pharmacogenomics of medicinal plants from traditional Korean medicine. Evidence-Based Complementary and Alternative Medicine 2013, 2013**.**

April 2009	First State Examination
April 2007- October 2011	Studies of pharmacy, Johannes Gutenberg University of Mainz
August 2006- February 2007	On the job training: Pharmaceutical technical assistant, Marienapotheke, Mainz
August 2004- February 2007	Off the job training: Pharmaceutical technical assistant, PTA-Schule Mainz
August 2001- June 2004	Oberstufengymnasium, Alfred-Delp-Schule, Dieburg General qualification for university entrance

Peer reviewed publications

Oswald, M.; Geissler, S.; Goepferich., *Targeting the blood-brain-barrier: a review of rabies-virus-targeting strategies*. Submitted to Molecular Pharmaceutics. (c**hapter 1**)

Oswald, M.; Platscher, M.; Geissler, S.; Goepferich, A., *HPLC analysis as a tool for assessing targeted liposome composition*. International Journal of Pharmaceutics 2016, 497 (1–2), 293-300. (**chapter 4**)

Oswald, M.; Geissler, S.; Goepferich, A., *Determination of the activity of maleimide-functionalized phospholipids during preparation of liposomes*. International Journal of Pharmaceutics 2016, 514 (1), 93-102. (**chapter 5**)

Conference abstracts

Oswald, M.; Geissler, S.; Goepferich, A., *Quantitative analysis of functionalized phospholipids in targeted liposomal formulations*, 2015 Annual Meeting and Exposition, American Association of Pharmaceutical Scientists, October 25-29, 2015, Orange County Convention Center, Orlando, Florida.

Ich möchte allen Menschen danken, die mich die letzten vier Jahre während meiner Promotion begleitet haben.

Mein besonderer Dank geht an Herrn Prof. Dr. Achim Goepferich für seine Betreuung während der aktiven Durchführung und im besonderen Maße während des Schreibens dieser Arbeit. Ich danke ihm für die wertvollen Hinweise und sein Blick auf die Wissenschaft, die mich stets motiviert haben.

Mein Dank geht an Eva Wrobel für ihre organisatorische Unterstützung während der letzten vier Jahre.

Weiterhin möchte ich Dr. Simon Geissler meinen Dank für diese intensive Zeit aussprechen. Ich denke gerne an die Diskussionen während unserer wöchentlichen Besprechungen. Ich danke ihm dafür, dass er ausnahmslos ein offenes Ohr für mich hatte. Er hat mich durch all meine Höhen und Tiefen begleitet. Besonders danke ich ihm für seine Unterstützung und sein Verständnis während mein Vater im Sterben lag.

Mein Dank gilt weiterhin Dr Markus Weigandt, der mir die Promotion bei Pharmaceutical Technologies und die Teilnahme an nationalen und internationalen Kongressen ermöglicht hat. Ich danke ihm vor allem für die schöne Zeit, die ich bei Pharmaceutical Technologies erleben durfte.

Weiterhin möchte ich vor allem meinen lieben Doktoranden-Kollegen danken, mit den ich die Promotion bei Merck bestritten habe. Mein besonderer Dank geht an Steffen Woell. Für sein kritisches Auge und die tiefe Auseinandersetzung mit meiner Arbeit. Sowie Stefan Schiller, Robert Hennig und Markus Riehl für die vielen wichtigen Ratschläge, die mich in meiner Arbeit weitergebracht haben. Melanie Hofman, Magdalena Münster und Carolin Auch für die vielen schönen, gemeinsamen Stunden und ihr offenes Ohr.

Nicht zuletzt möchte ich mich bei Katrin Grieser, Vicky Schmitt, Corinna Schoch und Meike Harms dafür bedanken, dass sie mein Leben neben der Doktorarbeit durch gemeinsames Ski fahren, Fastnacht, Yoga und Laufen bereichert haben.

Für eine tolle Unterstützung während meiner Promotion möchte ich weiterhin all meinen Kollegen bei Drug Delivery and Innovation sowie Research Pharmaceutics danken.

Ganz besonders geht mein Dank an Rike Ullrich, Sabine Bellers, Laura Tretzel und Astrid Morras-Ganskow, die mich seit meinen ersten Schritten in der Pharmaziewelt begleiten. Meiner

Familie möchte ich ganz besonders dafür danken, dass sie immer an mich geglaubt und mich ausnahmslos in jedem meiner Schritte bestärkt haben.

Zum Schluss möchte ich meinem Freund Jannis Papoutsakis für seine unendliche Unterstützung und Geduld danken.

Eidesstattliche Erklärung

(1) Ich erkläre hiermit an Eides statt, dass ich die vorliegende Arbeit ohne unzulässige Hilfe Dritter und ohne Benutzung anderer als der angegebenen Hilfsmittel angefertigt habe; die aus anderen Quellen direkt oder indirekt übernommenen Daten und Konzepte sind unter Angabe des Literaturzitats gekennzeichnet.

(2) Bei der Auswahl und Auswertung folgenden Materials haben mir die nachstehend aufgeführten Personen in der jeweils beschriebenen Weise entgeltlich/unentgeltlich geholfen:

1. .....

2. .....

3. .....

(3) Weitere Personen waren an der inhaltlich-materiellen Herstellung der vorliegenden Arbeit nicht beteiligt. Insbesondere habe ich hierfür nicht die entgeltliche Hilfe eines Promotionsberaters oder anderer Personen in Anspruch genommen. Niemand hat von mir weder unmittelbar noch mittelbar geldwerte Leistungen für Arbeiten erhalten, die im Zusammenhang mit dem Inhalt der vorgelegten Dissertation stehen.

(4) Die Arbeit wurde bisher weder im In- noch im Ausland in gleicher oder ähnlicher Form einer anderen Prüfungsbehörde vorgelegt.

Mainz, 21.04.2017